U.PORTO

MESTRADO ONCOLOGIA

ESPECIALIDADE EM ONCOLOGIA LABORATORIAL

Development of a 3D biomimetic *in vitro* platform to study EV cargo in rectal cancer radio-response

Miguel da Cruz Ribeiro

M

2022

U.PORTO

Miguel da Cruz Ribeiro. **Development of a 3D biomimetic *in vitro* platorm to study EV cargo in rectal cancer radio-response**

M.ICBAS.**2022**

INSTITUTO DE CIÊNCIAS BIOMÉDICAS ABEL SALAZAR

MESTRADO EM ONCOLOGIA

ONCOLOGIA LABORATORIAL

U.PORTO

Development of a 3D biomimetic *in vitro* platform to study EV cargo in rectal cancer radio-response

Miguel da Cruz Ribeiro

INSTITUTO DE CIÊNCIAS BIOMÉDICAS ABEL SALAZAR

M

2022

SUPERVISOR: DOUTORA TÂNIA CARINA BÉRTOLO CRUZ, PhD

Junior Researcher, "Tumour and Microenvironment Interactions" group, i3S - Instituto de Investigação e Inovação em Saúde da Universidade do Porto

CO-SUPERVISOR: MARIA JOSÉ CARDOSO OLIVEIRA, PhD

Group Leader, "Tumour and Microenvironment Interactions" group, i3S - Instituto de Investigação e Inovação em Saúde da Universidade do Porto; Invited Associated Professor at ICBAS-Institute Biomedical Sciences Abel Salazar, University of Porto

CO-SUPERVISOR: OLIVIER DE WEVER, PhD

Principal Investigator, Laboratory of Experimental Cancer Research; Full professor at Faculty of Medicine and Health Sciences, University of Ghent; Co-founder of the Cancer Research Institute Ghent (CRIG); Chairman of CRIG Steering Committee;

Acknowledgements

Durante o último ano, comecei a “trabalhar”. Deixando o panorama letivo, tive de ganhar capacidade de trabalho, sentido de responsabilidade, autonomia e resiliência mental para superar desafios que ainda não me tinham aparecido pela frente até agora. Este crescimento científico e pessoal só foi possível graças às pessoas que me rodearam durante este processo.

Gostaria de começar por agradecer à minha orientadora, a Tânia. De todos os meus colegas, neste e outros mestrados, creio ter sido o mais sortudo no que tocou à orientação. Trabalhar contigo (e não “para ti”) foi e continuará a ser um privilégio. A tua capacidade de delegar, ao mesmo tempo que ouves e integras as opiniões da equipa no trabalho, foram excecionais e criaram um ambiente que me permitiu sentir confortável em errar. E toda a gente sabe que errar é a melhor forma de aprender. Obrigado por me teres deixado errar, por me teres ensinado a trabalhar e a crescer a nível científico. E acima de tudo, em momentos difíceis, obrigado por te teres “desmascarado” do papel de orientadora e de seres minha amiga. O teu apoio em momentos difíceis foi fulcral para a minha motivação e confiança no meu trabalho.

Quero agradecer à equipa que me co-orientou, professores Maria Oliveira e Olivier de Wever, pela oportunidade de ter passado não por um, mas dois laboratórios de investigação em oncologia. A oportunidade que me foi concedida de executar parte do meu trabalho da tese em Ghent permitiu-me ter perspetivas diferentes do que é trabalhar em ciência, deu-me confiança nas minhas capacidades de adaptação a diferentes ambientes socio-culturais e de trabalho, e fez-me crescer imensamente num curto espaço de tempo. O período em que estive na Bélgica é um que vou valorizar para toda a vida.

Também quero deixar agradecimentos especiais a quem me ajudou no dia a dia, ensinando-me a trabalhar e a resolver problemas. O Diogo Estêvão, no Tumour and Microenvironment Interactions, recebeu-me de braços abertos no dia 1 e ajudou-me desde início no dia a dia laboratorial, uma ajuda que foi crucial para a minha aprendizagem. No Laboratory for Experimental Cancer Research em Ghent, a presença portuguesa do Cláudio Pinheiro fez-me sentir um pouco mais em casa estando tão longe dela, e o acompanhamento que ele me deu-me capacidade, conhecimento e confiança no meu trabalho.

Gostaria de agradecer a todos os elementos do TMI e LECR pelas receções calorosas e ajuda no trabalho diário. Fizeram-me aprender que dinâmicas animadas em contexto de trabalho são importantíssimas para não baixar a cabeça nos dias que não correm tão bem.

Nada do que alcancei neste último ano teria sido possível sem o apoio dos que me são mais queridos.

“Galáticos”, André, Bernardo, e Filipe, vocês são os maiores. Não tenho dúvidas que, por mais que uns “emigrem” ou outros trabalhem, nada vai abalar a nossa unidade. Obrigado por me fazerem rir, pelos vossos conselhos, pelas pulhices que são cometidas por causa de futebol, pelos torneios de sueca que eu e o Filipe nunca ganhamos, pelas horas infindáveis de entretenimento, diversão e apoio. Graças a vocês, na generalidade do trabalho apresentado, pude concluir que este foi executado com sucesso.

O “sofrimento conjunto” de saber que a Catarina e a Luísa estiveram em países diferentes enquanto eu também estava, e saber que compreendiam o que estava a sentir, fez-me saber que tudo passa. E sabia que íamos voltar todos, que ia voltar a rir convosco, e a força que isso me deu nos momentos mais críticos teve um peso imensurável. Obrigado por me ajudarem a crescer (algo que os rapazes não fazem) nos últimos 5 anos. E que contemos com muitos mais anos disto.

À Laura, porque te amo. E ter-te ao meu lado em toda e qualquer adversidade faz-me sentir que estou no topo do mundo. Tudo o que é mau voa pela janela na tua presença. Às vezes, em dias cinzentos, em que as experiências não corriam bem, em que estava longe de casa, em que tinha saudades tuas e de tudo, uma simples videochamada contigo iluminava o meu dia, não importa onde estivesse, e permitia que acordasse no dia seguinte com vontade de resolver os problemas do dia anterior. O teu carinho é tudo. Obrigado.

Por fim, gostaria de agradecer à minha família. Os meus pais, que para além do esforço financeiro que permitiu o estudo longe de Lisboa e até de Portugal, me fizeram o que sou. Os valores que aprendi deles guiar-me-ão para a vida, e ajudam-me a tomar decisões todos os dias. Mais do que saber que os orgulho, eles fazem-me sentir que tenho razões para me orgulhar de mim mesmo. A mana? É uma chata, portanto não me podia ter calhado ninguém melhor para atanazar o juízo aos pais sempre que possível. Amo-vos.

Obrigado a todos os que, de alguma forma, tenham contribuído para o meu crescimento pessoal e cientifico, permitindo que tenha chegado e aqui e que chegue mais longe ainda.

Summary

Rectal cancer (RC) is responsible for over 30% of the colorectal cancer burden worldwide, contributing heavily for the high incidence and mortality rates of gastrointestinal tract malignancies in 2020. Importantly, in Portugal, rectal cancer alone, represents the fifth most incident cancer, surmounting to almost half of all new colorectal cancer diagnoses in 2020. Moreover, due to the thriving of unhealthy lifestyles, rectal cancer is growing exponentially and it is expected, by 2030, an increase of 124% cases in patients under 35 years of age. Neo-adjuvant radiotherapy is usually the standard treatment method for RC. Although effective, radiotherapy still leaves over 30% of the patients experiencing no response or local recurrence after treatment, due to variable levels of radioresistance. As such, there is an urgent need for more efficient therapies to be combined with ionising radiation.

One of the strategies to search for new drug targets is to explore the radioresistance mechanisms. However, the mysteries behind such processes, within the tumour microenvironment, are still unsolved. The answer could partly reside in intercellular communication inside the tumour microenvironment and systemically. Having this in mind, this thesis aimed at developing a platform suitable for the uncovering of radioresistance molecular players enclosed in extracellular vesicles (EVs). This platform consisted of a biomimetic *in vitro* 3D rectal cancer model, to develop improved therapies that assist disease regression and to increase patient overall survival. This development consisted of *i)* optimising and characterising a biomimetic multicellular RC spheroid model; *ii)* implementing and optimising a protocol for the recovery of EVs from 3D RC spheroids; *iii)* studying the EV protein contents in the search for radioresistance players.

The data presented herein corroborates the success of this work in accomplishing its aim, resulting in a fully optimised and characterised platform for radiobiology studies, suitable for quality EV isolation and subsequent proteomic analysis, showing preliminary evidence of the influence of radiotherapy in the rectal cancer secretome.

Importantly, through the full characterisation and optimisation of the platform, this work lays strong foundations for more thorough multi-omics studies, which will include RNA sequencing of EV isolates, comparison of radioresistance and respective multi-omic EV signatures between RC cell lines, and inclusion of tumour microenvironment players such as immune cells in the RC spheroids.

Resumo

O cancro retal (CR) é responsável por mais de 30% do impacto do cancro colorretal (CCR) a nível mundial, contribuindo significativamente para as altas taxas de incidência e mortalidade de neoplasias malignas do trato gastrointestinal em 2020. Neste ano, em Portugal, o CR foi o 5º mais incidente, perfazendo quase metade dos novos diagnósticos de CCR. Adicionalmente, com a generalização de estilos de vida menos saudáveis, espera-se que o diagnóstico de CR suba em 124% em sujeitos com menos de 35 anos, até 2030. A radioterapia neoadjuvante é o tratamento padrão em CR. Ainda que a sua eficácia esteja comprovada, a radioterapia apresenta limitações, tendo taxas superiores a 30% no que toca a recorrência local após cirurgia, devido a variados níveis de radio-resistência. É, então, urgente encontrar novas terapias que possam ser combinadas com radioterapia.

Uma das estratégias para a pesquisa de novos fármacos passa pela exploração dos mecanismos de radio-resistência no microambiente tumoral, no entanto estes ainda foram desvendados. Alguns destes mecanismos poderão estar relacionados com a comunicação intercelular a nível tumoral e sistémico. Com base nesta premissa, esta tese teve por objetivo desenvolver uma plataforma que permita a investigação dos conteúdos de vesiculas extracelulares (VEs) que possam estar envolvidos em radio resistência. Esta plataforma consiste num modelo *in vitro* tridimensional biomimético de CR, que sirva para o desenvolvimento de novas terapias combinatórias que ajudem na regressão da doença e melhorem a sobrevivência dos pacientes. Este desenvolvimento consistiu em *i)* otimizar e caracterizar o modelo biomimético de CR; *ii)* implementar e otimizar o protocolo de isolamento de VEs a partir dos modelos 3D; *iii)* estudar os conteúdos proteicos das VEs isoladas, pesquisando por intervenientes em radio-resistência.

Os dados aqui apresentados corroboram o cumprimento destes objetivos, que resultou na implementação de uma plataforma completamente otimizada e caracterizada para estudos de VEs em radiobiologia, permitindo o isolamento de VEs com qualidade e passíveis de serem analisadas por proteómica. Este trabalho também apresenta evidências preliminares da influência da irradiação no secretoma do CR.

Através desta completa caracterização e otimização protocolar, este trabalho estabelece bases para estudos de multiómica mais detalhados, como sequenciação de RNA presente nas VEs, a comparação de modelos celulares com diferentes radio-resistências e seus secretoma, e a inclusão nos esferoides de CR de outros intervenientes do microambiente tumoral como células imunes.

Table of Contents

Figure Index

Table Index

List of Abbreviations

AGO-2 – Argonaute-2

AGRN - Agrin

ALIX – ALG-2 interacting protein X

ARF6 – ADP ribosylation factor 6

ARRDC1 - Arrestin domain-containing protein 1

ATCC – American Type Culture Collection

ATP – Adenosine triphosphate

BSA – Bovine Serum Albumin

CAD- carbamoyl-phosphate synthetase 2, aspartate transcarbamylase, and dihydroorotase

CAPOX – Capecitabine and Oxaloplatin

CD – Cluster of Differentiation (numbered after, e.g CD9)

CMS – Consensus Molecular Subtypes

Cox2 – Cyclooxygenase 2

CRC – Colorectal cancer

CTLA-4 – Cytotoxic T-Lymphocyte Associated-antigen 4

DAPI - 4',6-diamidino-2-phenylindole

DMEM – Dulbecco's Modified Eagle Medium

DMSO - Dimethyl Sulfoxide

DNA – Deoxyribonucleic Acid

ECM – Extracellular Matrix

EGF(R) – Epidermal Growth Factor (Receptor)

EMT – Epithelial to Mesenchymal Transition

EpCAM – Epithelial Cellular Adhesion Molecular

ESCRT – Endosomal Sorting Complex Required for Transport

ESMO – European Society for Medical Oncology

EVs – Extracellular Vesicles

FBS – Foetal Bovine Serum

FOLFOX – Folinic Acid, Fluorouracil and Oxaliplatin

GLUT1 – Glucose Transporter Type 1

GTPases – Guanosine Triphosphate Hydrolases

Gy - Gray

HE – Haematoxylin and Eosin

HIF-1α – Hypoxia Inducible Factor I-α

HSCs – Hepatic Stellate Cells

Hsp – Heat-shock protein

HSPG – Heparan Sulfate Proteoglycan Core Protein

hTERT – Telomerase Reverse Transcriptase gene

IL – Interleukin, usually numbered (e.g.: IL-1)

IL1RAP – Interleukin-1-receptor accesory protein

ILVs – Intraluminal Vesicles

ISEV – International Society for Extracellular Vesicles

KLF – Kruppel-like Factor

LC-MS/MS – Liquid Chromatography coupled to tandem mass spectrometry

LRP1 – Lipoprotein receptor-related protein 1

MDSCs – Myeloid-Derived Suppressor Cells

MHC – Major Histocompatibility Complex

MIF – Macrophage migration Inhibition Factor

miRNA – micro RNA

mRNA – messenger RNA

MSI – Microsattelite Instability

MVBs – Multivesicular Body

NF-κB - Nuclear factor of kappa light polypeptide gene enhancer in B-cells 1

NK – Natural Killer

NTA – Nanoparticle Tracking Analysis

ODG – Optiprep Density Gradient

PBS – Phosphate-Buffered Saline

PCA – Principal Component Analysis

PD-1 – Programmed cell Death protein 1

PD-L1 - Programmed cell Death protein 1 Ligand

P-gp – P-glycoprotein

PI – Propidium Iodide

PTEN – Phosphatase and Tensin homolog

Rab – Ras-associated binding GTPases

Ral – Ras-associated GTPase

RC – Rectal Cancer

RNA – Ribonucleic Acid

ROS – Reactive Oxygen Species

RPMI – Roswell Park Memorial Institute culture medium formulation 1640

RT – Room Temperature

SDS – Sodium Dodecyl Sulfate

SEC – Size Exclusion Chromatography

SNARE - (Soluble N-ethylmaleimide-sensitive fusion Attachment Protein Receptor

STAT3 - Signal Transducer and Activator of Transcription 3

TAp73 – Tumour protein p73

TEM – Transmission Electron Microscopy

TGF – Tumour Growth Factor

TLN-1 – Talin-1

Treg – Regulatory T cell

VEGF(R) - Vascular Endothelial Growth Factor (Receptor)

Wnt – Wingless-related integration site

ZO-1 – Zonula-occludens 1

1. Introduction

1.1. Rectal cancer

1.1.1. Epidemiology and specificities

Colorectal cancer (CRC) was the second most diagnosed malignancy in the world in the year 2020, with nearly two million new registered cases [3]. This disease was also the second deadliest, with almost one million of cancer related deaths being registered [3]. Importantly, the rectum alone, highly impacts colorectal epidemiology being responsible for over 30% of the CRC burden, comprising of 38% of all new CRC cases diagnosed worldwide and of 36% of all CRC-related deaths. In Portugal, specifically, rectal cancers (RC) corresponded to 47% of all the colorectal malignancies diagnosed in 2020 [3].

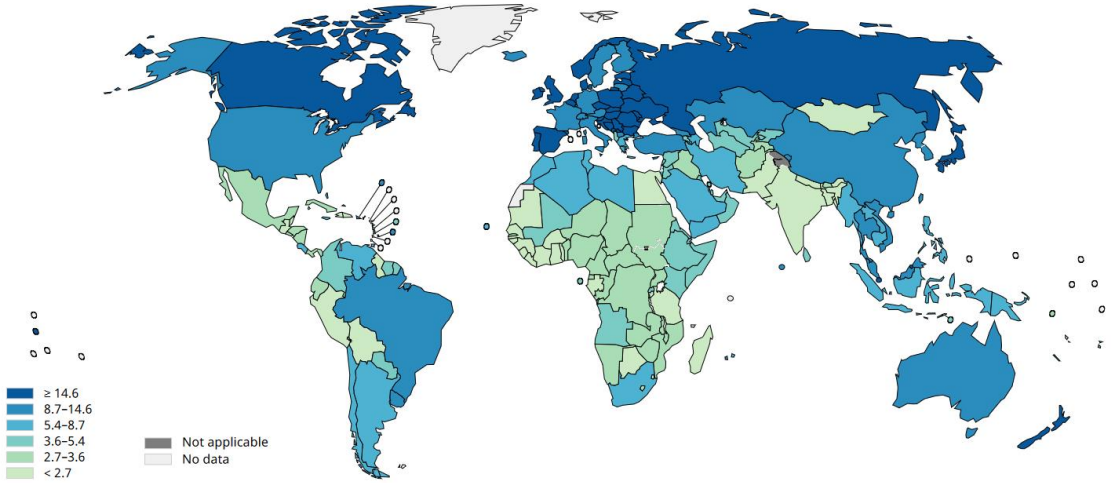

Figure 1 | Age standardised incidence rates for rectal cancer worldwide, in 2020. Adapted from GLOBOCAN 2020.

Colon and RC share some similarities, by virtue of arising in the same organ. Still, there are many molecular and physiological differences and therapeutic options and responses between colon and rectum malignancies. As such, there have been several proposals by the scientific community to abandon the term “colorectal” and to classify these tumours as different entities [4].

As previously stated, epidemiology of RC plays a major role in total CRC epidemiology (**Figure 1**), despite corresponding only to the terminal 10% of the colorectal tract. Risk factors involved in neoplastic transformation vary between the two entities, including diet, exercise or a pH gradient along the colon and rectum [5, 6]. Furthermore, RC is usually detected earlier than colon cancers [7], since patients with RC will more easily experience and detect blood in faeces, pain while sitting or incontinence [4]. However, the 5-year survival rates for both cancers are very similar [8].

CRC arises from different mechanisms in the colon and rectum. For this reason, in an attempt to better stratify patients towards treatment, the Consensus Molecular Subtyping (CMS) was created. This classification, illustrated in **Figure 2**, subdivides CRC into four subtypes: CMS1, CMS2, CMS3, and CMS4 [9]. CMS1 subtypes are named the "MSI immune" due to their characteristic microsatellite instability (MSI), which leads to the frequent expression of neo-antigens, leading to the recruitment of immune cells, and high CpG island methylation; CMS2 is the "canonical" subtype, holding epithelial cells with high number of somatic copies, increased MYC and Wnt signalling in immune-excluded tumours; CMS3 are termed "metabolic", presenting a mixed MSI status, low number of somatic copies and CpG methylation, but frequent KRAS mutations and metabolic deregulation; and CMS4, the "mesenchymal" subtype, presents high number of somatic copies, stroma infiltration, TGF-β signalling and high angiogenesis, generally being the subtype that presents the worst prognosis. A study by Guinney and colleagues on CRC subtypes partly explained the variability observed in CRC outcome, and could help in therapy guidance [10]. For example, the European Society for Medical Oncology (ESMO) guidelines state that assessment of MSI is important to rule out Lynch syndrome and that these MSI positive

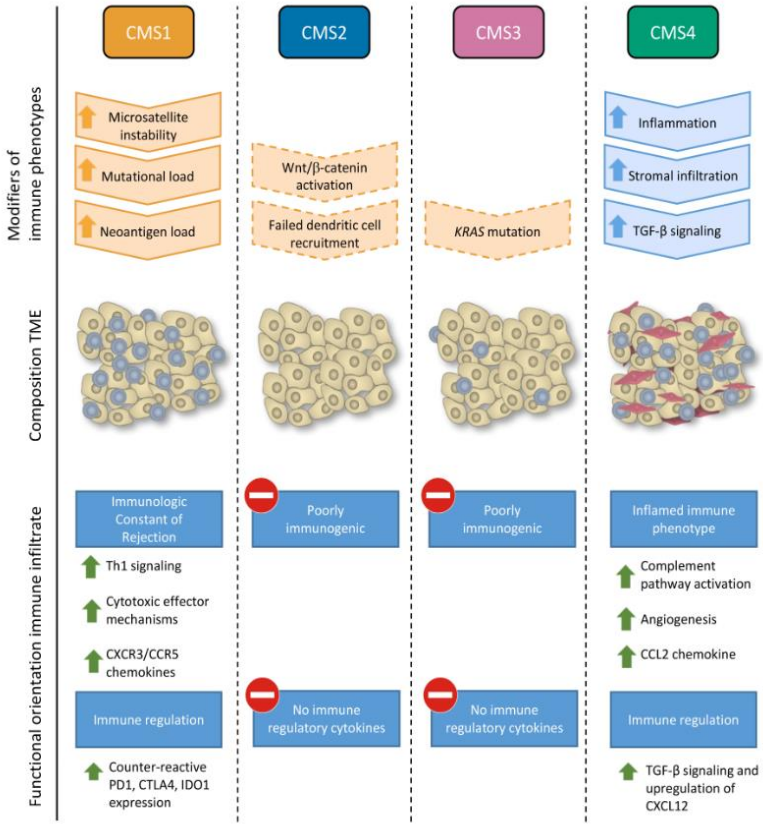

Figure 2 | Differential characteristics between all the Consensus Molecular subtypes employed to characterise CRC, obtained from Roelands et al. 2017 [2].

patients will benefit less from chemotherapy, but have better prognosis [11]. Also, screening for KRAS mutation is important to understand the benefit of using anti-EGFR (Epidermal Growth Factor Receptor) therapies. However, the usage of CMS subtyping for therapy guidance is still not recommended in international guidelines.

Importantly, Loree *et al.* [1] evaluated the distribution of CMS along the colorectal tract, concluding that the frequency of the different CMS varies according to the anatomical region. CMS1 is more frequent in the right side of the colon while CMS2 and CMS4 subtypes are the most commonly found in the rectum (**Figure 3**). This variability in CRC molecular subtypes is also related with the immune populations present at the tumour microenvironment, as shown by Becht *et al.* [12]. The expression of immune escape genes, as immune checkpoint and anti-phagocytic receptors is increased in CMS1 and CMS4 subtypes, which are the ones holding more immune cell infiltrates, while CMS2 and CMS3

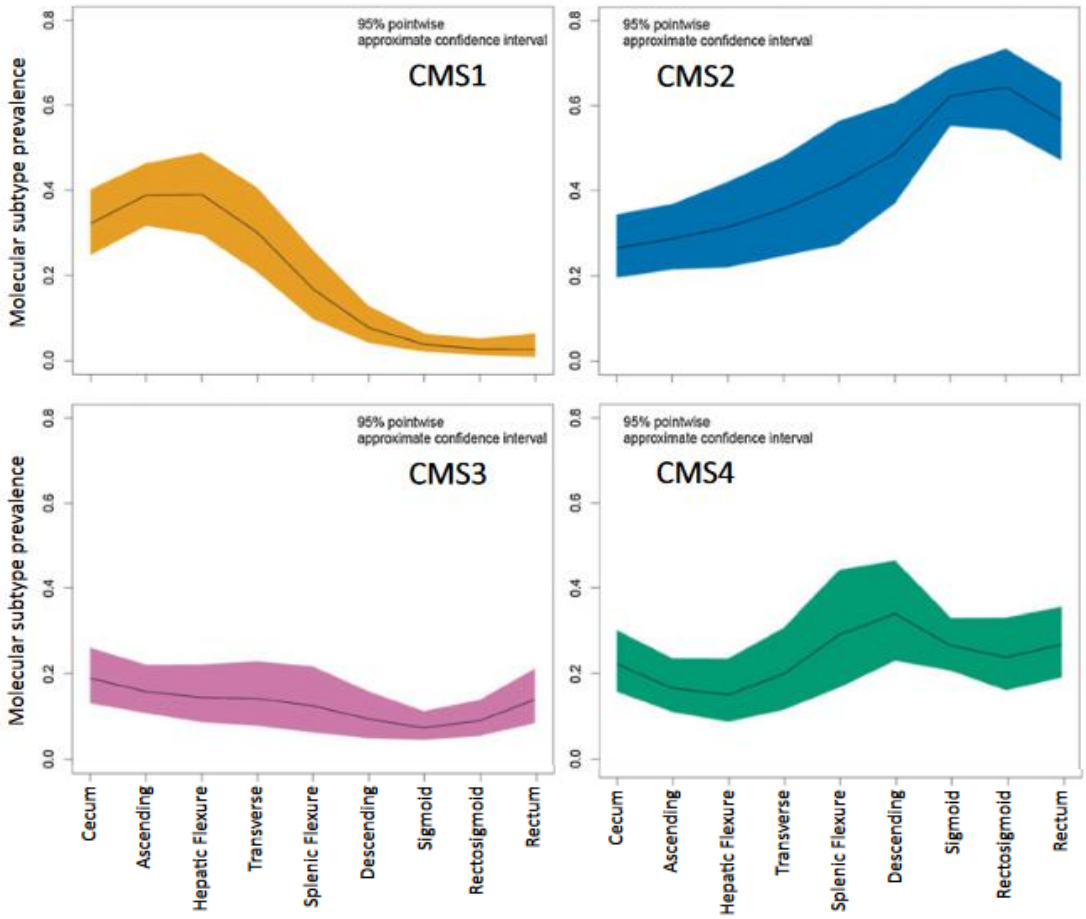

Figure 3 | Distribution of Consensus Molecular Subtypes along the colon and rectum, adapted from Loree *et al.* [1].

landscape is more immune-excluded, with limited to no infiltration of immune cells (frequently found in the rectum).

CRC and RC also display different metastatic patterns, which could, at least in part, be

explained by the differences in the vascular network that irrigates and drains both anatomical regions. In fact, the colonic blood drainage leads primarily to the liver, while rectal blood drainage leads both to the liver and to the lungs [13]. This could potentially drive rectal cancer spreading towards the lungs more frequently, when compared to the colon, while similar rates of liver metastases exist in both colon and rectal tumours [14]. Surgical resection effectiveness and post-surgical morbidity also differ from CRC to RC. Being approximately the last 16 cm of the larger intestine before the anocutaneous line, the rectum is very close to pelvic organs related to incontinence or impaired sexual function, which are innervated by the same nerves [4]. This makes RC resection a very difficult task, often impairing patients' quality of life, especially when it comes to defecation related problems [15]. Furthermore, in men, frequent urinary and sexual function problems arise upon an attempted curative resection [16]. Post-operative local recurrence is also higher in RC patients when compared to colon cancer patients [17]. One way to improve surgery effectiveness in RC is through neo-adjuvant treatments, which constitute, again, a difference between CRC and RC. In terms of colon cancers, localised disease management consists of colectomy followed by FOLFOX (Folinic Acid, Fluouracil and Oxaliplatin) or CAPOX (Capecitabine and Oxaliplatin) chemotherapy regimens, when endoscopic removal alone is not sufficient (locally invasive tumours), while metastatic disease includes adjuvant therapies that target VEGF and/or EGFR, in addition to chemotherapy and surgery [11, 18]. When it comes to RC, neo-adjuvant therapy is recommended for more advanced stages, in order to reduce local recurrence after total mesorectal excision, and relies on the use of radiotherapy that will often be accompanied by chemotherapy, both in short-course and long-course ionising radiation schemes. Short course preoperative radiotherapy consists in 5 fractions of 5 Gray (Gy) administered in 5 consecutive days, followed by surgery in less than 10 days, while long course fractionated radiotherapy is administered in 25-28 fractions of 1.8-2Gy, in a total of 45-50Gy, plus a possible preoperative boost [19].

1.1.2. Radiotherapy – "The 6 Rs"

The basic principle of radiotherapy is that cancer cells are less efficient in repairing DNA than normal cells, therefore, ionising radiation will induce DNA damage that is more easily repaired by the surrounding healthy cells when compared to cancer cells, which will accumulate damage and eventually die [20]. In 1975**,** Withers *et al.* proposed four principles of radiotherapy that supported the rationale for the use of fractioned ionising radiation [21]. The first principle of radiotherapy indicated in this publication – **Repair** – states that cells' capacity to fix repair DNA defects directly influences the effectiveness of radiation therapy, and dose fractionation kept efficient repairers (in theory, healthy cells) alive while killing

poor repairers (*i.e.* cancer cells) through the accumulation of sub-lethal damage. This means that malignant cells struggle to repair DNA damage in between radiation fractions, thereby accumulating DNA defects until, eventually, this damage becomes lethal. Moreover, this principle was observed to be dose dependent and also dependent on the number of fractions (granted that each fraction was high enough to provoke sub-lethal DNA damage) [21]. In fact, the distribution of high doses in more fractions spared cells that were efficient DNA repairers, but had increased effectiveness in killing cells that struggled to repair the damage caused by irradiation. Another proposed radiotherapy principle, by Withers, was – **Reoxygenation** – given that, upon cell death of the outer layers of the tumour, fractionation of radiotherapy will allow hypoxic cells to gain access to oxygen, which will sensitise them for the next fraction of ionising radiation. This was demonstrated in the 1970s, when tumour oxygenation was observed to improve upon radiotherapy, with a 2.5 to 3 times sensitisation of formerly hypoxic cells to irradiation [21]. This occurs because irradiation induces the formation of reactive oxygen species (ROS), which is greatly enhanced if oxygen is present in the cells' vicinity. ROS are very destructive, inducing additional DNA damage to the irradiated cells [22]. Fractionation also allows for the third principle proposed by Withers [21] - **Redistribution** of the cell cycle within the tumour. Experiments by Sinclair and Morton, further corroborated by others, showed that the cell cycle directly influences cells' radiosensitivity to both X-Rays and ultraviolet (UV) rays [23]. Explicitly, cells in the S phase tend to be more resistant, while cells in the G2 and M phases are more sensitive. By dividing radiation therapy into smaller fractions, the cells in G2 and M phases will be killed in the earlier doses, while cells in S phase will progress in the cell cycle and be more susceptible in the following fractions. The fourth principle proposed by Withers [21] in 1975 was **Repopulation** – which relies on the fact that induction of DNA damage and subsequent cell death through irradiation leads to increased proliferation of the remaining cells, that rapidly repopulate the tumour environment previously destroyed [24]. This is an analogous phenomenon to what occurs in healthy tissues responding to injury. Furthermore, reoxygenation of the remaining cells could assist in such proliferation. Of note, repopulation is pointed to as one of the major causes of treatment failure, but can be prevented through long exposure to irradiation as intended in long term radiotherapy schemes. The 5th "R" was proposed by Steel in 1989 [25], adding to the original 4 Rs proposed by Withers over 14 years earlier – **Radiosensitivity** – an intrinsic property that varies from tissue to tissue, since the initial damage done to the cells' DNA, with the same radiation dose, was proven to be tissue dependent [25]. This was supported by the observation that tumours with different curabilities, measured through the analysis of the survival curves of different cell lines exposed to fractionated radiotherapy, had corresponding radioresistances [26]. This helped to explain the variability in radiotherapy effectiveness between different tumours,

which the four original principles didn't. More recently, a 6th principle was proposed. Radiotherapy, by killing tumour cells, induces the release of tumour associated antigens into the microenvironment. These antigens can be taken up by antigen presenting cells which can then activate T effector cells [27], reverting the immune escape mechanisms acquired by the tumour over time. This is the **Reactivation** of the immune system's anti-tumour functions mediated by radiotherapy. Irradiation also affects the tumour microenvironment, for example, by disrupting endothelial cells and thereby increasing leukocyte adhesion and infiltrating capacity [28]. This reactivation is also responsible for the abscopal effect, which is the capacity of radiotherapy to affect "out-of-field" tumours, *i.e* tumours that weren't directly irradiated [29], because the newly activated immune effectors are able to act systemically on other tumour masses. The reactivation effectiveness will depend on total dose and its fractionation, and therefore the radiotherapy regimen that needs to be applied to each patient is still an object of research. This includes research on combinatory therapies with immune modulators or immune checkpoints, with the aim of improving the immune reactivation mediated by radiotherapy [30]. Thus the effectiveness of fractionated radiotherapy is guided by six principles (the "6 Rs"): **Radiosensitivity, Repair/Recovery, (Re)Oxygenation, Redistribution, Repopulation, and Reactivation** of the immune system.

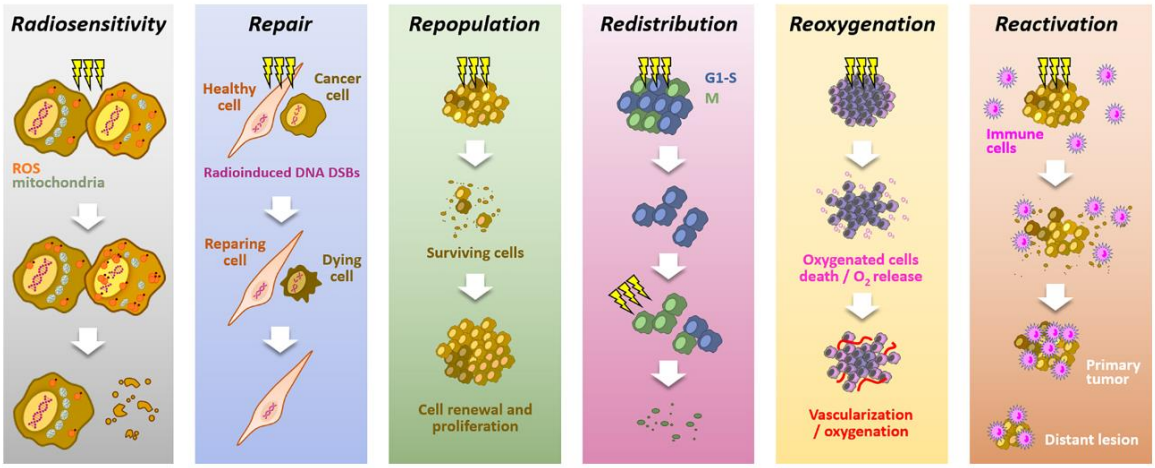

Figure 4 | Summary of the mechanisms underlying the 6 Rs of Radiotherapy, adapted from Rakotomalala *et al.* [31]. Radiosensitivity can be perceived as the intrinsic capacity of cells to survive a certain irradiation treatment, which will vary with its contents and stress conditions. Cancer cells also have, generally, impaired DNA Repair mechanisms when compared with their environment. Dose fractionation helps in the control of increased Repopulation rates verified in cancer cells, and in striking cells when they are most vulnerable by allowing cell cycle Redistribution, as well as the Reoxygenation of hypoxic areas, which are more radioresistant. DNA damage and cell death will release tumour neo-antigens and inflammatory factors into its microenvironment, leading to a Reactivation of the immune system.

1.2. Extracellular vesicles

1.2.1. History, classification, and trafficking

Extracellular vesicles (EVs), as defined by the International Society of Extracellular Vesicles (ISEV) [32, 33], are extracellular compartments naturally emitted from cells, enveloped in a lipid bilayer, that do not replicate due to the lack of a functional nucleus. Despite being a hot topic of discussion in basic and translational research in the past 15 years, with increasing number of publications from year to year, these vesicles are hardly a new concept – they were first observed by Chargaff and West in 1946, as particles that aided blood clotting [34]. This "platelet dust", as described by Wolf in 1967, was rich in phospholipids and presented "platelet-like" activity by containing "Platelet Factor 3" [35]. In 1977, De Broe *et al.* isolated "plasma membrane fragments" from both culture medium of HeLa cells and urine, that presented similarities in enzymatic activity to that of the parent cells [36]. In the 1980's, EVs started to gain traction as a relevant study topic, although they were mostly perceived as vehicles for selective externalisation of certain cell contents. While studying reticulocyte maturation, Harding and colleagues saw exocytosis of the transferrin receptor, through one of the first suggestions of multivesicular bodies (MVB) as exocytosis mediators, at the time termed multivesicular endosomes [37]. In the same decade, the term "exosome" arose in a study by Johnstone *et al.*, as the characterisation of these reticulocyte vesicles started gaining shape, again, considering them solely as a mechanism of expelling material to aid cell maturation [38]. In the following decade, after the discovery of intracellular MVBs enriched in Major Histocompatibility Complex (MHC) class II molecules in antigen-presenting cells, the function of these vesicles was found to be more than secretion of cellular "waste" [39, 40]. Raposo *et al.* found that these exosomes, "analogous to those released from reticulocytes", were released by B lymphocytes and were capable of presenting antigens to T cells, eliciting a response from them [41]. In the following decade, both microvesicles and exosomes were explored as an intercellular medium of communication [42-44].

The discovery that nucleic acids (specifically, mRNAs and microRNAs) were contained in these particles [45-47], captured, once again, the interest in EVs among the scientific community. This increasing interest in EVs led to their isolation from virtually all body fluids (blood, urine, seminal fluid, nasal and bronchial lavage fluid, saliva, amniotic fluid, and breast milk), indicating that EVs are not only an important effector in paracrine communication, but could also partake in distant cell-cell content interchange and, be a potential source of pathological biomarkers [48-52]. Their contents include all types of biomolecules, which is why EVs are capable of eliciting an effect in the target cell. The more common contents are summarised in **Figure 5**.

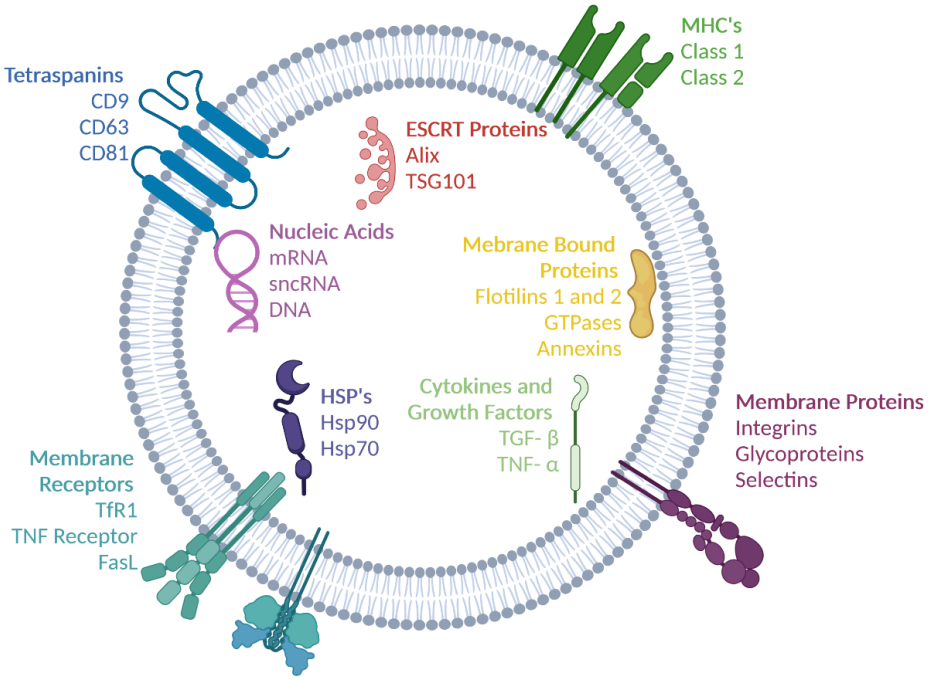

Figure 5 | The variety of EV contents. At their membrane, EVs may present a variety of signalling proteins such as MHC molecules, integrins, selectins, glycoproteins, membrane receptors or agonists and tetraspanins. In their core, they may hold molecules related to their biogenesis such as ESCRT proteins and lipid raft-associated proteins such as flotilins, but also cytokines, growth factors and heat-shock proteins (HSPs). Furthermore, they usually contain nucleic acids. ESCRT proteins, lipid raft-associated proteins and tetraspanins are commonly used as EV markers. Scheme made with BioRender.

These vesicles can be classified according to their biogenesis into three different classes: exosomes, microvesicles, and apoptotic bodies. Apoptotic bodies are the larger class in size, ranging from 1-5 μm and, as the name implies, are shed by dying cells in their natural blebbing process of disintegration. Microvesicles are intermediate in size, ranging from 100 nm to 1 μm, originating directly from the cell membrane through outwards shedding and can be also called ectosomes. Exosomes, are smaller than 200 nm, arise from MVBs, are a product of endosome processing and are carried to the cell membrane and released in a similar process to exocytosis [32]. In more detail, an exosome is the name given to an Intraluminal Vesicle (ILV) upon its release from the MVBs (late endosome) into the extracellular compartment [32, 53]. ILVs are formed through accumulation lipid raft-mediated mechanisms in the endosome membrane, aided by the Endosomal Sorting Complexes Required for Transport (ESCRT), both mechanisms that mediate membrane invagination and cargo loading into ILVs [53, 54]. Generally, MVBs can follow one of two paths: *i)* they can merge with a lysosome and be degraded, or *ii)* they can be transported to the plasma membrane in a process that involves cytoskeletal interaction mediated by the Rab family of small GTPases such as Rab27 [55], Rab35 [56], Rab11 [57] and Rab7 [58].

This is supported by the observations that different cells can hold different types of MVBs at the same time [59]. The secretion pathway of endosomes/MVBs is also controlled by the referred small GTPases [56, 57], with Rab27a and Rab27b isoforms playing a crucial role in exosome secretion. Rab27a silencing markedly increases MVB size near the plasma membrane and Rab27b silencing leads to intracellular MVB accumulation in the perinuclear region, both of the mechanisms hindering exosome secretion [55]. Rab11 and Rab35 are GTPases of the early endocytic pathway [60] that participate in exosome secretion through interaction with myosin Va [61], or by mediating docking to the plasma membrane [56]. Furthermore, Rab7 is capable of mediating transport of MVBs in the late endosomal trafficking system through interaction with the microtubule-dynein axis of transport [62]. Lastly, the exocytosis is complete through interaction with the SNARE (Soluble N-ethylmaleimide-sensitive fusion Attachment Protein Receptor) complexes, which mediate membrane fusion of the MVB with the plasma membrane [54].

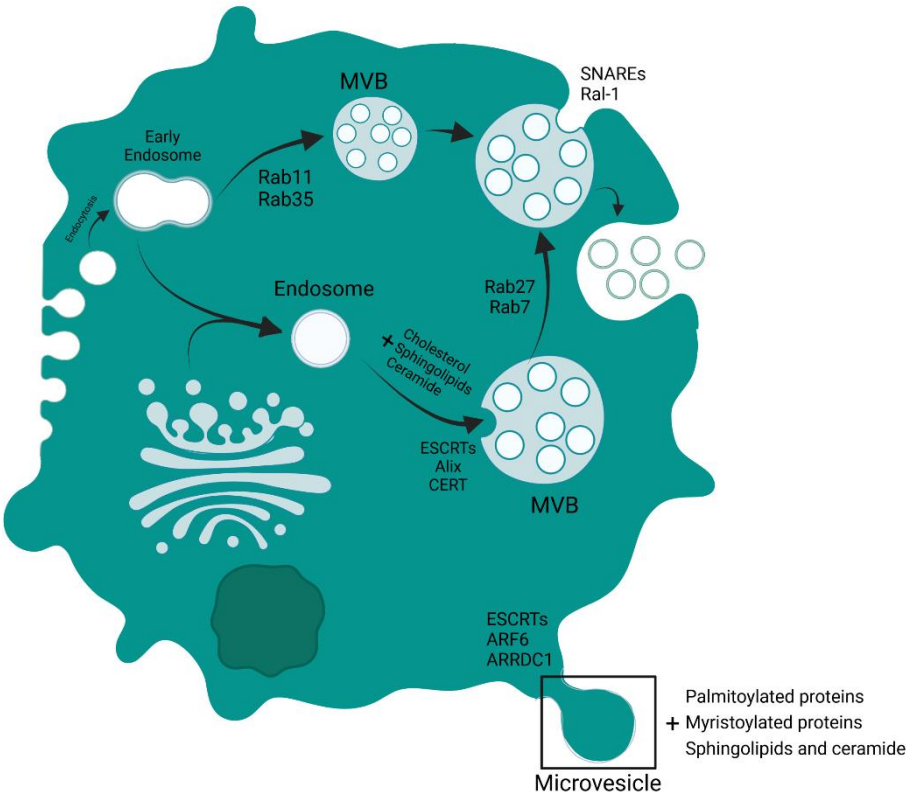

Figure 6 | EV biogenesis, a schematic summary. Early in the endosome maturation process, Rab11 and Rab35 mediate exosome release. With maturation, endosomes become enriched in cholesterol, sphingolipids and ceramide, which, with aid of the ESCRT machinery, leads to the genesis of ILVs. Rab27A, Rab27B and Rab7 mediate MVB transport towards the plasma membrane, where SNAREs and Ral-1 mediate membrane fusion and exosome release. Microvesicles originate directly from the plasma membrane, with ESCRT machinery intervention aided by ARF6 and ARRDC1. Microvesicles usually contain membrane-addressed proteins, and are also enriched in sphingolipids and ceramides. Original scheme created with BioRender.

In summary, the mechanisms by which ILVs are formed, transported, and released to the extracellular space are complementary leading to difficulties in completely inhibiting exosome release when manipulating these secretory pathways. This intricate system is illustrated in **Figure 6**.

1.2.2. Uptake

EVs carry surface proteins liable to recognise or be recognised by target cells and thus, may trigger signalling receptors directly upon cell-vesicle interaction [54, 63]. EVs may also be internalised via endocytosis or phagocytosis, or even fuse to the plasma membrane of the recipient cell, releasing its contents directly to the cytosol [64]. The fusion of the EV membrane to the recipient plasma membrane likely occurs through a similar mechanism to that of MVB to plasma membrane fusion, being mediated by SNARE complexes and Rab proteins. It is also likely that tetraspanin domains from EVs participate in EV-cell membrane fusion through the recognition of integrins in the target cell [65]. The incorporation of EVs may follow multiple mechanisms at the same time, therefore inhibiting endocytosis or inhibiting membrane fusion alone doesn't fully prevent EV content delivery to the recipient cell [66]. While further understanding of membrane fusion is still needed, mechanisms of EV internalisation via endocytosis have been more thoroughly explored. These can be clathrin or caveolin mediated, lipid raft assisted, phagocytosed or internalised through macropinocytosis [67]. In fact, Horibe *et al.* [68] showed that different colon cancer cells can prioritise different EVs uptake mechanisms, through inhibition of caveolin, clathrin, or both. This illustrates the redundancy of the different EV uptake mechanisms, since different cell lines internalised EVs differently. Furthermore, Escrevente *et al.* [69] demonstrated that treating EVs with proteinase K partially inhibits EV integration in the target cells and that certain glycoproteins on the EV surface mediate EV-target cell interaction. In conclusion, EV uptake is mediated by various, redundant mechanisms employed by the target cells, ultimately leading to the release of their cargo into the recipient cytosol.

1.2.3. EVs and the *hallmarks of cancer*

(Review in preparation)

In the year 2000, Hanahan and Weinberg published an influential review titled "The hallmarks of cancer" [70]. In this publication, the authors described six capabilities that malignant cells acquire during their multi-step progression into becoming cancerous, namely: i) neoplastic cells become neoplastic through **sustained proliferative signalling**, while ii) **evading growth suppression** and iii) **enabling replicative immortality**, and the neoplasia progresses because these cells iv) acquire **invasion and metastatic**

capabilities, v) generate **angiogenic signals** to sustain themselves, and vi) **resist cell death** by a variety of mechanisms that include acquired drug resistance [71]. In an updated version, in 2011, two hallmarks were added to the original six, and two "enabling characteristics". Added to these original hallmarks: neoplastic cells are capable of vii) **avoiding the action of the immune system** and commonly present a viii) **deregulated metabolism** [72]**.** Still, individually, these hallmarks are insufficient to fully describe the mechanism of tumour development, and even taken all together, fail to fully describe the complexity of cancer development. Mechanisms such as cell dedifferentiation, epigenetic regulation, influence of the microbiota, and induction of senescence within the microenvironment are not contemplated within the hallmarks, but are known mediators of cancer progression [73]. These eight common traits are enabled by the genetic instability of cancer cells and general inflammation of the tumour microenvironment [72, 73].

EVs, extensively studied in the past 15 years, are known to have a relevant role in the referred hallmarks of cancer. They have been described as carriers of signals to evade cell death, either by aiding in the suppression of apoptotic signals or by transferring drug resistance traits from cell to cell. Soldevilla and colleagues, working on the TAp73 protein family (a tumour suppressor gene, TP73), showed that a truncated version of this protein (ΔNp73), increased drug resistance and cell survival in colorectal tumours, through inhibition of p53 and p73, thereby aiding cells to escape cell death [74, 75]. Studying this truncated protein, their group found that CRC cells secrete exosomes enriched in ΔNp73 protein and mRNA, and that these exosomes are incorporated in target cells, stimulating cell survival and tumour growth in xenograft mice models [76]. To evade therapy effects, cancer cells evolved different mechanisms, as the overexpression of drug efflux pumps that remove chemotherapeutic agents from the intracellular space [77], leading to multi-drug resistance. This selective advantage can be transferred through EVs to more sensitive cells [78], as reported for the transmembrane protein of the ATP-binding cassette P-gp that exports a variety of amphipathic drugs in an energy dependent manner [77, 79, 80]. This protein has been shown to be enriched in EVs secreted from several cancer cell lines, being transferred to cells more susceptible to drugs, P-gp will confer its recipient cells drug resistance. This has been seen in a neuroblastoma cell line both *in vitro* and *in vivo* [81], in *in vitro* co-cultures with a breast cancer cell line [82], and in a leukaemia cell line [83].

Drug resistance associated to metabolic dysregulation can also be mediated by EVs. This is achieved through horizontal transfer of many effectors of metabolic reprogramming within EVs, for example the horizontal transfer of glucose receptor GLUT1, which seems to be enriched in mutant KRAS-derived exosomes and delivered to $KRAS^{wt}$ [84]. Another study by Lopes-Rodrigues *et al.*, on which multi-drug resistant cells exhibited increased glycolytic activity, reported that EVs from lung cancer and chronic leukaemia cells induced an

increase in metabolic activity in their non-resistant counterparts [85]. Alternatively, drug resistance may be mediated by metabolic detoxifying pathways. These can also be horizontally transferred within EVs. Specifically, it was reported that EVs derived from adriamycin-resistant breast cancer cells were enriched in gluthatione S-transferase P1 both on the protein and mRNA levels, and the drug resistance and expression levels were both transferred from drug-resistant to drug-sensitive cells via EV delivery [86].

Apart from drug resistance, EVs were also implicated in replicative immortality. Recently, it has been shown that mRNA encoding the human telomerase reverse transcriptase (hTERT) protein, released from various cancer cell lines, is enclosed in EVs that are capable of inducing hTERT activity in fibroblasts with no prior hTERT expression [87].

EVs, in particular cancer-derived exosomes, carrying micro RNAs (miRNAs), are also capable of inducing endothelial growth and increase vessel permeability by affecting a multiplicity of metabolic pathways related to endothelial cell proliferation, as observed in several types of tumours [88-92], thereby participating in angiogenesis. In a study published in 2018, using a variety of colon cancer cell lines, Zeng *et al.* investigated whether exosomal miR-25-3p could have an influence in angiogenesis. Using the CRC cell line SW480, transfected with miR-25-3p, they demonstrated that transfected cells secreted more miR-25-3p than controls [93]. These enriched exosomes were then utilised to treat human endothelial cells and were shown to affect blood vessel permeability and angiogenesis positively. The mechanism by which miR-25-3p acts in endothelial cells was proven to be associated with the silencing of two Kruppel-like transcription factors KLF2 and KLF4, that inhibit angiogenesis and dampen vessel permeability, respectively [93-95]. Another study, by Huang and Feng, explored the role of hypoxia in the exosome content and the effects that arise from these hypoxic exosomes in endothelial cells. By treating endothelial cells with colon cancer-derived exosomes, isolated from control and hypoxic conditions, they demonstrated that exosomes originating from hypoxic cells induced more proliferation and migration in endothelial cells. These exosomes contained higher amounts of a Wnt-family mRNA, Wnt4, which led to a higher level of translocation of β-catenin into the nucleus, ultimately leading to higher growth of xenograft tumours *in vivo* [96].

Perhaps the most broadly studied effect of EVs in the hallmarks of cancer is that of influencing invasion and metastasis, specifically through the establishment of a pre-metastatic niche in several cancers. Very recently, using EVs isolated from three different lung cancer cell lines, Hasan and colleagues saw that these isolated EVs were taken up by normal lung epithelial cells, affecting their epithelial barrier function by inducing a reduction in the expression of E-cadherin and ZO-1, and increasing the invasion ability of recipient tumour cells [97]. Similarly, invasive breast cancer cells are known to secrete EVs capable of inducing motility and invasion of less aggressive cells and also affect EMT (Epithelial to

Mesenchymal Transition) gene expression [98]. In CRC, EVs secreted from patient-derived cancer associated fibroblasts were proven to deliver miR-92a-3p to colon cancer cells, enhancing stemness and EMT, as well as increasing therapy resistance [99]. In addition, colon cancer-derived EVs also carry miR-181a-5p which activates the inflammatory pathway of IL-6/STAT3 in hepatic stellate cells (HSCs), in a positive feedback loop that has been proposed to be a driver of liver metastasis in CRC [100].

Another report showing that colon-derived EVs hold a tropism towards the liver, demonstrated that colon cancer-derived EVs by carrying miR-21 and increasing the secretion of the pleiotropic cytokine IL-6, promote a pro-inflammatory phenotype of liver resident macrophages (Kuppfer cells) [101]. The increase of IL-6, and also of IL-8, in the liver microenvironment, is achieved by activating HSCs through the NF-κB pathway, in a process that is mediated, once again, by colon cancer-derived EVs, rich in integrin beta-like 1 [102]. The modulation of the immunological properties by EVs is directly associated with immune escape mechanisms, for example the activation of immune suppressive cells, such as T regulatory cells (Treg) or myeloid derived suppressor cells (MDSCs), inhibition of effector cells such as T $CD4^+$ or and cytotoxic T $CD8^+$ and Natural Killer (NK) cells, or polarisation of macrophages towards an immune suppressive, tumour supportive phenotype [63, 103-112]. MDSC expansion in the tumour context has for long been observed, and their infiltration in the tumour is associated with worse prognosis [113]. Their expansion, activation, and infiltration are promoted by tumour cells through the secretion of soluble factors and of EVs containing for example Prostaglandin E2, TGF-β. The latter have been described to activate secretion of IL-6, Cox2, and VEGF from MDSCs in a murine model of breast cancer [105]. Hsp72, is also found in the cargo of cancer cell-derived EVs and was reported to promote the activation of STAT3 in colon cancer and other tumour models [104]. The activation of MDSCs may also be triggered by miRNAs contained in tumour-derived EVs, as exemplified by miR-107 which seems to mediate the expansion of myeloid cells through the activation of PTEN and DICER1 in a gastric cancer mouse model [103]. Tumour-derived EVs in comparison with normal EVs, have also been shown to have a positive effect in Treg function through their TGF-β and IL-10 contents. Such cytokines interact with Tregs through surface receptors and increase their FasL, TGF-β, IL-10, CTLA-4, granzyme, and perforin expression [106, 108]. This was reported for colon cancer-derived EVs which have TGF-β in their cargo, holding the capacity to upregulate Treg associated genes [107]. Additionally, PD-L1 has been found in multiple tumour-derived EVs, in different cancer models, which allows tumour cells to inhibit T effector cell function from a distance [114-120], mediating immune escape and hinting for its use as a circulating biomarker for immunotherapy allocation [120].

Finally, tumour-derived EVs can play a role in macrophage polarisation. The plasticity of these immune cells allows tumour cells to “hijack” their function, directing them towards a tumour-associated macrophage phenotype that help disease progression [121]. Once again, tumour-derived EVs participate in this hijacking process through the delivery of a variety of contents. miRNAs such as miR-145 and miR-203 derived from CRC EVs drive macrophage polarisation to an anti-inflammatory phenotype [109, 110]. Furthermore, long non-coding RNAs with the same origin also help in the process of anti-inflammatory phenotype acquisition by macrophages [112].

1.2.4. EVs and radiotherapy

More recently, radiobiology and EV studies in the context of cancer have emerged. The knowledge that EVs can aid in apoptosis escape, cancer cell proliferation, and EMT hints towards their role in mediating therapy resistance, which includes radiotherapy. Furthermore, both EVs and radiation therapy have a role in immune modulating and in systemic cancer control: while EVs can generally be immune suppressive and promote metastasis, radiotherapy contribute to immune reactivation and induces abscopal effects, in which non-irradiated distant tumour metastasis may still react to irradiation and regress [122].

Interestingly, recent insights point towards a role of EVs in radiotherapy-mediated abscopal effects. In a recent study with cervical cancer patient samples, macrophage infiltration in the primary tumour increased upon irradiation, with a concomitant shift from the anti-inflammatory to the pro-inflammatory phenotype. This shift in phenotype was mediated by cervical cancer EVs isolated from the plasma of irradiated patients, but not of non-irradiated patients [123]. This macrophage activation was also observed in a mixed colon and RC model, where the authors observed the same phenotypic shift in the tumour infiltrating macrophages upon irradiation, which was mediated by irradiated cell-derived EVs [124]. Other immune cells, $CD4^+$ and $CD8^+$, were activated by irradiated-cell EVs in a murine breast cancer model. In this study, the authors isolated EVs from 2D cell cultures, controls and irradiated, and injected such EVs on mice, 25 days before inoculating tumour cells. Mice treated with EVs from irradiated cells presented exacerbated immune responses with increased infiltration of T lymphocytes, reduced tumour burden and increased survival [125]. Interestingly, experiments using irradiated mouse fibroblast-derived EVs showed that such vesicles hold the capacity to inhibit colony formation of non-irradiated cells, while promoting oxidative stress, in a miR-34c mediated mechanism [126].

1.3. Biomimetic *in vitro* model - The 3D multicellular spheroid

Translational capability between *in vitro* drug screenings and actual clinical application is very difficult. It is estimated that only 5-10% of anticancer drugs find some success in reaching patients [127, 128]. Enhancement of this percentage would greatly improve the cost-effectiveness of translational research, which is why an effort must be made to better recapitulate tumours in *in vitro* models. Such models should especially consider the different features of the tumour microenvironment. This has been the reasoning for usage of 3D multicellular spheroids.

Hardly a new concept, multicellular spheroids "suffer" from being too versatile: these can be cultured in bulk, or in a single spheroid per well; they can include extracellular matrix; they may include different cellular populations or a single population; and the experiments outcome can be varied. This versatility has led to under reporting in the field, which makes reproducibility almost impossible [129]. Nevertheless, spheroids provide many advantages when compared to 2D conventional cell cultures. An immediate difference between spheroids and 2D cultures is physical. By assembling cells in 3D, in a compact manner, cells in the inner layers of the spheroid will immediately be restricted when it comes to nutrient and oxygen access, when compared to the outer layers [130]. This is already an advantage because it better mimics what happens *in vivo*, in solid tumours, where they outgrow their blood vessels and do not generate enough new vascular structures to support their growth, leading to the formation of an acidic, necrotic, and hypoxic region [131].

Likewise, the core of a sufficiently large multicellular spheroid will have such characteristics [130]. Hypoxia on the spheroids core will drive cells towards anaerobic respiration, through stabilisation of HIF-Iα and consequent expression of glycolytic enzymes, in what is termed the Warburg effect, as it occurs in solid tumours but not in 2D cell cultures [132].

Additionally, in a spheroid, cells don't have a forced basal-apical asymmetry as it happens in 2D cultures [133], which leads to a more biomimetic behaviour due to different DNA condensation in the nuclei and consequently more trustworthy RNA, protein, and even miRNA expression [134-136]. Also, spheroids don't have to be made of a single type of cells, and are a platform that promotes (and increases) direct cell-cell contact between cancer cells, and microenvironment important players such as tumour-associated macrophages, T cells, fibroblasts or endothelial cells, in multiple combinations depending on the goal of the study. This allows researchers to investigate how these tumour microenvironment players affect cancer cell survival in hostile environments such as the application of chemotherapeutic agents, radiation therapy or immunotherapy [130]. For example, Djordjevic and Lange tested how the presence of normal fibroblasts affected HeLa

cell radiosensitivity, and that previously irradiated fibroblasts were capable of sensitising cancer cells by direct contact [137]. Additionally, when it comes to radiobiology studies, it has been shown that DNA will have different sensitivity to radiotherapy induced damage in 2D and 3D cultures, because of different chromatin condensation states [138]. Moreover, many 3D cell cultures will include a more developed extracellular matrix, which has been proven to increase survival and proliferative signalling in cancer cells [139]. In summary, 3D models, particularly spheroids, are reliable, biomimetic, and suitable models for oncology research conveying improved and more translation results (**Figure 7**).

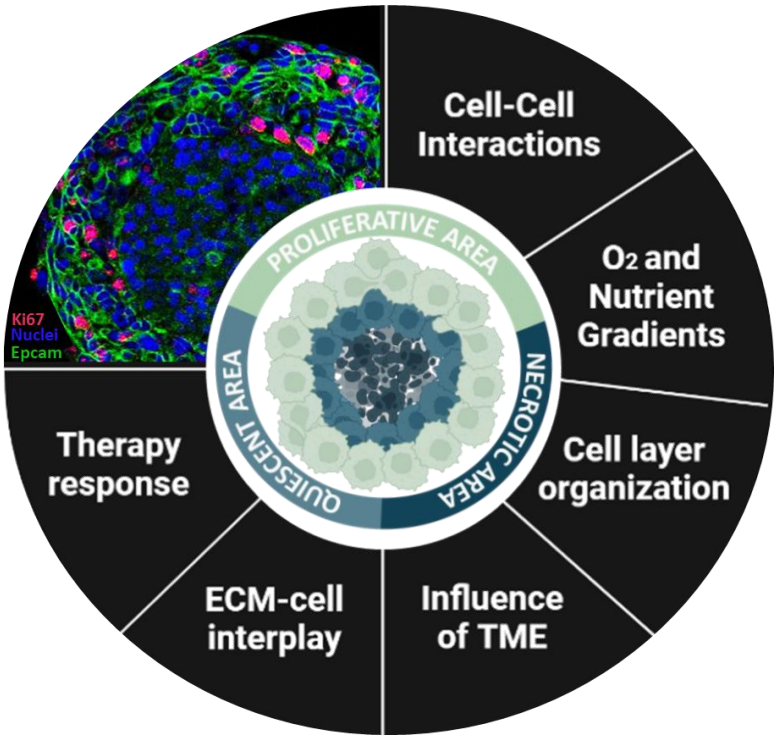

Figure 7 | The advantages of 3D cultures versus 2D cultures and schematic spheroid representations.

2. Aims

Rectal cancer local recurrence rates after curative resection can still rise above 30% [140] even with the usage of radiotherapy, with variable response rates for similar patients. This poses an important problem for RC management since the uncertainty regarding radiotherapy effectiveness is impossible to predict. Therefore, it is essential to identify novel predictive factors to therapy response, to better allocate patients to effective treatment. Moreover, it is imperative to uncover the radioresistance mechanisms that sustain cancer cell survival to develop upgraded combinatory therapies that could improve patient overall survival.

With this in mind, we set out to study the relatively unexplored world of rectal cancer secretome, specifically its relationship with radioresistance. Our major aim was to study EV secretion in response to irradiation by resorting to a novel multicellular spheroid model that better mimics tumour features. To achieve our main goal, the specific aims were:

1. To develop and characterise a biomimetic multicellular RC spheroid model. This will also contribute to the open database MISpheroID, created by our collaborators at Ghent University that aims to improve transparency of reporting and reproducibility within the 3D *in vitro* model's field;
2. To implement a protocol for the recovery of EVs from 3D RC spheroids. This includes optimisation of the quality and quantity of EVs collected according to ISEV guidelines;
3. To study the EV contents regarding protein and miRNAs in the search for novel biomarkers of radioresistance and response to therapy.

3. Materials and methods

3.1. Cell subculturing

Spheroids were assembled with SW837 cells, an epithelial RC cell line, kindly provided by Dr. K. Haigis (Boston, USA). Subculturing methodology used was based on ATCC guidelines. Briefly, cells were kept in cryovials at -80ºC in a maximum concentration of $5x10^6$ cells/mL until needed. Then, quick thawing at 37ºC degrees was applied, and cell suspension was transferred to a 15 mL tube, on which 9 mL of culture medium, DMEM/F-12 supplemented with 10% heat-inactivated foetal bovine serum (FBS) and 1% penicillin/streptomycin (Pen/Strep), were added drop by drop. This cell suspension was centrifuged at 300 *x g* for 5 minutes at room temperature (RT), the supernatant was discarded, cells were ressuspended in 5 mL of culture medium and kept in a vented flask at 37ºC with 5% CO_2. These cultures grew until approximately 70% confluence before being subcultured. The latter was performed by removing the culture media from the flask, washing with an appropriate volume of PBS, and then adding the required volume of trypsin (2 mL/T75 flask). Incubation with trypsin lasted 5 minutes at 37ºC, and then inactivation occurred by adding culture medium in 3-4x the volume of trypsin in the flask. The cell suspension was transferred to a Falcon tube and centrifuged at 300 *x g* for 5 minutes at RT. Supernatant was discarded and cells resuspended in culture medium, which was then passed to a new tissue culture flask according to the desired dilution. At the third passage after a thawing process, some of the cells were collected to be stored at -80ºC degrees to guarantee a SW837 stock. For that, cells were counted and resuspended into a $5x10^6$ cells/mL concentration in freezing medium (50% culture medium, 40% FBS and 10% DMSO), and then transferred to cryovials in 1mL aliquots. These cryovials were placed in liquid nitrogen where they can be kept for long periods.

3.2. Spheroid assembly method

3.2.1. Agarose gel matrix formation

The spheroid support was performed in an agarose matrix with 81 micro-wells of approximately 800 μm in diameter. In order to establish this agarose support, Sigma Aldrich MicroTissues 3D Petri Dishes® moulds were used.

A 0,9% NaCl (weight/volume) solution and the desired weight of agarose were autoclaved before dissolution into a final concentration of 2%. Usually, 5g of agarose were added to 250 mL of NaCl (in sterile conditions) solution and dissolved by heating. The agarose solution was taken to a laminar flow chamber, where the spheroid agarose matrix was

prepared as follows: 550 µl of agarose solution was carefully but swiftly pipetted in a corner of the autoclaved 3D Petri Dish® mold to form the negative microchip. After drying, these microchips were passed to each well of a 12 well plate and observed under the microscope, to check if bubbles caused by flawed pipetting affected the integrity of the wells. After that, 2 mL of culture media were added to the wells to equilibrate the agarose micro-molds for at least 2 hours or overnight at 37ºC.

3.2.2. Cell seeding

SW837 cells lines were cultured in T75 flasks until they reached approximately 70% confluence.

Then they were collected and a very small fraction (20 µL) of cells was taken and mixed with Trypan Blue, in a 1:2 dilution, placed in a Neubauer chamber, and counted. After counting, viable cell number in the suspension was determined, and the procedure was followed according to the conditions to be assessed. Briefly, if the conditions of the experiment determined that spheroids should have 10.000 SW837 cells, an 81-well chip should contain 810.000 cells in total, which were to be suspended in 190 µL of culture medium. To do so, after counting, cells were centrifuged at 300 *x g* for 5 minutes at RT, media was discarded, and cells were resuspended according to the experimental needs. After that, 190µL of the cell suspension was added to each agarose microchip. Cells were then left to settle into the wells for 30 minutes at 37ºC. Finally, 2mL of culture medium were added to each 12-well plate well, outside the seeded micro-mould, and the forming spheroids were incubated in 37ºC, 5% CO_2, for 8 days. Of note, three cell culture media were used to assemble RC spheroids, DMEM/F-12, RPMI 1640, and DMEM low glucose (1g/L of glucose), all supplemented with 10% heat-inactivated FBS and 1% Pen/Strep.

3.3. Computational spheroid measurement

To perform morphological measurements, pictures were taken at established time points, and measurements were attained using the program AnaSP. We did so based on methodology proposed by our collaborators from Ghent University, published in 2021, regarding the standardisation of spheroid-related methodologies {Peirsman, 2021 #51}. For that, 8 to 10 micrographs were taken per condition, in a Leica optical microscope using a 10x magnification. The measurements were returned in pixels and converted to micrometres upon checking the conversion rate of the DCC camera and magnification that was used. This conversion was done with the aid of ImageJ and an empty Neubauer chamber. Each pixel was equivalent to approximately 0,5 µm when observing spheroids in the 10x objective lens. Using AnaSP data analysis spheroid size, compactness, and

circularity were obtained.

3.4 Histology and immunofluorescence assay

Haematoxylin and Eosin (HE) staining was performed at the i3S Histology core facility after spheroid fixation in formalin. In short, culture medium was removed from the outside and the inside of the agarose microchip and the spheroids were washed once with PBS. Pipetting inside the agarose support was always done slowly and in the same corner, in order to avoid spheroid loss during the process. In the fume hood PBS was pipetted out and replaced by formalin, both on the inside and the outside of the agarose support. These were incubated overnight at RT. The next day, formalin was removed, and 1,5% agarose solution was added on top of the micro-mould to enclose the spheroids. The moulds were then embedded in paraffin, sliced with a microtome (3μm slices), and set onto glass slides. The spheroid sections were then deparaffinised and rehydrated by a graded series of xylene and ethanol solutions and stained with haematoxylin followed by eosin. After staining, dehydration was performed and slides were observed under the Light microscope Olympus coupled with a DP 25 Camera and the Software Cell B.

Slides were also allocated for immunofluorescent detection of EpCAM, Ki67 and phosphorylated γ-H2AX. For that, deparaffinisation and rehydration were performed followed by antigen retrieval achieved with citric acid incubation at 96ºC for 30 minutes. Permeabilisation was done with 0.05% Tween-20 detergent in PBS for 20 minutes at RT. For blocking non-specific interactions, BSA 1% and FBS 10% in PBS were used for 60 minutes at RT. Blocking solution was then used to dilute the primary antibodies, which were incubated over-night at 4ºC. For EpCAM detection, direct immunofluorescence was performed using AlexaFluor® 488 anti-EpCAM rabbit recombinant monoclonal antibody from Abcam (Ab237395). For Ki67, same methodology was employed using recombinant AlexaFluor® 647 conjugated anti-Ki67 rabbit monoclonal antibody (Ab196907), also from Abcam. These were both used in 1:100 dilutions. For phosphorylated γ-H2AX, indirect immunofluorescence was performed. Primary antibody incubation was achieved over-night at 4ºC with Phospho-Histone H2A.X (Ser139) (20E3) rabbit monoclonal antibody (9718s, Cell Signalling) in 1:500 dilution followed by secondary anti-rabbit antibody conjugated with AlexaFluor® 488 incubation, at RT for 1 hour in a 1:500 dilution. After washing, DAPI counterstain was employed by incubating the sections 15 minutes at RT. Observation and image capture was performed in a Leica Laser scanning confocal microscope SP5II.

3.5. Cell viability assays - propidium iodide and calcein staining

To assess the distribution of dead and metabolically active cells within RC spheroids, 8-day culture spheroids were used. For that, multiple spheroids from each condition were collected, washed once with PBS, and then incubated for 45 minutes, at RT and with agitation, with 200 µL of a staining solution that contained 1 µM of calcein and 4 µg/mL of propidium iodide (PI). Then, spheroids were washed twice with PBS and transferred to a glass-bottom 96-well plate. Visualisation was performed in the fluorescence microscope INCELL Analyzer 2000. Quantification of the PI signal was performed using ImageJ software.

3.6. Metabolism assays - ATP level measurements

To assess the metabolic activity of SW837 spheroids, the CellTiter-Glo® 3D Cell Viability Assay was used, according to manufacturers' protocol. Briefly, three spheroids were collected from the agarose micro-mould at each experimental endpoint and transferred onto opaque walled 96-well plates to a final volume of 100 µL of culture medium. The same volume of Cell Titer Glo 3D reagent was added to the wells, and the contents of the well plate were mixed with the assistance of a shaker for 5 minutes, at RT. Then, the samples underwent an additional 25 minutes of incubation at RT, covered from light. Luminescence was then recorded with the aid of Biotek's Synergy MX Multiplate Reader, with an integration time of 1 second per well.

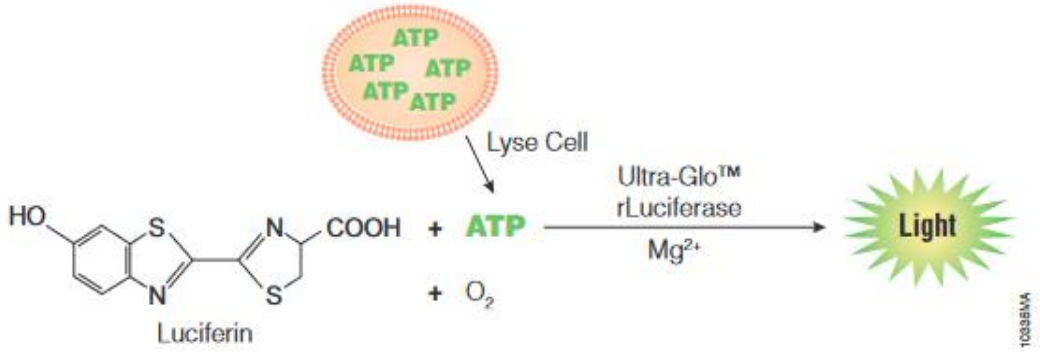

Figure 8 | CellTiter-Glo Luciferase reaction

Adapted from the manufacturer's protocol sheet found, in October 2022 (last accessed), at https://worldwide.promega.com/products/cell-health-assays/cell-viability-and-cytotoxicity-

3.7. Spheroid-applied radiotherapy

In collaboration with the Medical Physics department of IPO – Porto, spheroids were submitted to ionising radiation mimicking the RC patient short-scheme radiotherapy treatment: 5Gy during 5 consecutive days. For that, after cell seeding on the agarose microchips, spheroids were left to assemble and compact for three days. At day 4, the 12-well plates containing spheroids were submitted to radiation therapy and kept at 37ºC with 5% CO_2. Culture media was changed only after the last irradiation dose. Twenty-four hours after the last dose (at the ninth day), spheroids were allocated for CellTiter-Glo 3D viability assay, HE and immunofluorescence staining, and culture media was collected for EV studies.

3.8. Extracellular vesicle isolation

EV isolation was performed from the culture media of 9-day cultures, controls and irradiated RC spheroids. This protocol was performed according to the expertise learned at the LECR, led by professor Olivier de Wever and Dr. An Hendrix, in Ghent. In these cultures, RPMI 1640 was supplemented with 1% Pen/Strep and 10% heat-inactivated FBS previously **ultracentrifuged** for 18 hours, at 100.000 x *g* and 4ºC, in order to deplete bovine EV contents (EV-depleted FBS). Moreover, for the last 24 hours of culture, the spheroid media was replaced with media containing only 0,5% (volume/volume) of EV-depleted FBS. The culture media was then collected from the 12-well plates and pooled onto control or irradiated samples. In each experiment, four 12-well plates, containing secretions from almost 40 million cells, were used, resulting in over 100 mL collected media for each condition, as this methodology is already established at LECR. The collected volume was then reduced and concentrated to 1mL samples using Centricon® Plus-70 centrifugal filters with a nominal cut-off of 10 kDa. Centrifugation was performed at 3200 x *g* at 4ºC, for as long as necessary to obtain a 1mL sample (usually, two 30-minute centrifugations per sample were required). This 1mL sample was kept at -80ºC until the ultracentrifugation protocol was executed. Next, an Optiprep™ Density Gradient (ODG) was applied as exemplified in Figure 9. This was achieved by diluting the stock solution of ODG to a 60% iodixanol solution in Tris-HCl buffer with 0,25M of sucrose, as previously described in works from LECR [141, 142], followed by different density solution preparation namely, 5%, 10%, 20% and 40% iodixanol solutions. These were then placed in 17 mL Beckman Coulter open-top polypropylene tubes for ultracentrifugation as follows, 4 mL of 40% iodixanol solution, 4 mL of 20% iodixanol solution, 4 mL of 10% iodixanol solution, and at the top 3.5 mL of 5% iodixanol solution. With the discontinuous gradient established, 1 mL of concentrated culture media was placed on top. The tubes were then centrifuged for 18 hours at 100.000 x *g* at 4ºC. Fractions of 1 mL were collected and pooled, knowing that the fractions of interest

were between the 7th and 10th millilitres – see Quality Control of EV isolates results and discussion for reasoning. These 4 mL of interest then underwent Size Exclusion Chromatography (SEC) in a 10 cm tall Sepharose CL-2b columns. The EV fraction eluted right after the void volume, in the 4th to 7th millilitres of eluate were collected, pooled, and concentrated using centrifugal filters Amicon® Ultra - 2 mL, with a nominal cut-off of 10 kDa, until the final volume was 100 µL. This concentration was performed in a table top centrifuge, at 4ºC and 3200 x *g*. The collected 100 µL constituted the final EV isolate, and were allocated to several analyses according to the experiments objectives.

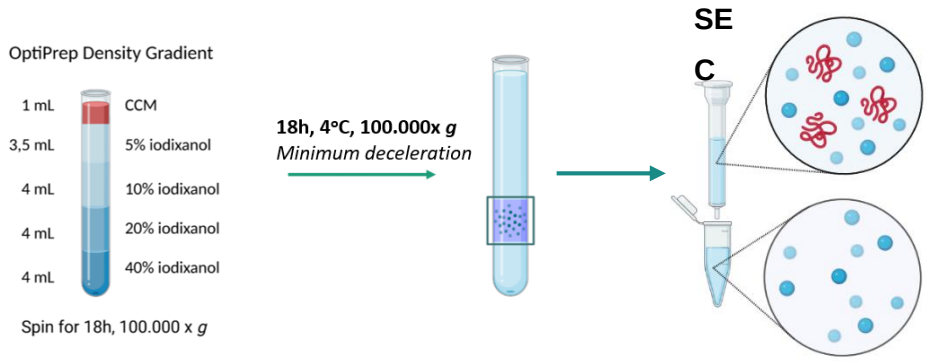

Figure 9 | EV isolation simplified protocol. The 7th to 10th millilitres are collected from the ultracentrifugation final suspension. The 4th to 7th eluates are collected from SEC as the EV containing eluates. The scheme is preceded by culture media concentration and followed by EV isolate concentration using centrifugal filters. Figure made with the help of BioRender.

3.9. Spheroid-applied transmission electron microscopy

In order to observe spheroid organelles in detail, specifically the presence of MVBs and shedding of microvesicles, a standard electron microscopy protocol with more contrast was used.

For ultrastructure analysis, spheroids were fixed in a solution of 2.5% glutaraldehyde with 2% formaldehyde in 0.1 M sodium cacodylate buffer (pH 7.4) for 1 day at RT. Spheroids were then incubated in 1% osmium tetroxide and 1.5% potassium ferrocyanide in 0.1 M cacodylate buffer for 1 hour. After centrifugation, the pellet was stained with aqueous 1% uranyl acetated solution overnight, dehydrated, and embedded in Embed-812 resin. Ultra-thin sections (50 nm thickness) were cut on a RMC Ultramicrotome using Diatome diamond knifes, mounted on mesh copper grids, and stained with uranyl acetate substitute and lead citrate for 5 minutes each. Samples were viewed on a JEOL JEM 1400 transmission electron microscope and images were digitally recorded using a CCD digital camera Orius 1100W. The transmission electronic microscopy (TEM) was performed at the HEMS core facility at i3S, University of Porto, Portugal with the assistance of Ana Rita Malheiro and Rui

Fernandes.

3.10. Extracellular vesicle quality control and analysis

As per the guidelines proposed by the International Society for Extracellular Vesicles, three different techniques were utilised to assess the efficacy and quality of the EV isolation: Western Blotting, Nanoparticle Tracking Analysis (NTA) and TEM.

3.10.1. Nanoparticle tracking analysis

NTA allows us to check the approximate concentration of particles in the EV isolate, which, together with other techniques, we can infer are EVs. To do so, we diluted a fraction of the EV isolate in filtered PBS to a dilution factor of 1:500 and made use of the NanoSight LM10 microscope (in Ghent) or the NanoSight NS300 (in Porto), equipped with a 405nm laser. Three videos of 30s each were recorded for each analysis, and if the EV concentration landed in between $3x10^8$ and $1x10^9$, it was considered satisfactory – concentrations outside this window are not accurately measured by this methodology and therefore the dilution factor had to be adjusted accordingly.

3.10.2. Western blotting

Protein quantification was assessed at the intra- and extravesicular level. This was performed with the Bradford method-based kit from BioRad, the DC protein assay kit. Firstly, a 1:2 dilution of the EV isolates was performed in lysis buffer to expose intravesicular proteins to the kit's reagents. After, BSA standard solutions and the EV isolates were diluted in 1:45 dilution factor with the reagents from the kit, according to manufacturer's instructions. BSA standards were used in concentrations between 0 and 3 mg/mL to elaborate the calibration curve. Measurement of absorbance was done in a 750nm wavelength with the BioTek PowerWave XS plate reader.

EV lysates were obtained by incubating EV isolates in Laemmli buffer with SDS and glycerol, pre-prepared with 0.5% β-mercaptoethanol and 0.5% bromophenol solution. Protein was further denatured for 5 minutes at 96^{o}C before electrophoresis. EV lysates were then resolved on a 10% SDS polyacrylamide gel and transferred onto nitrocellulose Hybond-C membranes. After transfer the membranes were incubated in blocking solution containing 5% low fat milk or 4% BSA for phosphorylated protein detection. Primary antibodies rabbit anti-CD9 antibody (ref. D3H4P) from Cell Signalling, mouse anti-Flotilin-1 (ref. 610820) from BD BioSciences, and mouse anti-ALIX (ref. 2171 S) from Cell Signalling, diluted in the respective blocking solution at 1:1000 dilutions, were used. Primary antibodies were incubated at 4^{o}C over-night followed by washing steps. Secondary antibodies,

conjugated with horseradish peroxidase, were used in 1:4000 (anti-rabbit, NA934V, Cytiva) and 1:3000 (anti-mouse, NA931V, Cytiva) dilutions in 45 minutes incubations at RT. Additionally, a rabbit anti-Ago2 (ref. Ab32381) from Abcam was used. After horseradish peroxidase chemiluminescent reaction with a SuperSignal™ Western Blot Substrate kit, the signal was developed for variable time periods (up to 7 minutes) under the iBright CL750 chemiluminescence detector.

3.10.3. Transmission electron microscopy (TEM)

To observe the morphology of the EVs, checking their size more accurately, as well as checking for the purity of isolation, we proceeded with TEM at i3S core facility, recurring to a uranyl acetate negative staining. For negative staining, 5 µL of samples were mounted on Formvar/carbon film-coated mesh nickel grids and left standing for 1 minute. The liquid in excess was removed with filter paper, and 5 µL of 1% uranyl acetate were added onto the grids. After liquid excess removal with filter paper, visualisation was carried out on a JEOL JEM 1400 TEM at 120 kV. Images were digitally recorded using a CCD digital camera Orious 1100W. EV observation using TEM was performed with the assistance of Ana Rita Malheiro and Rui Fernandes.

3.11. Proteomic analysis of EV content

Proteomic analysis was performed at i3S Proteomics core facility with the help of Dr. Hugo Osório. The protocol described in [143] was used by the core facility operators, with minimal adaptations. Briefly, 50 µL of EV isolate per sample were treated with trypsin/LysC at 37ºC with 1000 rpm shaking over-night. Next, 500 ng of peptides were loaded into a nano-LC-MS/MS (high pressure liquid chromatography coupled to tandem mass spectrometry), which consisted of the Ultimate 3000 liquid chromatography system coupled to Q-Exactive Hybrid Quadrupole-Orbitrap mass spectrometer. The peptides were loaded onto a trapping cartridge for 3 minutes loading, after which the trap column was switched in-line to a 50 cm × 75 µm inner diameter EASY- Spray column (ES803, PepMap RSLC, C18, 2 µm, Thermo Scientific, Bremen, Germany) at 250 nL/minute. Data acquisition was controlled by Xcalibur 4.0 and Tune 2.9 software. The Eletro-spray Ionisation voltage was 1.9 kV. The raw data were processed using the Proteome Discoverer 2.5.0.400 software. Protein identification analysis was performed with the data available in the UniProt protein sequence database for the *Homo sapiens* and the *Bos Taurus* (to control for FBS contaminants), Proteome 2020_05 and a common contaminant database from MaxQuant Version 1.6.2.6. Two protein search algorithms were considered: (i) the mass spectrum library search software MSPepSearch, with the NIST human HCD Spectrum Library (1,127,970 spectra and (ii) the

Sequest HT tandem mass spectrometry peptide database search program. For determination of differentially expressed proteins between the irradiated and control groups, the following filters were applied, (1) the minimum number of samples that a protein must be detected to be used was set to 50% per experimental group, (2) the use of at least two unique peptides and the p-value adjusted using Benjamini-Hochberg correction for the False Discovery Rate set to ≤0.05, (3) the Radio/Control considered ratio was set to ≥1.50 for the selection of enriched proteins and to ≤0.5 for decreased proteins, and (4) at least 51% of samples (minimum 2 out of 3 or 2 out of 2) with protein-related peptides sequenced by MS/MS. Volcano plot analysis was performed with the Proteome Discoverer software after applying the above described filters.

3.12. Statistical analysis

Statistical analysis was performed making use of GraphPad Prism 9 software. Spheroid diameter and compactness were compared in regard to changes dependent on time, using a Mixed Effects models fitted by Prism to the data, since 2-way ANOVA cannot handle missing values, which were missing rarely and for random reasons. Multiple comparisons were run using Tukey's test and significance was considered at 5%. Within each day of culture (Row), columns' means (mean size of a given spheroid in a given culture media) were compared against each other; and within each culture condition (grouped columns), row means were compared to test the effect of days of culture on spheroid size and compactness.

PI signal quantification was performed in triplicate and the mean was used for comparison between conditions. Considering the control group of spheroids with 1000 cells, for each different culture media used, 2-way ANOVA was performed using the multiple comparisons Dunnett's test. Significance was set at 5%, so statistical differences were considered when the p-value was below 0.05.

4. Results

4.1. Multicellular rectal cancer spheroid as a biomimetic model to study tumour radioresistance

(Manuscript in preparation)

In the oncology field, research that is rectum specific is rare and often diluted or not approached in “colorectal” cancer-related studies. Furthermore, the few rectum-dedicated reports centred in *in vitro* assays rely on 2D cultures. However, the use of monolayers is rather limiting, lacking tumour features such as metabolic gradients, and holding low translational capability between *in vitro* drug screenings and actual clinical application. Therefore, to study RC in the context of radioresistance, we first developed a 3D multicellular spheroid rectal cancer model.

Spheroid morphology is affected by cell density and culture media

Part of the justification for spheroid model usage is the possibility to mimic, as close as possible, the tumor heterogeneity and complexity. Therefore, this model should contain oxygen, nutrient and pH gradients from the outside layers to the inside, forming a proliferative outer layer, quiescent intermediate region, and a necrotic core. Although varying according with the cell line, in general, spheroids with over 300 μm in diameter achieve this necrotic core formation. Therefore, we firstly attested how many cells per spheroid were necessary to achieve such dimension, and how the culture medium could affect the shape/size of the spheroid. The RC cell line SW837 was isolated from a Caucasian 53-year-old patient with stage IV adenocarcinoma of the rectum. Exhibiting an epithelial morphology, this cell line didn’t grow in a perfect monolayer, but in islands aggregates that possibly had more than one layer. Additionally, these cells are relatively small, which led us to ascertain that T75 cm^2 flasks always contained over 12 million cells when they were 70% confluent. This notion of how many cells were in a flask was important when planning the experiments, since a high number of cells was required for spheroid assembly. To develop the SW837 rectal cancer spheroid model, we started by assessing the morphological features along eight days of culture, in spheroids composed of 1.000, 2.000, 5.000, 8.000, 10.000, 15.000, or 20.000 SW837 RC cells, cultured in DMEM/F-12, RPMI 1640, or DMEM Low Glucose, and how these culture conditions would affect spheroid morphology. To do so, spheroid diameter and circularity/compactness was evaluated through brightfield photographs taken on days 1, 2, 4, and 8 of culture. All analyses were

performed with assistance of the AnaSP software.

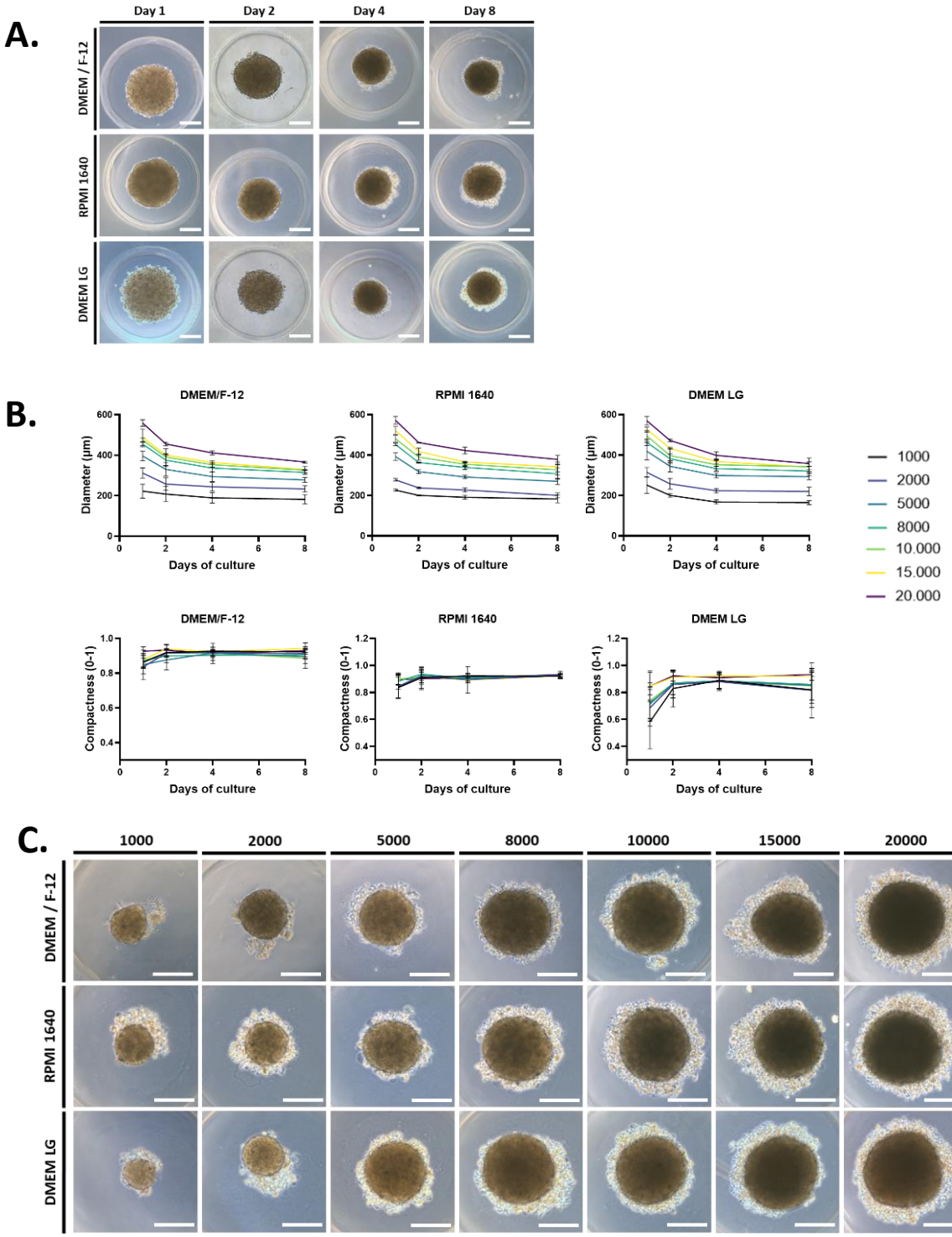

Figure 10 | SW837 spheroid brightfield microscopy images and morphological analysis.

A) Progression of 10.000 cell spheroids along 8 days of culture in DMEM/F-12, RPMI 1640, or DMEM Low Glucose (LG). Scale bar: 200 µm. B) Morphological analysis of spheroids composed of increasing cell-seeding densities, a long time. The average diameter and compactness of spheroids from 3-independent experiments ± SD, in all tested conditions, are shown. C) Brightfield micrographs of 8-day culture spheroids from all experimental conditions (from 1000 to 20.000). Scale bar 200µm. Depicted are illustrative images from 3-independent experiments.

Our data revealed that, along one week of culture, regardless of the media used, spheroids did not grow. Spheroids took 3 to 4 days to compact and then their diameter stabilised until the eighth day. Spheroids composed of 10.000, or more, SW837 RC cells maintained a size above 300 µm in diameter after compaction. Furthermore, the combination of number of cells and used culture medium tended to affect the spheroids shape. The spheroid culture in richer media DMEM/F-12 appeared to result in higher circularity on smaller spheroids. Larger spheroids also tended to acquire a more circular shape, although the compactness did not significantly vary with culture conditions, nor with time (**Figure 10** and **Supplementary Table 1**). Regarding the diameter, significant differences in size were observed mostly due to time progression, since in almost all culture conditions Day 1 spheroids presented significantly higher diameter when compared to Day 4 and Day 8 spheroids. Between different culture media, in the same cell seeding conditions, no significant differences regarding spheroid size were found (**Supplementary Table 2**).

Larger spheroids contain less ATP per cell than smaller spheroids

With the objective of measuring the ATP production within the spheroids in each condition, at the end of 8 days of culture, 2 spheroids were collected from each experimental setting (in triplicate), to undergo the CellTiter-Glo® 3D assay. This reagent works by lysing the cells and relies on luciferin molecule binding to ATP. In the presence of the commercial recombinant Luciferase, a green fluorescence signal is produced, which can be linked to more ATP molecules and, therefore, indicating the levels of metabolically active cells. CellTiter-Glo® 3D is optimised from its "2D" counterpart to specifically penetrate multicellular spheroids with higher efficacy, avoiding confounding results when assessing cell viability in spheroids. In the SW837 spheroids, our data indicated that size, but not the culture medium, affected ATP production. Also, the increase of cell-seeding numbers per spheroid impacted positively the ATP production, as expected. However, normalising the luminescence values to the number of cells in each spheroid, resulted in decreased ATP production "per cell" (**Figure 11**). This pinpoints to a decrease of ATP levels in spheroids with higher diameter. Such observation could be explained by the formation of a necrotic core in spheroids holding 10.000 SW837 cells or more, probably associated to a decrease access to nutrients and oxygen at the centre of these spheroids. Statistical differences of luminescence (ATP production) induced by different cell seeding were found, represented in **Supplementary Table 3**.

A. **B.**

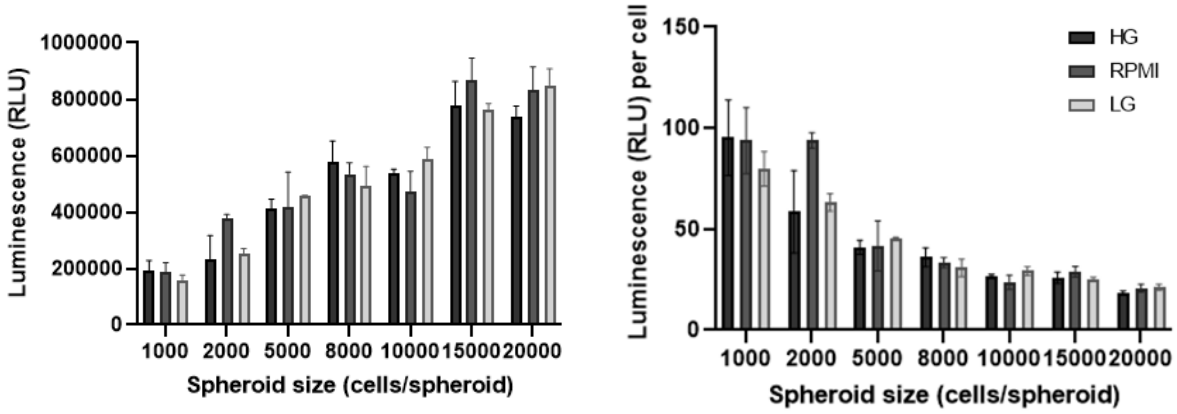

Figure 11 | Spheroid ATP production measured by luciferase assay (CellTiter-Glo ® 3D assay).

A) Shown are the ATP levels per spheroid in all culture conditions. B) Production of ATP per cell after normalisation to the number of cells per spheroid. Luminescence represented by relative light units (RLU) is illustrated. Each plot represented herein shows the average of RLU values obtained from 3-independent experiments ± SD.

Formation of a necrotic core in RC spheroids is size and culture media-dependent

To understand whether cell death was occurring in the higher diameter spheroids, we performed calcein (for live cells) and Propidium iodide (PI- for dead cell identification) stainings, in live spheroids, and quantified the intensity of the PI signal.

The cell membrane is impermeable to PI, but when it loses integrity in the event of cell death, allowing PI to bind to DNA (at the Guanine – Cytosine pairs) [144] there is emission of signal with a maximum intensity at the 617 nm wavelength. Calcein AM (acetoxymethyl), on the other hand, is able to cross the cell membrane of viable cells, however, it is not fluorescent in its AM form. Upon crossing the cell membrane, these acetomethoxy groups are hydrolised by cytosolic esterases, which are only active in viable cells, and the calcein fluorescence is restored and trapped inside the viable cell, with a maximum intensity of signal emission at 515-520 nm. Through fluorescence microscopy, we were able to observe PI and calcein staining in all conditions (**Figure 12A**), although PI signal (red) appeared to be stronger in the larger spheroids. Through ImageJ software, quantification of PI signal was performed and compared amongst all conditions. **Figure 12B** shows that, indeed, PI signal is increased particularly in larger spheroids cultured in RPMI 1640 and DMEM Low Glucose medium. In addition, a statistical difference between 1.000 cell spheroids and

larger, 8.000 or more cells, in RPMI 1640 or DMEM Low Glucose was observed. Regarding the generation of a necrotic core, we could observe that it was reproducibly induced in spheroids with over 10.000 cells and was more easily formed in DMEM Low Glucose and RPMI 1640 than in DMEM/F-12. Furthermore, HE staining performed at i3S HEMS core facility, clearly illustrated that there is a loss of cell density in the centre of the spheroids with over 10.000 cells, particularly when these were cultured in RPMI 1640 and DMEM Low Glucose, which is in agreement with the results observed in live spheroids fluorescence microscopy images (**Figure 12C**). Of note, in all conditions, there is indication for scattered cell death, as evidenced by the large intercellular spaces found in the HE stainings. These data corroborate the ATP measurements, showing that spheroids with more than 300 µm hold a necrotic core and have less ATP production.

Irradiation promotes DNA damage and exacerbates the necrotic core size

Evaluating the integrity of the spheroid is of great importance to certify the uniformity of nutrient and O_2 gradients highly relevant for therapy response studies. After the successful development of a 3D biomimetic rectal cancer spheroid model, we proceeded then to evaluate its response to a therapeutic agent, as ionising radiation. Therefore, spheroids of 5.000, 10.000 and 20.000 cells cultured in DMEM/F-12, RPMI 1640, and DMEM Low Glucose were irradiated with the same scheme used to treat RC patients, namely 5 doses of 5 Gy during five consecutive days. The effect of radiotherapy on DNA damage was assessed by the phosphorylation of the histone γ-H2AX. In **Figure 13A** one can clearly observe that irradiated spheroids present increased levels of γ-H2AX phosphorylation, indicating that the treatment was effective in promoting DNA damage. This was achieved regardless of the spheroid cell density or culture medium. Through HE stainings we observed an increase in the necrotic core size of the irradiated SW837 spheroids, when compared to non-irradiated controls. This was associated to the induction of cell death promoted by irradiation, which leads to unrepairable DNA damage, as previously mentioned. Nevertheless, the fact that higher diameter spheroids cultured in media with less glucose hold more death at their core strongly indicates that, apart from radiation, the size of the spheroid also impacts the formation of a central necrotic core.

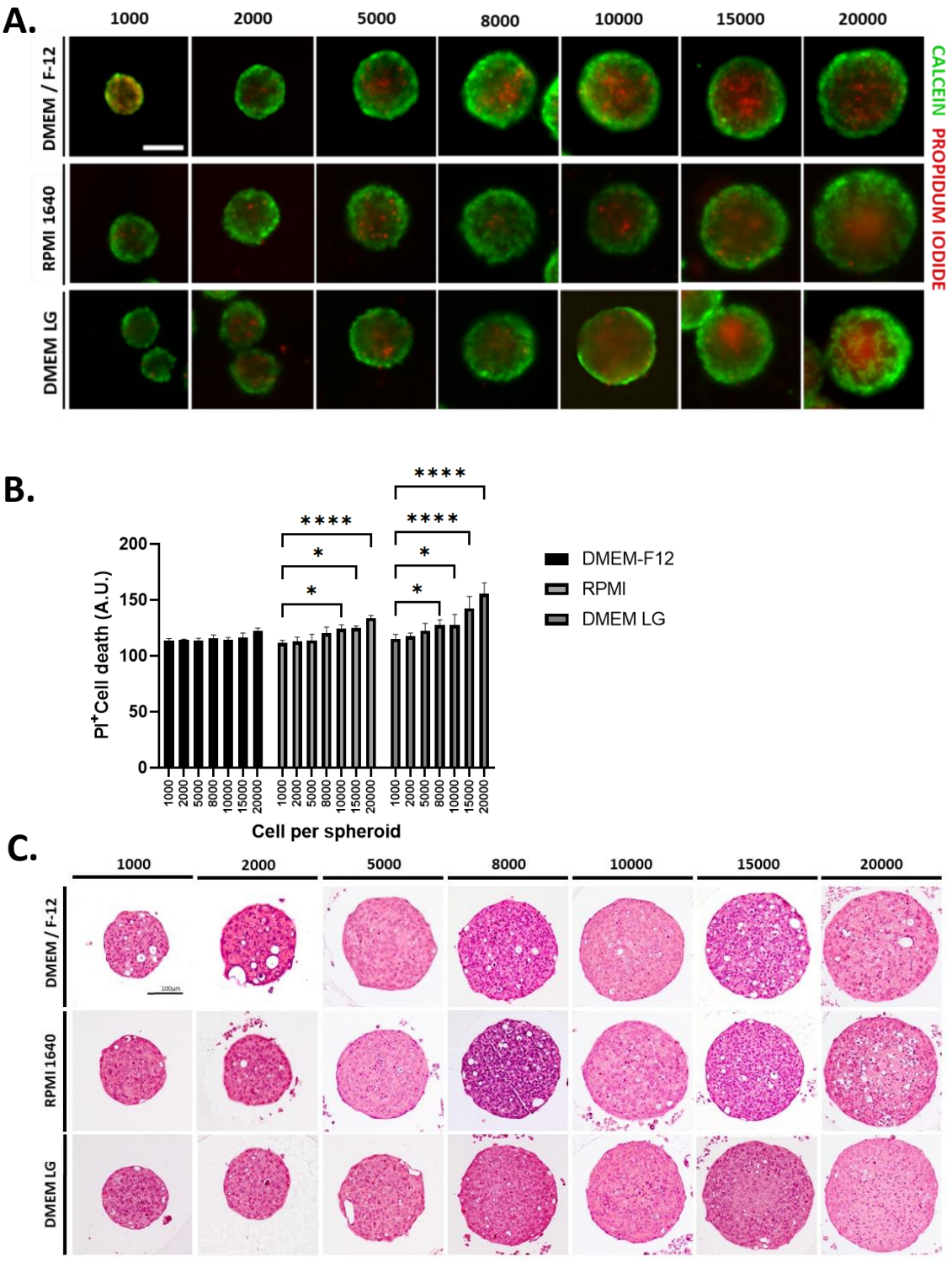

Figure 12 | Cell death visualisation and quantification among all culture conditions at the 8th day of culture. **A)** Fluorescence microscopy of spheroids with multiple cell-seeding numbers, cultured in three different media. PI (red) and Calcein (green) stainings are illustrated. Scale bar for 120 µm. **B)** Graphical representation of PI signal intensity, as measured by ImageJ. Significant differences ** $p \leq 0.05$; **** $p \leq 0.0001$;* with Dunnet's multiple comparisons test. **C)** Representative images of HE stainings for all culture conditions. Scale bar for 100 µm. Data from 3-independent experiments ± SD.

Radiotherapy increases spheroids' necrotic core without affecting proliferative cells

The impact of radiotherapy on the necrotic core size of spheroids and on the cancer cells proliferative status was also assessed, using immunofluorescence assays. As observed in **Figure 14**, through a loss of EpCAM (which indicates a loss in membrane organisation), control spheroids with 10.000 and 20.000 cells, cultured in RPMI 1640 or DMEM Low Glucose, presented a clear necrotic region in their core. This necrotic core increased upon ionising radiation treatment, becoming evident in spheroids comprised of 20.000 cells, independently of the used culture media. Regarding proliferation, ki67 positive cells were found scattered in the control spheroids and seem to be maintained in irradiated conditions (**Figure 14A**). Interestingly, the density of proliferative cells on the periphery of the spheroid appears to increase with spheroid size and exacerbated by irradiation. Furthermore, this increased proliferation seems to compensate for the enhanced cell death in the spheroids core, as there were no differences in ATP production between irradiated and non-irradiated multicellular spheroids (**Figure 14B**).

4.2. 3D Multicellular tumour spheroids as a source of EVs to study rectal cancer radioresistance

One of the main goals of this work was to develop a more biomimetic 3D rectal cancer model as a source of EVs for proteomics studies, as these particles play a crucial role in intercellular communication by carrying signals (protein and RNA content) horizontally in the tumour microenvironment. Being a relatively new field, the EV studies tend to have include heterogeneous methodologies that differ among different laboratories when it comes to their isolation. Furthermore, it is very difficult to distinguish between EV populations when performing isolation (specifically, microvesicles from exosomes) due to their overlapping sizes and similar densities, which is why, for most methods, the term "Extracellular Vesicle" should be kept when addressing what has been isolated [33]. The impact of disparate methods of isolation in EV studies has been and continues to be studied, but it is known that the quality of the isolates, efficiency and cost of methodology have a broad range among the most common protocols used in research. A study by Olivier de Wever's group compared the four most common methods for EV isolation and their impact on EV, protein and RNA yields and profiles [141]. This report showed that making use of the ODG method markedly improved the quality of EV isolation, by reducing extravesicular contaminants, such as RNA-binding proteins (an important confounding factor when performing RNA profiling) and non-vesicular compartments, increasing CD63-positive

vesicle yield and having a more reproducible RNA profile when compared to other methods [141]. This led us to select the ODG methodology, although with higher cost and time consumption than the required for other methods.

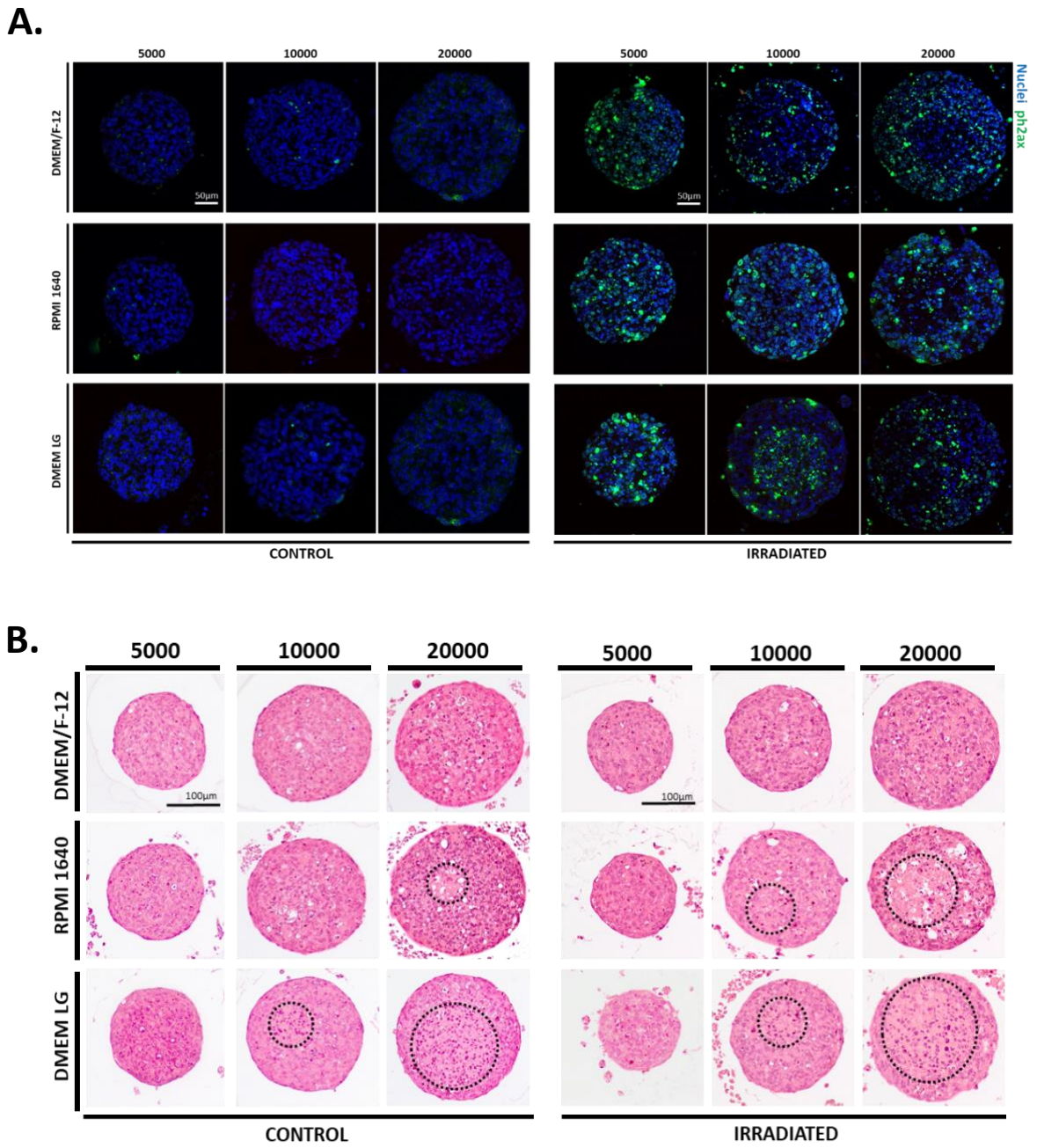

Figure 13 | Effects of short scheme radiation therapy on multicellular RC spheroids.

A) Detection of early DNA damage marker γ-H2AX through immunofluorescence (green). Comparison between cell density per spheroid and culture media is shown. Representative images from controls (left panel) and irradiated samples (right panel). Scale bar for 50 µm. B) HE stainings of irradiated and control spheroids in different culture conditions. Scale bar for 100 µm. Dashed circumference around low density cell area, indicating necrotic core. Representative images from 3-independent experiments.

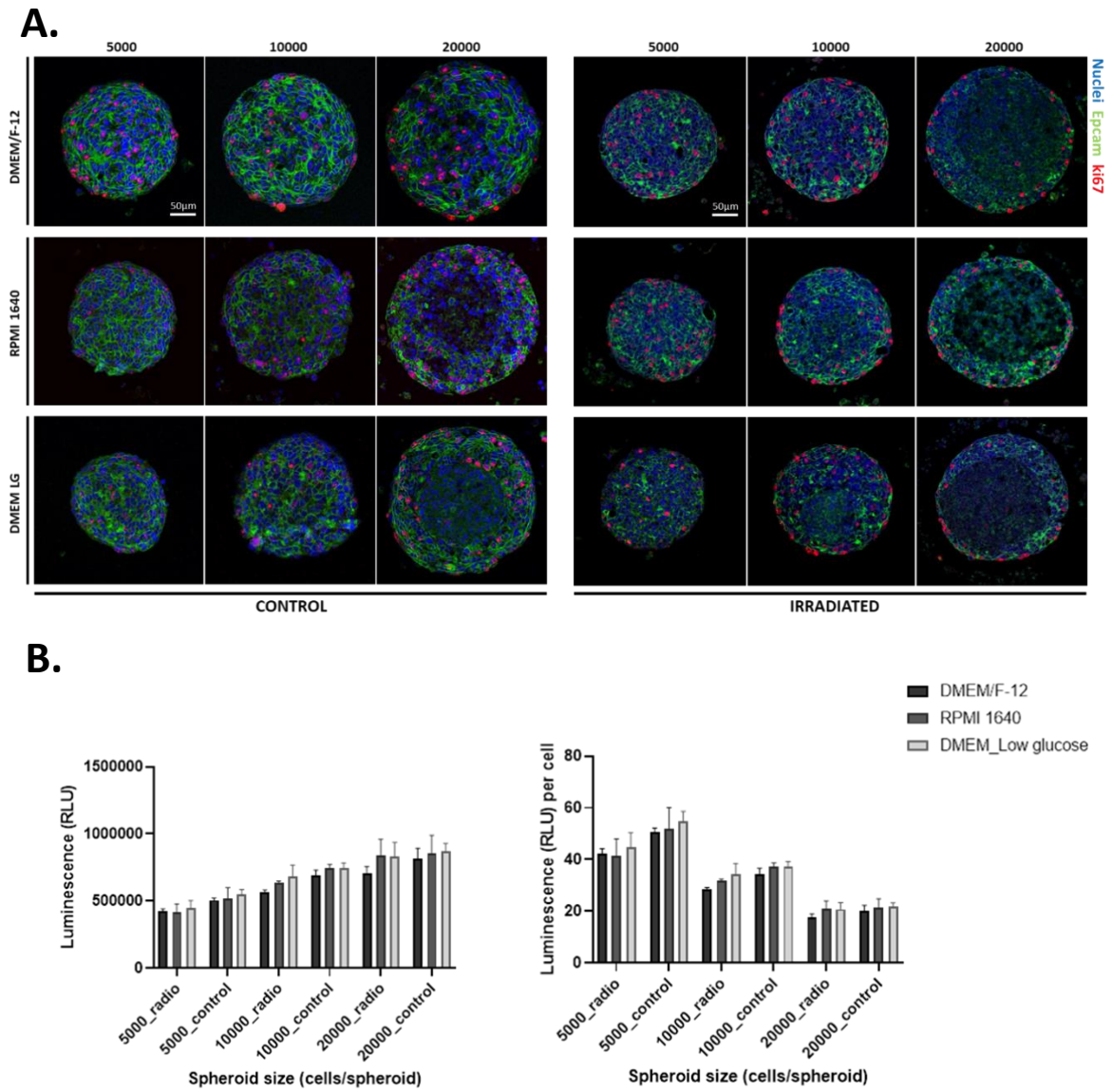

Figure 14 | Effects of short scheme radiation therapy on the necrotic core area and proliferation of multicellular RC spheroids. A) Detection of EpCAM (green), Ki67 (red) and nuclei (blue) on multicellular spheroids composed of 5.000, 10.000, and 20.000 SW837 cells cultured in different media. Controls are shown in the left panel and irradiated spheroids are illustrated in the right panel. Representative images from 3-independent experiments are illustrated. Scale bar for 50 µm. **B)** ATP production per spheroid (left panel) and per cell (right panel). The latter was obtained after normalisation to the number of cells per spheroid. Luminescence represented by relative light units (RLU) is depicted. The plots hold the average of data from 3-independent experiments ± SD.

Quality control of EV isolations proves the reliability of SW837 RC spheroids as a source omics-grade EVs

Initially, a proof of concept regarding the ODG followed by SEC protocol was applied, to confirm that EVs were present in the 9th and 10th millilitres of the gradient and eluted in the 4th to 7th eluates of the SEC column. With this approach an apparent enrichment of particle numbers in fractions 9 and 10 of the density gradient was observed (**Supplementary Figure 1**). This result was likely exaggerated due to the inherent bias of NTA towards larger particles, and lower sensitivity when it comes to detecting particles under 70 nm in size. The presence of particles was exclusive to the eluates 4 to 7 in SEC (**Supplementary Figure 2**). To verify that the protein content in the samples, for both western blotting and proteomics, was sufficient and arose from EV lysis, and not from extravesicular proteins, we performed protein quantification based on the Bradford method using lysis buffer to disrupt EV lipid bilayers. This showed a doubling in protein contents on the EV isolates when lysis buffer was used, meaning that EVs indeed contain protein on their lumen, but half of the protein contents in the sample were either membrane proteins or extravesicular (**Supplementary Figure 3**). With these results we then followed with the quality control steps.

Firstly, NTA was used to assess the number of particles arising from isolates of both irradiated spheroids and non-irradiated controls. To do so, four 12-well plates filled with 972 spheroids each (81 per well), of 10.000 cells per spheroid, were used per condition. Therefore, to obtain a control and irradiated pair, roughly 80x10^{6} SW837 cells were used per experimental replicate. Of note, in one experiment, a sample of spheroids was taken to be submitted to TEM, where it was possible to obtain illustrative images showing both microvesicle shedding and MVB-like structures, which indicates that, although small EVs are being isolated, these may originate from both EV pathways (**Supplementary Figure 5**). The NTA analysis indicated that the mean number of particles recovered from the spheroid isolates were of 4,36x10^{10} for controls and of 3,58x10^{10} for irradiated spheroids. Particle size distribution displayed some variance, as illustrated in **Figure 15A**, with mean sizes of 118,6 nm for controls and of 125,9 nm for irradiated spheroids (**Supplementary Figure 4**). The isolates were then analysed by western blotting to confirm that the particles measured by NTA were indeed EVs, through the detection of common, previously described, EV markers. The EV markers chosen for detection were tetraspanin CD9 (membrane protein), Flotillin-1 (intravesicular, membrane bound) and ALIX (associated with the Endosome Sorting Complex), as well as the relative presence of the extravesicular contaminant Argonaute-2 (AGO-2), a well characterised RNA chaperone that could confound RNAseq results.

Data obtained evidenced that, as expected, EVs concentrated along the 9th and 10th mL of the gradient, as previously described, however, EV markers were also found in fraction 7-8 (7th and 8th mL) (**Figure 15B**). Therefore, for proteomic studies, fractions 7 to 10 of the density gradient were collected to increase the recovery of EVs. Importantly, the low signal of AGO-2 observed in the fractions of interest was also in agreement with the loss of the RNA chaperone from EV isolates. To comply with the EV quality control guidelines, a third technique to check EV morphology and size distribution should be used. For that we resorted to TEM and as shown in **Figure 15C**, a satisfactory enrichment of EVs with some extravesicular protein contaminants was found in EV isolates. Altogether, these results indicated that EV isolation protocol was successfully optimised and that EVs from both control and irradiated RC spheroids could now be used for further studies.

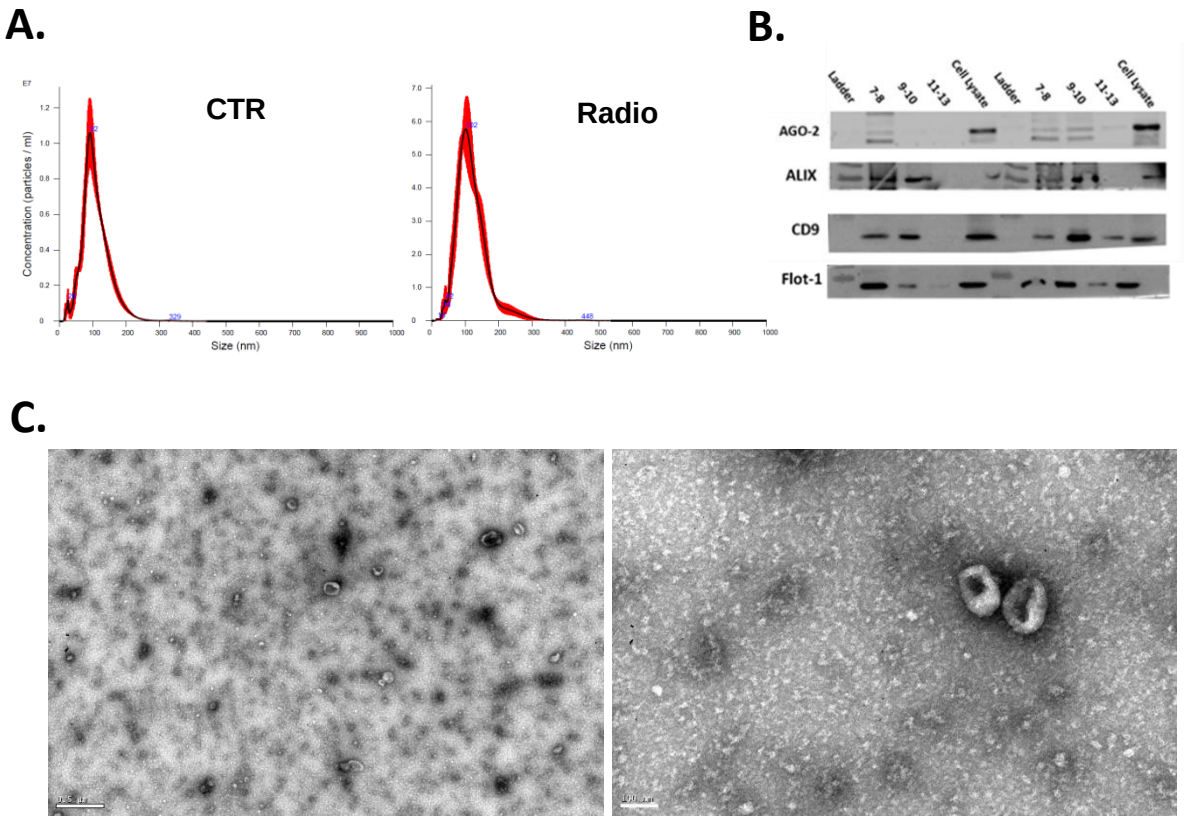

Figure 15 | Quality control of RC spheroid-derived EV isolates.

A) Particle size distribution and concentration, measured through NTA in a 1:500 dilution from the original samples. B) Protein expression assessed by western blotting. Three common EV markers were detected, ALIX, CD9, and Flotilin-1 (Flot-1). For contaminants AGO-2 was used. C) TEM representative images from EV isolates. Scale bars: 500 nm (left) and 100 nm (right).

4.3. Preliminary data reveals EV cargo of irradiated rectal cancer cells

To investigate the content of EVs from both control and irradiated spheroids 50 µl of each EV isolates was forwarded to the i3S Proteomics platform to undergo mass spectrometry LC-MS/MS analysis. Three pairs (control vs. irradiated) of samples were evaluated (n=3), one of them isolated from a Ghent paired sample, and the other two generated at i3S, using exactly the same methodology and reagents. Analysis of the data obtained was performed using the Proteome Discoverer software.

A total of 2120 proteins were found, including human and bovine proteins, the last derived from the EVs-depleted serum used along spheroids culture conditions. Applied filters excluded *Bos taurus* and proteins identified by less than two unique peptides to provide trustworthy identification. The application of the referred filters resulted in the identification of 606 proteins in the EV isolates. Additional filters were then applied to compare between the cargo of EVs obtained from control and irradiated spheroids. Protein enrichment was considered when one condition registered over 50% more of a given protein relative to the other, which was detected through the abundance ratio (R/C). The five most common proteins found in general (as per number of Unique Peptide hits) were Agrin (AGRN), Filamin-A, Pro low-density lipoprotein receptor-related protein (LRP1), Talin-1 (TLN-1), and Basement membrane-specific heparin sulfate proteoglycan core protein (HSPG), of which AGRN and HSPG were significantly more abundant in controls when compared to irradiated in the six samples (**Supplementary Table 4**).

Through Principal Component Analysis (PCA), it was observed that most of the differences between all samples could be explained by inter-laboratory variability. Sample 3 was generated at the Laboratory for Experimental Cancer Research (LECR), in Ghent, and the major differences between samples may be explained by possible differences between working places. With these effects in mind, we excluded Sample 3 from the analysis and performed a new PCA analysis (**Figure 16**). In this second analysis, only considering samples generated at i3S, 1612 proteins were found. After applying the previously referred filters, bovine proteins and protein groups with less than 2 unique peptides were excluded. Even though this analysis resulted in a loss of statistical significance, due to the absence of one replicate, 435 candidate proteins were identified in the EV isolates. The five most abundant proteins in general, considering all samples, (as per number of Unique Peptide hits) were Thrombospondin-1, Agrin, Fibronectin, Actin, and HSPG (**Supplementary Table 5**).

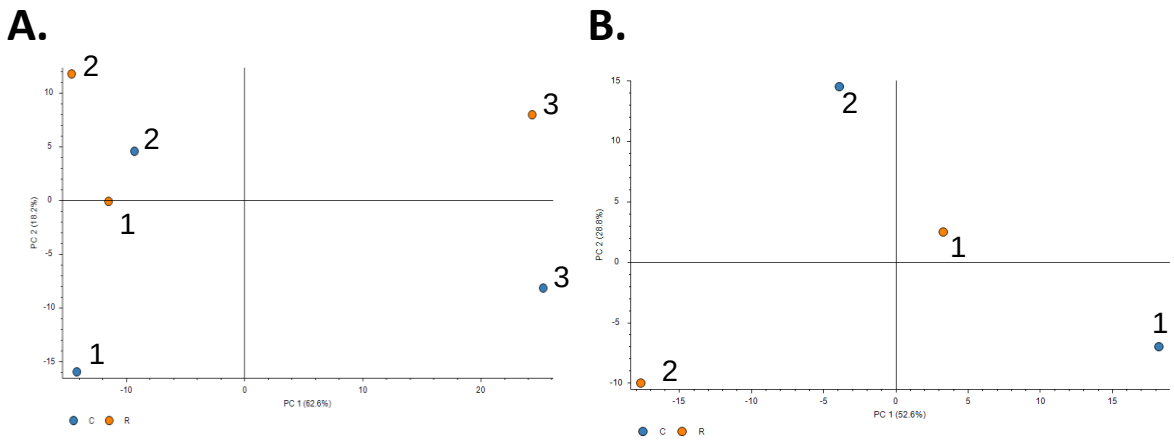

Figure 16 | Principle Component Analysis of proteomics data. A) Analysis of the 3-independent experimental data. Sample 3 is shown to differ from samples 1 and 2. B) Principal Component Analysis of samples 1 and 2 alone.

Eight proteins were 50% more abundant in EVs from radiotherapy-treated spheroids when compared to controls, of which five were present in both "irradiated EVs" (**Table 1**). On the other hand, 14 proteins decreased in EVs by 50% after irradiation, of which 11 appeared in both control samples. A summary of the differentially abundant proteins in control and irradiated samples is present in **Table** 1.

From a universe of 435 proteins, only 13 registered a 2-fold difference in abundance when comparing controls and irradiated samples (11 more abundant in controls and 2 in irradiated). The distribution of proteins between controls and irradiated samples is summed up in **Figure 17**, where controls seemed to have more proteins enriched and more protein variety, when compared to irradiated samples. Although these results are still preliminary, we can already observe that irradiation of cells elicits a response evidenced on the spheroids' secretome. These changes, if further explored, could uncover novel therapeutic targets to be used in combination with radiotherapy and possibly, biomarkers of radiotherapy response.

Table 1 | Differentially abundant proteins in control and irradiated EV isolates.

Abundance ratios under 0.50 indicate proteins 50% more abundant in controls then in irradiated EVs (in green). Abundance ratios over 1.5 indicate a 50% increase in the protein's abundance in irradiated samples in comparison with their paired controls (in red).

Protein	Abundance Ratio (Radiotherapy/Control)	Function
Agrin	0.442	Basement membrane and extracellular matrix protein, participates in integrin and Wnt signalling
Laminin Subunit α5	0.428	Cell adhesion protein, participates in ECM remodelling
Alkaline phosphatase	0.010	Participates in GPI-anchored proteins
CAD protein	0.492	Participates in pyrimidine synthesis and metabolism
Arrestin domain-containing protein 1 (ARRDC1)	0.411	Extracellular vesicle protein loading (microvesicles)
Integrin-linked protein kinase	0.500	Integrin signalling
Serine incorporator 5	0.378	Serine incorporation into sphingolipids
Laminin subunit β2	0.010	Cell adhesion protein, participates in ECM remodelling
Lactadherin	0.438	Promotes mucosal healing and VEGF-dependent neo-angiogenesis
Interleukin-1 receptor accessory protein	0.357	IL-1β receptor in association with IL1R1, activates NFκB pathway
Macrophage migration inhibition factor	0.010	Pro-inflammatory cytokine
Keratin, type II cytoskeletal1	1.937	Keratinisation
Keratin, type I cytoskeletal 9	2.393	Keratinisation
Cartilage oligomeric matrix protein	1.571	ECM interactions, blocks apoptosis in chondrocytes
Protocadherin Fat 1	100.000	Cell polarisation, migration and cell-cell contact
Fructose-bisphosphatase aldolase B	1.524	Glycolytic protein

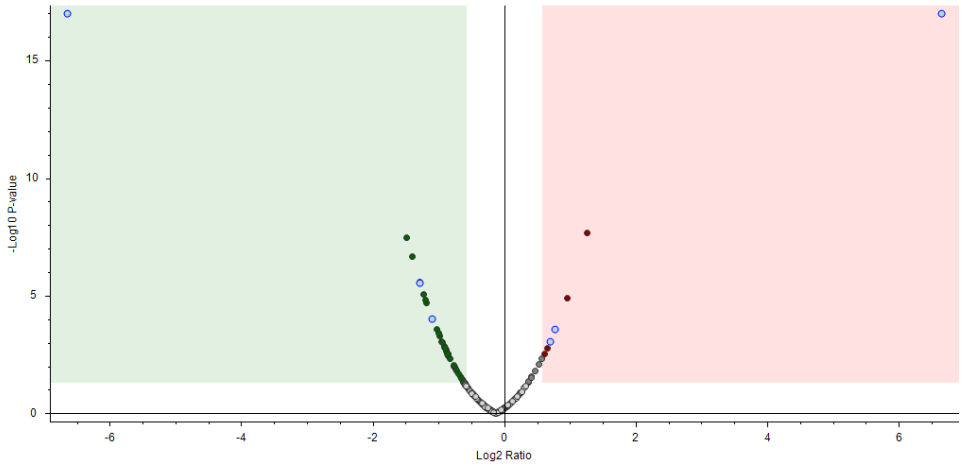

Figure 17 | Volcano plot representing differentially abundant proteins in controls and irradiated samples. The green side indicates increased abundance in controls, whereas the red side indicates increased abundance in irradiated samples.

5. Discussion

Rectal cancer is responsible for over 30% of the CRC burden worldwide, contributing heavily for the high incidence and mortality rates of gastrointestinal tract malignancies in 2020 [3]. Importantly, in Portugal, RC alone represents the fifth most incident cancer [3]. Moreover, due to thriving unhealthy lifestyles, RC is growing exponentially and the expectations are that by 2030, an increase of 124% cases under 35 year-old patients occurs. Neo-adjuvant radiotherapy is usually the standard treatment method [19, 145] since more than 50% of the patients present an advanced disease at diagnosis [140, 146]. Although effective, radiotherapy still leaves over 30% of the patients experiencing no response or local recurrence after treatment, due to variable levels of radioresistance [147]. As such, there is an urgent need for more efficient therapies to be combined with ionising radiation. One of the strategies to improve radiotherapy response and to search for new drug-target molecules is to explore the radioresistance mechanisms. However, the mysteries behind such processes, within the tumour microenvironment, are still unsolved.

The answers to the aforementioned questions could reside in intercellular communication, in particular, in the secretome of the tumour microenvironment, where EVs have a preponderant role [71]. EVs are defined as particles naturally released by cells, delimited by a lipid bilayer that do not contain a functional nucleus [33]. Their contents include virtually all biomolecules, namely proteins, lipids and nucleic acids, such as small RNAs and microRNAs (miRNAs), which are carried to neighbouring cells and have the capacity to elicit a phenotypical response [32]. These vesicles are emitted by all cells, but more proficiently by tumour cells [148]. The contents of EVs can support tumour progression, influencing several *hallmarks of cancer*, namely, the promotion of proliferation, angiogenesis, immune escape, invasion and metastasis, or even drug resistance [71, 73, 78]. Some of the EV functions have been described in CRC [110, 112, 149-151], but never in RC specifically. It is also known that, by reflecting the nature of their parent cells, circulating EVs are potential biomarker sources for diagnostic and patient stratification. In CRC, there are studies that identify EVs cargo namely, proteins and nucleic acids, as risk of progression markers [152-154], however, these studies were not focused in RC. Only recently there were published two studies regarding EVs as carriers of RC biomarkers: T. Bjornetro *et al.* explored the applicability of microRNAs miR-486-5p, miR181a-5p and miR-30-5p as circulating indicators of high RC risk [155], and U. Strybel *et al*, which investigated the proteome of circulating EVs, isolated from patients with high stage RC, as a potential discriminator of neo-adjuvant therapy response (making use of the long neo-adjuvant radiotherapy scheme applied to RC patients, of ~45Gy). Although there are some limitations in this study's

methodology, they still found that exosomes carry numerous proteins related to processes that are influenced by radiotherapy, such as an enrichment in antioxidant protein on good responders' circulating exosomes, and the enrichment of glucose transporter GLUT1 on poor responders [156]. Still, so far, there are no studies on the role of EVs in RC radioresistance mechanisms. Having this in mind, through the use of innovative tools, this thesis aimed at uncovering radioresistance molecular players enclosed in EVs secreted by irradiated RC tumour cells to develop improved therapies that assist in disease regression and increase patient overall survival. For this we sought to develop a novel 3D cell culture methodology that better mimics tumour features, from which omics-grade EVs where isolated and further submitted to proteomic analysis.

5.1. Development of a biomimetic rectal cancer spheroid model for radiobiology research

Multicellular spheroids offer a multiplicity of advantages, such as increased cell-cell and cell-ECM interactions, and tumour mimetic gradients (nutrients, O_2, pH) and drug responses, when compared to conventional monolayer cell cultures. We believe 2D cell cultures still have a place in oncology research, due to their low cost and high throughput traits. Nevertheless, there are also protocols for spheroid assembly that allow high throughput assays and have the added benefit of being more biomimetic (through higher complexity) and versatile. Therefore, we believe that 3D models should be considered for drug screening and radiobiology studies over 2D cell cultures, before moving into animal models. For these reasons, we have chosen multicellular spheroids as a platform to study radioresistance in RC, making use of the SW837 cell line.

The multicellular spheroid 3D culture methodology is gaining traction in basic and translational research, thus it is important to accurately report the followed methodology and optimisation steps to produce reproducible results. As is the case with EV isolation or any new methodology in a scientific field, multicellular spheroids count on several, very distinct, protocols that are viable for their assembly, which is why accurate reporting of minimal information is important in such a heterogeneous field. For the effects of standardisation, Professor Olivier de Wever and his research group created an open access online platform called MISpheroID, on which experiment conditions can be transparently reported and kept in a database. Accompanying this, they published a study that demonstrates how many variables dramatically affect multicellular spheroid morphology and behaviour [129], highlighting the importance of minimal information reporting for spheroid studies and existence of a transparent report repository in the MISpheroID platform. Recognising the importance of the work developed by our collaborators, we set

out to develop and thoroughly characterise the RC spheroid model. Since one of the project's objectives was to produce EVs in sufficient amounts for proteomics, and eventually RNAseq studies, avoiding the more common "one well, one spheroid" approaches was necessary and the 3D MicroTissues Micromolds methodology was chosen. The latter is a platform that allows culturing 81 spheroids per well in a 12-well plate, in microwells of approximately 800 μm in diameter, in a non-adherent agarose mould. The data collected herein confirmed that the RC 3D model developed presents all the features that justify the use of multicellular spheroids over 2D cultures. Spheroids with 10.000 cells or more had over 300 μm in diameter, developed a necrotic core, and held for 8 days in culture without losing shape severely, even without medium change. Although spheroid growth was not observed, cells maintained metabolic activity and viability during all the experimental timeline.

After developing the RC spheroid model, short scheme radiotherapy that mimicked the one applied to RC patients was employed. The irradiation effects on the multicellular tumour spheroids were assessed using a variety of techniques. Since the SW837 cell line is of epithelial origin, we could rely on immunohistochemically stained sections of fixed spheroids, using anti-EpCAM to label the cell membrane of the cancer cells. Cell proliferation was checked by Ki67 positivity and phosphorylation of γ-H2AX was used to assess DNA damage. Our results indicated that fractioned ionising radiation in a total of 25 Gy effectively promoted DNA damage and altered the spheroid features, exacerbating necrotic core formation without affecting ATP production. Moreover, cancer cell proliferation, after irradiation, seemed to compensate for the loss of cells in the spheroid. This may explain the absence of differences regarding ATP levels after radiotherapy.

Altogether, our data supports the development of RC 3D biomimetic spheroid model, proven to be suitable for radiobiology studies, with detectable radiation-induced DNA damage but no disruption of the spheroid morphology. Despite being significantly more labour intensive, time consuming, and costly than traditional 2D cell cultures, 3D *in vitro* models may effectively contribute for reducing drug attrition rates and increasing drug testing effectiveness and, consequently, clinical trial success.

However, the methodology herein employed failed to induce spheroid growth in normal conditions. This can be attributed to the high duplication time registered for this cell line (roughly 40 hours) together with stressful culture conditions. The low proliferation rate, together with the short scheme radiotherapy application, and the fact that the necrotic core is exacerbated (core cells die first) under radiation therapy, pinpoints a lack of compliance with the Reoxygenation and Repopulation radiotherapy principles. Nevertheless, SW837 cell line was reported as being radioresistant when compared to other RC cells such as SW1463, for example [157]. Thus, comparison with spheroids comprised of different cell

lines, inclusion of fibroblasts and immune cells, and application of larger but more fractionated doses (radiotherapy long scheme) will be interesting to test the compliance of the RC spheroid with other Rs of radiotherapy in the future.

5.2. Successful implementation of a spheroid-secreted EV isolation method

The need for a more adequate *in vitro* model that better mimics the tumour properties, including extracellular vesicles shedding, seems apparent, since the EVs research field has relied mostly on 2D cell cultures or blood/plasma samples isolations. Although some hallmarks of cancer, such as exacerbated proliferative signalling or enhanced replicative immortality, aren't among the most important effects mediated by EVs, their ability to mediate most of the hallmarks of cancer evidences their versatility and importance as propagators of such features, both within the tumour microenvironment and systemically. This characteristic makes them an ideal target to develop new anti-cancer drugs against, with special focus on invasion, metastasis, immune modulation and angiogenesis. Therefore, blocking EV secretion or uptake, or targeting specific EV contents, such as those that propagate invasive traits, EMT, establishment of a pre-metastatic niche, angiogenic factors, immune checkpoint ligands, and other immune modulators, are attractive strategies for anti-cancer drug development.

After developing and characterising the RC spheroid model, our data has proven that this platform is suitable for EV multi-omics studies. Thus, we chose to proceed to EV studies with the 10.000 cell spheroids cultured in RPMI 1640 medium. These seemed to be the ideal conditions to study radiotherapy effects since spheroid formation was between the absence of a necrotic core or being too necrotic and too fragile to irradiate. Also, 10.000 cell-spheroids contained the minimal amount of cells to obtain a spheroid with 300 μm in diameter and RPMI 1640 likely offers better options for future work, allowing the inclusion of immune cells, such as macrophages, on the spheroid model.

The quality control assays, that followed the proof of concept for the coupling of ODG to SEC, all delivered satisfactory results, with a high number of particles recovered, on the small EV size range, EV-like morphology, and positive staining for three different EV markers ALIX, CD9, and Flotilin-1. Irradiation did not affect the number of particles recovered, which additionally proves that this platform is adequate for radiobiology studies focused on complete secretome studies. Furthermore, sufficient yield of EVs was obtained from this method to undergo proteomic analysis, which makes it a very interesting platform for EV studies and drug development.

However, this method also holds some disadvantages. As mentioned before, the chosen

methodology for spheroid assembly was based on the high throughput, cost-effective properties of 3D MicroTissues Micromolds, still, a large density of cells was required to obtain sufficient EV content for -omics assays. Choosing the 10.000 cell per spheroid condition, as the platform for EV studies translated into a total of 80 million cells per experiment. This was, therefore, a time consuming, labour intensive, and somehow costly protocol. An additional limitation relates with the presence of a significant amount of extravesicular protein in the EV isolates which, even though all technical precautions were taken, was still registered. Such contaminants may result from i) the bursting of EVs in the isolate during the isolation procedure and/or ii) bovine proteins from the FBS present in the cell culture medium. Slight tweaks in the protocol, such as increasing the number of washings when transitioning from 10% FBS to 0.5% FBS supplemented medium, and working with samples in the shortest time span possible to reduce the number of thawing cycles, will likely improve sample quality in the future.

Nevertheless, the narrow spikes registered in the NTA analysis showed that the applied EV isolation method is highly reproducible (**Supplementary Figure 4**), which taken together with the presence of common EV markers in the collected fractions, highlights the reliability of the previously described ODG method [141].

5.3. Identification of potential candidates for radio-communication

Although in early steps of proteomic analysis, our preliminary data on the secretome characterisation of SW837 spheroid-derived EVs has already started to yield some interesting results. A total of 435 proteins were identified, from which 13 registered a 50% alteration in abundance when comparing controls and irradiated samples. This means there is a cellular response to radiation-induced stress, evidenced by a change in cell secretions, which may constitute a mean of propagation of radioresistant traits within the tumour microenvironment, and therefore, a possible adjuvant therapy target.

In more detail, irradiation led to a reduction of IL1RAP in SW837 EVs. This IL-1 receptor accessory protein, a member of IL-1 receptor family, is necessary for IL-1 signalling transduction, since IL-1R cannot transduce signal alone. This signal transduction leads to the activation of the NF-κB pathway, which is responsible for increased proliferation in cancer cells and angiogenesis [158]. One may speculate that, by reducing this protein's presence in the tumour microenvironment, on the one hand, cancer cells may be losing their ability to respond to radiation-induced stress and, in the other hand, irradiation may be affecting immune cell sensitivity to IL-1 signalling. It would be interesting to assess whether T cells, included in this irradiated spheroid setting, maintain their IL-1 response.

Furthermore, there are clinical trials in lung and pancreatic cancer testing the effectiveness of antibodies targeting IL1RAP, which inhibit the ability of this protein to associate with IL-1R1 [159], however without contemplating radiotherapy. The functional relevance of the IL1RAP decrease in EVs shed by irradiated RC cells represents an interesting line of future research.

Another immunologically-related protein downregulated in irradiated samples was the Macrophage migration inhibition factor (MIF), a cytokine that is overexpressed in colon cancer [160]. This molecule was described as a cancer promotor through the enhancement of EMT and metastasis [161], due to its pleiotropic functions that can cause chronic inflammation and increased angiogenesis. Moreover, MIF has been reported to function as a radiotherapy resistance mediator in glioblastoma [162]. It will be interesting to investigate if EVs secreted by RC cell lines holding different sensitivities to radiotherapy have differences in MIF content.

From the proteins identified, Protocadherin Fat1 was increased in irradiated samples, which may indicate a possible therapy resistance mechanism employed by RC SW837 cells. In fact, Fat1 has been reported as overexpressed in CRC [163]. In this study, Pileri and colleagues explored the internalisation of Fat1, induced by a multiclonal antibody, as mechanism of reducing metastasis. However, the role of this membrane protein is still not fully understood, and even controversial, being described as a tumour suppressor gene or as an oncogene in different studies [164, 165].

The increase of keratinisation-related proteins upon irradiation also constitutes an interesting result. In nasopharyngeal carcinoma, it was observed that keratinising tumours have a worse response to radiotherapy, and, despite having lower metastases rates than their non-keratinising counterparts, keratinising tumours registered a worse loco-regional control of disease upon radiotherapy and worse 5-year survival [166]. Similar effects have been observed in squamous cell lung cancers [167]. This keratinisation increase in epithelial carcinomas upon irradiation may be a radioresistance mechanism, and should be explored upon further validation.

Another protein that was pinpointed in the proteomic analysis was the CAD protein, a trifunctional molecule involved in the pyrimidine metabolism: carbamoyl-phosphate synthetase 2, aspartate transcarbamylase, and dihydroorotase. This multifunctional protein is frequently deregulated in cancer [168, 169], including colon cancer. It supports cancer cell proliferation by assisting in nucleic acid synthesis. Intriguingly, CAD protein was found downregulated in the radiotherapy settings, which seems paradoxical. However, the regulation of this protein's expression under radiotherapy hasn't yet been explored, paving the way for future studies.

Proteins that influence epithelial cell polarisation, ECM remodelling, and integrin signalling,

detected in the proteomic analysis were depleted in the context of radiotherapy. This hints for a role of EVs cargo in the axis of ionising radiation with EMT and invasion regulation, a phenomenon that has been previously proposed [170, 171] and reviewed in [172]. Nevertheless, more samples must be generated to reach a satisfactory statistical power, since it was not possible to have a uniform trio of samples due to interlaboratorial variance factors. This will allow further exploring the EV proteome in the context of radiotherapy to draw significant and biologically relevant conclusions.

6. Conclusion and future work

Cancer progression is heavily promoted by the paracrine network signalling mediated by EVs. These particles, which also participate in establishing the metastatic niche and long distance communication, can transport all types of biomolecules, and participate in virtually all cancer hallmark mechanisms. This makes them a very interesting target when it comes to researching new anti-cancer therapies. To tackle EVs or their common contents as drug targets, biomimetic *in vitro* models are needed in order to improve the low drug approval rates in the oncology field. For this reason, we developed a platform that better recapitulated the RC *in vivo* characteristics, without losing the ability to work in medium-to-high-throughput, allowing the isolation of high amounts of pure EVs. The data presented in this thesis demonstrated that we successfully accomplished our goals. We were able to fully develop and characterise, using multiple conditions, the RC SW837 multicellular spheroid model and up scaled this model to suit the need for EV studies. EV isolates were quality controlled and successfully submitted to proteomic analysis. This platform, which withstood the application of radiotherapy for a week, will, in the future, be suitable for more thorough -omics studies, which will potentially assist in the discovery of novel therapeutic targets.

In the future, we intend to use the multicellular spheroid model to expand the understanding of radiation on RC, particularly of the acquisition of radioresistance mechanisms, through RNA sequencing of the EV contents. Furthermore, another RC cell line, SW1463, which has been described as having less radioresistance than SW837 cells in monolayer culture [157] will also be included in future studies. The secretome of such cell lines, in 3D spheroid models, may help to explain their different radioresistance levels, and signal potential proteins and nucleic acid components as mediators of ionising radiation resistance. After this comparison, validation, and functional relevance of the uncovered differences will be investigated. The secretomes role may be validated by treating radiosensitive cells with radioresistant-derived EVs, and assessing their effect on the radiotherapy response. Alternatively, molecular candidates, mediators of radioresistance can be inhibited to prove their influence in radioresistance. Additionally, we aim to apply the long course radiotherapy scheme on the spheroids, to assess long term spheroid behaviour under radiation therapy. Multicellular spheroids that include immune cells are already being characterised within our group, for breast and RC, and will be also used to understand the EV role on immune (in)activation. Finally, our long term perspectives are to use this platform with patient-derived RC cells, attempting to develop a personalised therapy platform with high throughput capacity without losing tumour microenvironment mimicry.

Funding

This work was financed by Portuguese funds through FCT - Fundação para a Ciência e a Tecnologia/Ministério da Ciência, Tecnologia e Ensino Superior in the framework of the project READOUT (EXPL/BIA-CEL/1225/2021) and in part by Programa Operacional Regional do Norte and co-funded by European Regional Development Fund under the project "The Porto Comprehensive Cancer Center" with the reference NORTE-01-0145-FEDER-072678 - Consórcio PORTO.CCC – Porto.Comprehensive Cancer Center.

Development of this work in Ghent, Belgium, for 4 months, was supported by the European Erasmus+ program.

Contribution to the scientific community in oncology

This work will be included, in the future, in two separate original scientific articles, one on rectal cancer spheroid development, and one on rectal cancer EV characterisation. Furthermore, related to this work, we will produce a review on the role of EVs in the hallmarks of cancer.

During the past year, the author of this thesis contributed to the production of a review article entitled “IRON METABOLISM IN COLORECTAL CANCER: A BALANCING ACT”, which is, as of the date of this thesis final submission, under review at the Cellular Oncology Journal:

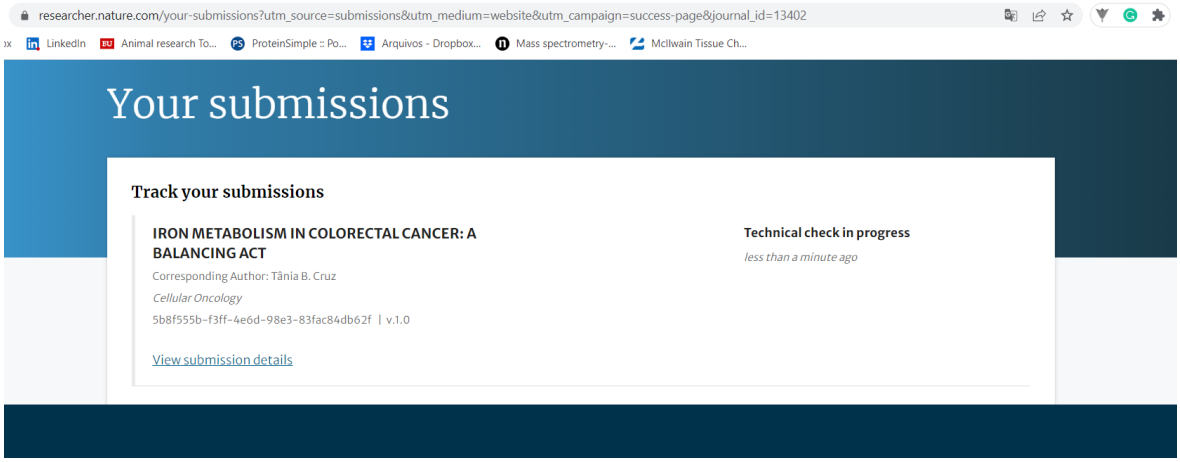

This manuscript can be found after the supplementary information, in this document.

References

[1] J. M. Loree *et al.*, "Classifying Colorectal Cancer by Tumor Location Rather than Sidedness Highlights a Continuum in Mutation Profiles and Consensus Molecular Subtypes," *Clin Cancer Res,* vol. 24, no. 5, pp. 1062-1072, Mar 1 2018, doi: 10.1158/1078-0432.CCR-17-2484.

[2] J. Roelands *et al.*, "Immunogenomic Classification of Colorectal Cancer and Therapeutic Implications," *Int J Mol Sci,* vol. 18, no. 10, Oct 24 2017, doi: 10.3390/ijms18102229.

[3] H. Sung *et al.*, "Global Cancer Statistics 2020: GLOBOCAN Estimates of Incidence and Mortality Worldwide for 36 Cancers in 185 Countries," *CA Cancer J Clin,* vol. 71, no. 3, pp. 209-249, May 2021, doi: 10.3322/caac.21660.

[4] S. Paschke *et al.*, "Are Colon and Rectal Cancer Two Different Tumor Entities? A Proposal to Abandon the Term Colorectal Cancer," *Int J Mol Sci,* vol. 19, no. 9, Aug 30 2018, doi: 10.3390/ijms19092577.

[5] B. Iacopetta, "Are there two sides to colorectal cancer?," *Int J Cancer,* vol. 101, no. 5, pp. 403-8, Oct 10 2002, doi: 10.1002/ijc.10635.

[6] E. K. Wei *et al.*, "Comparison of risk factors for colon and rectal cancer," *Int J Cancer,* vol. 108, no. 3, pp. 433-42, Jan 20 2004, doi: 10.1002/ijc.11540.

[7] J. Virostko, A. Capasso, T. E. Yankeelov, and B. Goodgame, "Recent trends in the age at diagnosis of colorectal cancer in the US National Cancer Data Base, 2004-2015," *Cancer,* vol. 125, no. 21, pp. 3828-3835, Nov 1 2019, doi: 10.1002/cncr.32347.

[8] Y. C. Lee, Y. L. Lee, J. P. Chuang, and J. C. Lee, "Differences in survival between colon and rectal cancer from SEER data," *PLoS One,* vol. 8, no. 11, p. e78709, 2013, doi: 10.1371/journal.pone.0078709.

[9] J. Guinney *et al.*, "The consensus molecular subtypes of colorectal cancer," *Nat Med,* vol. 21, no. 11, pp. 1350-6, Nov 2015, doi: 10.1038/nm.3967.

[10] M. Rebersek, "Consensus molecular subtypes (CMS) in metastatic colorectal cancer - personalized medicine decision," *Radiol Oncol,* vol. 54, no. 3, pp. 272-277, May 28 2020, doi: 10.2478/raon-2020-0031.

[11] G. Argiles *et al.*, "Localised colon cancer: ESMO Clinical Practice Guidelines for diagnosis, treatment and follow-up," *Ann Oncol,* vol. 31, no. 10, pp. 1291-1305, Oct 2020, doi: 10.1016/j.annonc.2020.06.022.

[12] E. Becht *et al.*, "Immune and Stromal Classification of Colorectal Cancer Is Associated with Molecular Subtypes and Relevant for Precision Immunotherapy," *Clin Cancer Res,* vol. 22, no. 16, pp. 4057-66, Aug 15 2016, doi: 10.1158/1078-0432.CCR-15-2879.

[13] A. Barleben and S. Mills, "Anorectal anatomy and physiology," *Surg Clin North Am,* vol. 90, no. 1, pp. 1-15, Table of Contents, Feb 2010, doi: 10.1016/j.suc.2009.09.001.

[14] M. Riihimaki, A. Hemminki, J. Sundquist, and K. Hemminki, "Patterns of metastasis in colon and rectal cancer," *Sci Rep,* vol. 6, p. 29765, Jul 15 2016, doi: 10.1038/srep29765.

[15] J. Scheele, J. Lemke, M. Meier, S. Sander, D. Henne-Bruns, and M. Kornmann, "Quality of Life After Sphincter-Preserving Rectal Cancer Resection," *Clin Colorectal Cancer,* vol. 14, no. 4, pp. e33-40, Dec 2015, doi: 10.1016/j.clcc.2015.05.012.

[16] T. Mori, K. Takahashi, and M. Yasuno, "Radical resection with autonomic nerve preservation and lymph node dissection techniques in lower rectal cancer surgery and its results: the impact of lateral lymph node dissection," *Langenbecks Arch Surg,* vol. 383, no. 6, pp. 409-15, Dec 1998, doi: 10.1007/s004230050153.

[17] M. Kornmann *et al.*, "Long-term results of 2 adjuvant trials reveal differences in chemosensitivity and the pattern of metastases between colon cancer and rectal cancer," *Clin Colorectal Cancer,* vol. 12, no. 1, pp. 54-61, Mar 2013, doi: 10.1016/j.clcc.2012.07.005.

[18] E. Van Cutsem, A. Cervantes, B. Nordlinger, D. Arnold, and E. G. W. Group, "Metastatic colorectal cancer: ESMO Clinical Practice Guidelines for diagnosis, treatment and follow-up," *Ann Oncol,* vol. 25 Suppl 3, pp. iii1-9, Sep 2014, doi: 10.1093/annonc/mdu260.

[19] R. Glynne-Jones *et al.*, "Rectal cancer: ESMO Clinical Practice Guidelines for diagnosis, treatment and follow-up," *Ann Oncol,* vol. 28, no. suppl_4, pp. iv22-iv40, Jul 1 2017, doi: 10.1093/annonc/mdx224.

[20] J. Sia, R. Szmyd, E. Hau, and H. E. Gee, "Molecular Mechanisms of Radiation-Induced Cancer Cell Death: A Primer," *Front Cell Dev Biol,* vol. 8, p. 41, 2020, doi: 10.3389/fcell.2020.00041.

[21] H. R. Withers, "The 4 R's of Radiotherapy," in *Advances in Radiobiology*, vol. 5: Elsevier, 1975, pp. 241-271.

[22] M. R. Horsman, L. S. Mortensen, J. B. Petersen, M. Busk, and J. Overgaard, "Imaging hypoxia to improve radiotherapy outcome," *Nat Rev Clin Oncol,* vol. 9, no. 12, pp. 674-87, Dec 2012, doi: 10.1038/nrclinonc.2012.171.

[23] W. K. Sinclair, "X-Ray and Ultraviolet Sensitivity of Synchronized Chinese Hamster Cells at Various Stages of the Cell Cycle " vol. 5, no. 1, 1965, doi: 10.1016/s0006-3495(65)86700-5.

[24] H. R. Withers, "Treatment-Induced Accelerated Human Tumor Growth," *Semin Radiat Oncol,* vol. 3, no. 2, pp. 135-143, Apr 1993, doi: 10.1054/SRAO00300135.

[25] G. G. Steel, T. J. McMillan, and J. H. Peacock, "The 5Rs of radiobiology," *Int J Radiat Biol,* vol. 56, no. 6, pp. 1045-8, Dec 1989, doi: 10.1080/09553008914552491.

[26] G. G. Steel, J. M. Deacon, G. M. Duchesne, A. Horwich, L. R. Kelland, and J. H. Peacock, "The dose-rate effect in human tumour cells," *Radiother Oncol,* vol. 9, no. 4, pp. 299-310, Aug 1987, doi: 10.1016/s0167-8140(87)80151-2.

[27] A. Gupta *et al.*, "Radiotherapy promotes tumor-specific effector CD8+ T cells via dendritic cell activation," *J Immunol,* vol. 189, no. 2, pp. 558-66, Jul 15 2012, doi: 10.4049/jimmunol.1200563.

[28] D. Hallahan, J. Kuchibhotla, and C. Wyble, "Cell adhesion molecules mediate radiation-induced leukocyte adhesion to the vascular endothelium," *Cancer Res,* vol. 56, no. 22, pp. 5150-5, Nov 15 1996. [Online]. Available: https://www.ncbi.nlm.nih.gov/pubmed/8912850.

[29] J. M. Kaminski, E. Shinohara, J. B. Summers, K. J. Niermann, A. Morimoto, and J. Brousal, "The controversial abscopal effect," *Cancer Treat Rev,* vol. 31, no. 3, pp. 159-72, May 2005, doi: 10.1016/j.ctrv.2005.03.004.

[30] B. Burnette and R. R. Weichselbaum, "Radiation as an immune modulator," *Semin Radiat Oncol,* vol. 23, no. 4, pp. 273-80, Oct 2013, doi: 10.1016/j.semradonc.2013.05.009.

[31] A. Rakotomalala, A. Escande, A. Furlan, S. Meignan, and E. Lartigau, "Hypoxia in Solid Tumors: How Low Oxygenation Impacts the "Six Rs" of Radiotherapy," *Front Endocrinol (Lausanne),* vol. 12, p. 742215, 2021, doi: 10.3389/fendo.2021.742215.

[32] M. Yanez-Mo *et al.*, "Biological properties of extracellular vesicles and their physiological functions," *J Extracell Vesicles,* vol. 4, p. 27066, 2015, doi: 10.3402/jev.v4.27066.

[33] C. Thery *et al.*, "Minimal information for studies of extracellular vesicles 2018 (MISEV2018): a position statement of the International Society for Extracellular Vesicles and update of the MISEV2014 guidelines," *J Extracell Vesicles,* vol. 7, no. 1, p. 1535750, 2018, doi: 10.1080/20013078.2018.1535750.

[34] E. Chargaff and R. West, "The biological significance of the thromboplastic protein of blood," *J Biol Chem,* vol. 166, no. 1, pp. 189-97, Nov 1946. [Online]. Available: https://www.ncbi.nlm.nih.gov/pubmed/20273687.

[35] P. Wolf, "The nature and significance of platelet products in human plasma," *Br J Haematol,* vol. 13, no. 3, pp. 269-88, May 1967, doi: 10.1111/j.1365-2141.1967.tb08741.x.

[36] M. E. De Broe, R. J. Wieme, G. N. Logghe, and F. Roels, "Spontaneous shedding of plasma membrane fragments by human cells in vivo and in vitro," *Clin Chim Acta,* vol. 81, no. 3, pp. 237-45, Dec 15 1977, doi: 10.1016/0009-8981(77)90054-7.

[37] C. Harding, J. Heuser, and P. Stahl, "Receptor-mediated endocytosis of transferrin and

recycling of the transferrin receptor in rat reticulocytes," *J Cell Biol,* vol. 97, no. 2, pp. 329-39, Aug 1983, doi: 10.1083/jcb.97.2.329.

[38] R. M. Johnstone, M. Adam, J. R. Hammond, L. Orr, and C. Turbide, "Vesicle formation during reticulocyte maturation. Association of plasma membrane activities with released vesicles (exosomes)," *J Biol Chem,* vol. 262, no. 19, pp. 9412-20, Jul 5 1987. [Online]. Available: https://www.ncbi.nlm.nih.gov/pubmed/3597417.

[39] S. Amigorena, J. R. Drake, P. Webster, and I. Mellman, "Transient accumulation of new class II MHC molecules in a novel endocytic compartment in B lymphocytes," *Nature,* vol. 369, no. 6476, pp. 113-20, May 12 1994, doi: 10.1038/369113a0.

[40] M. J. Kleijmeer, V. M. Oorschot, and H. J. Geuze, "Human resident langerhans cells display a lysosomal compartment enriched in MHC class II," *J Invest Dermatol,* vol. 103, no. 4, pp. 516-23, Oct 1994, doi: 10.1111/1523-1747.ep12395666.

[41] G. Raposo *et al.*, "B lymphocytes secrete antigen-presenting vesicles," *J Exp Med,* vol. 183, no. 3, pp. 1161-72, Mar 1 1996, doi: 10.1084/jem.183.3.1161.

[42] H. F. Heijnen, A. E. Schiel, R. Fijnheer, H. J. Geuze, and J. J. Sixma, "Activated platelets release two types of membrane vesicles: microvesicles by surface shedding and exosomes derived from exocytosis of multivesicular bodies and alpha-granules," *Blood,* vol. 94, no. 11, pp. 3791-9, Dec 1 1999. [Online]. Available: https://www.ncbi.nlm.nih.gov/pubmed/10572093.

[43] A. Janowska-Wieczorek *et al.*, "Platelet-derived microparticles bind to hematopoietic stem/progenitor cells and enhance their engraftment," *Blood,* vol. 98, no. 10, pp. 3143-9, Nov 15 2001, doi: 10.1182/blood.v98.10.3143.

[44] M. Baj-Krzyworzeka *et al.*, "Platelet-derived microparticles stimulate proliferation, survival, adhesion, and chemotaxis of hematopoietic cells," *Exp Hematol,* vol. 30, no. 5, pp. 450-9, May 2002, doi: 10.1016/s0301-472x(02)00791-9.

[45] M. Baj-Krzyworzeka *et al.*, "Tumour-derived microvesicles carry several surface determinants and mRNA of tumour cells and transfer some of these determinants to monocytes," *Cancer Immunol Immunother,* vol. 55, no. 7, pp. 808-18, Jul 2006, doi: 10.1007/s00262-005-0075-9.

[46] J. Ratajczak *et al.*, "Embryonic stem cell-derived microvesicles reprogram hematopoietic progenitors: evidence for horizontal transfer of mRNA and protein delivery," *Leukemia,* vol. 20, no. 5, pp. 847-56, May 2006, doi: 10.1038/sj.leu.2404132.

[47] H. Valadi, K. Ekstrom, A. Bossios, M. Sjostrand, J. J. Lee, and J. O. Lotvall, "Exosome-mediated transfer of mRNAs and microRNAs is a novel mechanism of genetic exchange between cells," *Nat Cell Biol,* vol. 9, no. 6, pp. 654-9, Jun 2007, doi: 10.1038/ncb1596.

[48] T. Pisitkun, R. F. Shen, and M. A. Knepper, "Identification and proteomic profiling of exosomes in human urine," *Proc Natl Acad Sci U S A,* vol. 101, no. 36, pp. 13368-73, Sep 7 2004, doi: 10.1073/pnas.0403453101.

[49] M. P. Caby, D. Lankar, C. Vincendeau-Scherrer, G. Raposo, and C. Bonnerot, "Exosomal-like vesicles are present in human blood plasma," *Int Immunol,* vol. 17, no. 7, pp. 879-87, Jul 2005, doi: 10.1093/intimm/dxh267.

[50] A. Poliakov, M. Spilman, T. Dokland, C. L. Amling, and J. A. Mobley, "Structural heterogeneity and protein composition of exosome-like vesicles (prostasomes) in human semen," *Prostate,* vol. 69, no. 2, pp. 159-67, Feb 1 2009, doi: 10.1002/pros.20860.

[51] S. Keller, J. Ridinger, A. K. Rupp, J. W. Janssen, and P. Altevogt, "Body fluid derived exosomes as a novel template for clinical diagnostics," *J Transl Med,* vol. 9, p. 86, Jun 8 2011, doi: 10.1186/1479-5876-9-86.

[52] C. Lasser, S. E. O'Neil, L. Ekerljung, K. Ekstrom, M. Sjostrand, and J. Lotvall, "RNA-containing exosomes in human nasal secretions," *Am J Rhinol Allergy,* vol. 25, no. 2, pp. 89-93, Mar-Apr 2011, doi: 10.2500/ajra.2011.25.3573.

[53] D. M. Pegtel and S. J. Gould, "Exosomes," *Annu Rev Biochem,* vol. 88, pp. 487-514, Jun 20 2019, doi: 10.1146/annurev-biochem-013118-111902.

[54] M. Colombo, G. Raposo, and C. Thery, "Biogenesis, secretion, and intercellular interactions of exosomes and other extracellular vesicles," *Annu Rev Cell Dev Biol,* vol. 30, pp. 255-89, 2014, doi: 10.1146/annurev-cellbio-101512-122326.

[55] M. Ostrowski *et al.*, "Rab27a and Rab27b control different steps of the exosome secretion pathway," *Nat Cell Biol,* vol. 12, no. 1, pp. 19-30; sup pp 1-13, Jan 2010, doi: 10.1038/ncb2000.

[56] C. Hsu *et al.*, "Regulation of exosome secretion by Rab35 and its GTPase-activating proteins TBC1D10A-C," *J Cell Biol,* vol. 189, no. 2, pp. 223-32, Apr 19 2010, doi: 10.1083/jcb.200911018.

[57] A. Savina, M. Vidal, and M. I. Colombo, "The exosome pathway in K562 cells is regulated by Rab11," *J Cell Sci,* vol. 115, no. Pt 12, pp. 2505-15, Jun 15 2002, doi: 10.1242/jcs.115.12.2505.

[58] M. F. Baietti *et al.*, "Syndecan-syntenin-ALIX regulates the biogenesis of exosomes," *Nat Cell Biol,* vol. 14, no. 7, pp. 677-85, Jun 3 2012, doi: 10.1038/ncb2502.

[59] I. J. White, L. M. Bailey, M. R. Aghakhani, S. E. Moss, and C. E. Futter, "EGF stimulates annexin 1-dependent inward vesiculation in a multivesicular endosome subpopulation," *EMBO J,* vol. 25, no. 1, pp. 1-12, Jan 11 2006, doi: 10.1038/sj.emboj.7600759.

[60] A. Wandinger-Ness and M. Zerial, "Rab proteins and the compartmentalization of the endosomal system," *Cold Spring Harb Perspect Biol,* vol. 6, no. 11, p. a022616, Oct 23 2014, doi: 10.1101/cshperspect.a022616.

[61] A. J. Lindsay *et al.*, "Identification and characterization of multiple novel Rab-myosin Va interactions," *Mol Biol Cell,* vol. 24, no. 21, pp. 3420-34, Nov 2013, doi: 10.1091/mbc.E13-05-0236.

[62] G. Cantalupo, P. Alifano, V. Roberti, C. B. Bruni, and C. Bucci, "Rab-interacting lysosomal protein (RILP): the Rab7 effector required for transport to lysosomes," *EMBO J,* vol. 20, no. 4, pp. 683-93, Feb 15 2001, doi: 10.1093/emboj/20.4.683.

[63] E. Segura, C. Guerin, N. Hogg, S. Amigorena, and C. Thery, "CD8+ dendritic cells use LFA-1 to capture MHC-peptide complexes from exosomes in vivo," *J Immunol,* vol. 179, no. 3, pp. 1489-96, Aug 1 2007, doi: 10.4049/jimmunol.179.3.1489.

[64] S. Gurung, D. Perocheau, L. Touramanidou, and J. Baruteau, "The exosome journey: from biogenesis to uptake and intracellular signalling," *Cell Commun Signal,* vol. 19, no. 1, p. 47, Apr 23 2021, doi: 10.1186/s12964-021-00730-1.

[65] S. Rana and M. Zoller, "Exosome target cell selection and the importance of exosomal tetraspanins: a hypothesis," *Biochem Soc Trans,* vol. 39, no. 2, pp. 559-62, Apr 2011, doi: 10.1042/BST0390559.

[66] Y. Zheng, C. Tu, J. Zhang, and J. Wang, "Inhibition of multiple myelomaderived exosomes uptake suppresses the functional response in bone marrow stromal cell," *Int J Oncol,* vol. 54, no. 3, pp. 1061-1070, Mar 2019, doi: 10.3892/ijo.2019.4685.

[67] L. A. Mulcahy, R. C. Pink, and D. R. Carter, "Routes and mechanisms of extracellular vesicle uptake," *J Extracell Vesicles,* vol. 3, 2014, doi: 10.3402/jev.v3.24641.

[68] S. Horibe, T. Tanahashi, S. Kawauchi, Y. Murakami, and Y. Rikitake, "Mechanism of recipient cell-dependent differences in exosome uptake," *BMC Cancer,* vol. 18, no. 1, p. 47, Jan 6 2018, doi: 10.1186/s12885-017-3958-1.

[69] C. Escrevente, S. Keller, P. Altevogt, and J. Costa, "Interaction and uptake of exosomes by ovarian cancer cells," *BMC Cancer,* vol. 11, p. 108, Mar 27 2011, doi: 10.1186/1471-2407-11-108.

[70] D. Hanahan and R. A. Weinberg, "The hallmarks of cancer," *Cell,* vol. 100, no. 1, pp. 57-70, Jan 7 2000, doi: 10.1016/s0092-8674(00)81683-9.

[71] C. P. R. Xavier, H. R. Caires, M. A. G. Barbosa, R. Bergantim, J. E. Guimaraes, and M. H. Vasconcelos, "The Role of Extracellular Vesicles in the Hallmarks of Cancer and Drug Resistance," *Cells,* vol. 9, no. 5, May 6 2020, doi: 10.3390/cells9051141.

[72] D. Hanahan and R. A. Weinberg, "Hallmarks of cancer: the next generation," *Cell,* vol. 144,

no. 5, pp. 646-74, Mar 4 2011, doi: 10.1016/j.cell.2011.02.013.
[73] D. Hanahan, "Hallmarks of Cancer: New Dimensions," *Cancer Discov,* vol. 12, no. 1, pp. 31-46, Jan 2022, doi: 10.1158/2159-8290.CD-21-1059.
[74] I. Fillippovich *et al.*, "Transactivation-deficient p73alpha (p73Deltaexon2) inhibits apoptosis and competes with p53," *Oncogene,* vol. 20, no. 4, pp. 514-22, Jan 25 2001, doi: 10.1038/sj.onc.1204118.
[75] B. Soldevilla *et al.*, "Prognostic impact of DeltaTAp73 isoform levels and their target genes in colon cancer patients," *Clin Cancer Res,* vol. 17, no. 18, pp. 6029-39, Sep 15 2011, doi: 10.1158/1078-0432.CCR-10-2388.
[76] B. Soldevilla *et al.*, "Tumor-derived exosomes are enriched in DeltaNp73, which promotes oncogenic potential in acceptor cells and correlates with patient survival," *Hum Mol Genet,* vol. 23, no. 2, pp. 467-78, Jan 15 2014, doi: 10.1093/hmg/ddt437.
[77] G. Bradley and V. Ling, "P-glycoprotein, multidrug resistance and tumor progression," *Cancer Metastasis Rev,* vol. 13, no. 2, pp. 223-33, Jun 1994, doi: 10.1007/BF00689638.
[78] D. Sousa, R. T. Lima, and M. H. Vasconcelos, "Intercellular Transfer of Cancer Drug Resistance Traits by Extracellular Vesicles," *Trends Mol Med,* vol. 21, no. 10, pp. 595-608, Oct 2015, doi: 10.1016/j.molmed.2015.08.002.
[79] C. A. Doige and G. F. Ames, "ATP-dependent transport systems in bacteria and humans: relevance to cystic fibrosis and multidrug resistance," *Annu Rev Microbiol,* vol. 47, pp. 291-319, 1993, doi: 10.1146/annurev.mi.47.100193.001451.
[80] I. L. Urbatsch, B. Sankaran, S. Bhagat, and A. E. Senior, "Both P-glycoprotein nucleotide-binding sites are catalytically active," *J Biol Chem,* vol. 270, no. 45, pp. 26956-61, Nov 10 1995, doi: 10.1074/jbc.270.45.26956.
[81] A. Levchenko *et al.*, "Intercellular transfer of P-glycoprotein mediates acquired multidrug resistance in tumor cells," *Proc Natl Acad Sci U S A,* vol. 102, no. 6, pp. 1933-8, Feb 8 2005, doi: 10.1073/pnas.0401851102.
[82] J. Pasquier, P. Magal, C. Boulange-Lecomte, G. Webb, and F. Le Foll, "Consequences of cell-to-cell P-glycoprotein transfer on acquired multidrug resistance in breast cancer: a cell population dynamics model," *Biol Direct,* vol. 6, p. 5, Jan 26 2011, doi: 10.1186/1745-6150-6-5.
[83] M. Bebawy *et al.*, "Membrane microparticles mediate transfer of P-glycoprotein to drug sensitive cancer cells," *Leukemia,* vol. 23, no. 9, pp. 1643-9, Sep 2009, doi: 10.1038/leu.2009.76.
[84] Q. Zhang *et al.*, "Mutant KRAS Exosomes Alter the Metabolic State of Recipient Colonic Epithelial Cells," *Cell Mol Gastroenterol Hepatol,* vol. 5, no. 4, pp. 627-629 e6, 2018, doi: 10.1016/j.jcmgh.2018.01.013.
[85] V. Lopes-Rodrigues *et al.*, "Identification of the metabolic alterations associated with the multidrug resistant phenotype in cancer and their intercellular transfer mediated by extracellular vesicles," *Sci Rep,* vol. 7, p. 44541, Mar 17 2017, doi: 10.1038/srep44541.
[86] S. J. Yang *et al.*, "Predictive role of GSTP1-containing exosomes in chemotherapy-resistant breast cancer," *Gene,* vol. 623, pp. 5-14, Aug 5 2017, doi: 10.1016/j.gene.2017.04.031.
[87] A. Gutkin *et al.*, "Tumor cells derived exosomes contain hTERT mRNA and transform nonmalignant fibroblasts into telomerase positive cells," *Oncotarget,* vol. 7, no. 37, pp. 59173-59188, Sep 13 2016, doi: 10.18632/oncotarget.10384.
[88] M. Mineo *et al.*, "Exosomes released by K562 chronic myeloid leukemia cells promote angiogenesis in a Src-dependent fashion," *Angiogenesis,* vol. 15, no. 1, pp. 33-45, Mar 2012, doi: 10.1007/s10456-011-9241-1.
[89] Y. Liu *et al.*, "STAT3-regulated exosomal miR-21 promotes angiogenesis and is involved in neoplastic processes of transformed human bronchial epithelial cells," *Cancer Lett,* vol. 370, no. 1, pp. 125-35, Jan 1 2016, doi: 10.1016/j.canlet.2015.10.011.
[90] C. T. Dickman *et al.*, "Selective extracellular vesicle exclusion of miR-142-3p by oral cancer cells promotes both internal and extracellular malignant phenotypes," *Oncotarget,* vol. 8,

no. 9, pp. 15252-15266, Feb 28 2017, doi: 10.18632/oncotarget.14862.

[91] B. Li *et al.*, "piRNA-823 delivered by multiple myeloma-derived extracellular vesicles promoted tumorigenesis through re-educating endothelial cells in the tumor environment," *Oncogene,* vol. 38, no. 26, pp. 5227-5238, Jun 2019, doi: 10.1038/s41388-019-0788-4.

[92] S. Masoumi-Dehghi, S. Babashah, and M. Sadeghizadeh, "microRNA-141-3p-containing small extracellular vesicles derived from epithelial ovarian cancer cells promote endothelial cell angiogenesis through activating the JAK/STAT3 and NF-kappaB signaling pathways," *J Cell Commun Signal,* vol. 14, no. 2, pp. 233-244, Jun 2020, doi: 10.1007/s12079-020-00548-5.

[93] Z. Zeng *et al.*, "Cancer-derived exosomal miR-25-3p promotes pre-metastatic niche formation by inducing vascular permeability and angiogenesis," *Nat Commun,* vol. 9, no. 1, p. 5395, Dec 19 2018, doi: 10.1038/s41467-018-07810-w.

[94] R. Bhattacharya *et al.*, "Inhibition of vascular permeability factor/vascular endothelial growth factor-mediated angiogenesis by the Kruppel-like factor KLF2," *J Biol Chem,* vol. 280, no. 32, pp. 28848-51, Aug 12 2005, doi: 10.1074/jbc.C500200200.

[95] J. Ma, P. Wang, Y. Liu, L. Zhao, Z. Li, and Y. Xue, "Kruppel-like factor 4 regulates blood-tumor barrier permeability via ZO-1, occludin and claudin-5," *J Cell Physiol,* vol. 229, no. 7, pp. 916-26, Jul 2014, doi: 10.1002/jcp.24523.

[96] Z. Huang and Y. Feng, "Exosomes Derived From Hypoxic Colorectal Cancer Cells Promote Angiogenesis Through Wnt4-Induced beta-Catenin Signaling in Endothelial Cells," *Oncol Res,* vol. 25, no. 5, pp. 651-661, May 24 2017, doi: 10.3727/096504016X14752792816791.

[97] H. Hasan *et al.*, "Extracellular vesicles released by non-small cell lung cancer cells drive invasion and permeability in non-tumorigenic lung epithelial cells," *Sci Rep,* vol. 12, no. 1, p. 972, Jan 19 2022, doi: 10.1038/s41598-022-04940-6.

[98] K. R. Jordan *et al.*, "Extracellular vesicles from young women's breast cancer patients drive increased invasion of non-malignant cells via the Focal Adhesion Kinase pathway: a proteomic approach," *Breast Cancer Res,* vol. 22, no. 1, p. 128, Nov 23 2020, doi: 10.1186/s13058-020-01363-x.

[99] J. L. Hu *et al.*, "CAFs secreted exosomes promote metastasis and chemotherapy resistance by enhancing cell stemness and epithelial-mesenchymal transition in colorectal cancer," *Mol Cancer,* vol. 18, no. 1, p. 91, May 7 2019, doi: 10.1186/s12943-019-1019-x.

[100] S. Zhao *et al.*, "Highly-metastatic colorectal cancer cell released miR-181a-5p-rich extracellular vesicles promote liver metastasis by activating hepatic stellate cells and remodelling the tumour microenvironment," *J Extracell Vesicles,* vol. 11, no. 1, p. e12186, Jan 2022, doi: 10.1002/jev2.12186.

[101] Y. Shao *et al.*, "Colorectal cancer-derived small extracellular vesicles establish an inflammatory premetastatic niche in liver metastasis," *Carcinogenesis,* vol. 39, no. 11, pp. 1368-1379, Dec 13 2018, doi: 10.1093/carcin/bgy115.

[102] Q. Ji *et al.*, "Primary tumors release ITGBL1-rich extracellular vesicles to promote distal metastatic tumor growth through fibroblast-niche formation," *Nat Commun,* vol. 11, no. 1, p. 1211, Mar 5 2020, doi: 10.1038/s41467-020-14869-x.

[103] W. Ren *et al.*, "Exosomal miRNA-107 induces myeloid-derived suppressor cell expansion in gastric cancer," *Cancer Manag Res,* vol. 11, pp. 4023-4040, 2019, doi: 10.2147/CMAR.S198886.

[104] F. Chalmin *et al.*, "Membrane-associated Hsp72 from tumor-derived exosomes mediates STAT3-dependent immunosuppressive function of mouse and human myeloid-derived suppressor cells," *J Clin Invest,* vol. 120, no. 2, pp. 457-71, Feb 2010, doi: 10.1172/JCI40483.

[105] X. Xiang *et al.*, "Induction of myeloid-derived suppressor cells by tumor exosomes," *Int J Cancer,* vol. 124, no. 11, pp. 2621-33, Jun 1 2009, doi: 10.1002/ijc.24249.

[106] M. Szajnik, M. Czystowska, M. J. Szczepanski, M. Mandapathil, and T. L. Whiteside, "Tumor-derived microvesicles induce, expand and up-regulate biological activities of human

regulatory T cells (Treg)," *PLoS One,* vol. 5, no. 7, p. e11469, Jul 22 2010, doi: 10.1371/journal.pone.0011469.

[107] N. Yamada, Y. Kuranaga, M. Kumazaki, H. Shinohara, K. Taniguchi, and Y. Akao, "Colorectal cancer cell-derived extracellular vesicles induce phenotypic alteration of T cells into tumor-growth supporting cells with transforming growth factor-beta1-mediated suppression," *Oncotarget,* vol. 7, no. 19, pp. 27033-43, May 10 2016, doi: 10.18632/oncotarget.7041.

[108] L. Muller *et al.*, "Human tumor-derived exosomes (TEX) regulate Treg functions via cell surface signaling rather than uptake mechanisms," *Oncoimmunology,* vol. 6, no. 8, p. e1261243, 2017, doi: 10.1080/2162402X.2016.1261243.

[109] H. Shinohara *et al.*, "Regulated Polarization of Tumor-Associated Macrophages by miR-145 via Colorectal Cancer-Derived Extracellular Vesicles," *J Immunol,* vol. 199, no. 4, pp. 1505-1515, Aug 15 2017, doi: 10.4049/jimmunol.1700167.

[110] Y. Takano *et al.*, "Circulating exosomal microRNA-203 is associated with metastasis possibly via inducing tumor-associated macrophages in colorectal cancer," *Oncotarget,* vol. 8, no. 45, pp. 78598-78613, Oct 3 2017, doi: 10.18632/oncotarget.20009.

[111] K. Gabrusiewicz *et al.*, "Glioblastoma stem cell-derived exosomes induce M2 macrophages and PD-L1 expression on human monocytes," *Oncoimmunology,* vol. 7, no. 4, p. e1412909, 2018, doi: 10.1080/2162402X.2017.1412909.

[112] Z. X. Liang *et al.*, "LncRNA RPPH1 promotes colorectal cancer metastasis by interacting with TUBB3 and by promoting exosomes-mediated macrophage M2 polarization," *Cell Death Dis,* vol. 10, no. 11, p. 829, Nov 4 2019, doi: 10.1038/s41419-019-2077-0.

[113] J. E. Talmadge and D. I. Gabrilovich, "History of myeloid-derived suppressor cells," *Nat Rev Cancer,* vol. 13, no. 10, pp. 739-52, Oct 2013, doi: 10.1038/nrc3581.

[114] G. Chen *et al.*, "Exosomal PD-L1 contributes to immunosuppression and is associated with anti-PD-1 response," *Nature,* vol. 560, no. 7718, pp. 382-386, Aug 2018, doi: 10.1038/s41586-018-0392-8.

[115] J. A. Lubin, R. R. Zhang, and J. S. Kuo, "Extracellular Vesicles Containing PD-L1 Contribute to Immune Evasion in Glioblastoma," *Neurosurgery,* vol. 83, no. 3, pp. E98-E100, Sep 1 2018, doi: 10.1093/neuros/nyy295.

[116] F. L. Ricklefs *et al.*, "Immune evasion mediated by PD-L1 on glioblastoma-derived extracellular vesicles," *Sci Adv,* vol. 4, no. 3, p. eaar2766, Mar 2018, doi: 10.1126/sciadv.aar2766.

[117] M. N. Theodoraki, S. S. Yerneni, T. K. Hoffmann, W. E. Gooding, and T. L. Whiteside, "Clinical Significance of PD-L1(+) Exosomes in Plasma of Head and Neck Cancer Patients," *Clin Cancer Res,* vol. 24, no. 4, pp. 896-905, Feb 15 2018, doi: 10.1158/1078-0432.CCR-17-2664.

[118] Y. Yang *et al.*, "Exosomal PD-L1 harbors active defense function to suppress T cell killing of breast cancer cells and promote tumor growth," *Cell Res,* vol. 28, no. 8, pp. 862-864, Aug 2018, doi: 10.1038/s41422-018-0060-4.

[119] V. Fleming *et al.*, "Melanoma Extracellular Vesicles Generate Immunosuppressive Myeloid Cells by Upregulating PD-L1 via TLR4 Signaling," *Cancer Res,* vol. 79, no. 18, pp. 4715-4728, Sep 15 2019, doi: 10.1158/0008-5472.CAN-19-0053.

[120] A. Lux, C. Kahlert, R. Grutzmann, and C. Pilarsky, "c-Met and PD-L1 on Circulating Exosomes as Diagnostic and Prognostic Markers for Pancreatic Cancer," *Int J Mol Sci,* vol. 20, no. 13, Jul 5 2019, doi: 10.3390/ijms20133305.

[121] J. Condeelis and J. W. Pollard, "Macrophages: obligate partners for tumor cell migration, invasion, and metastasis," *Cell,* vol. 124, no. 2, pp. 263-6, Jan 27 2006, doi: 10.1016/j.cell.2006.01.007.

[122] D. J. Craig *et al.*, "The abscopal effect of radiation therapy," *Future Oncol,* vol. 17, no. 13, pp. 1683-1694, May 2021, doi: 10.2217/fon-2020-0994.

[123] J. Ren *et al.*, "Extracellular vesicles mediated proinflammatory macrophage phenotype induced by radiotherapy in cervical cancer," *BMC Cancer,* vol. 22, no. 1, p. 88, Jan 21 2022, doi: 10.1186/s12885-022-09194-z.

[124] V. Stary *et al.*, "Short-course radiotherapy promotes pro-inflammatory macrophages via extracellular vesicles in human rectal cancer," *J Immunother Cancer,* vol. 8, no. 2, Aug 2020, doi: 10.1136/jitc-2020-000667.

[125] W. Lin *et al.*, "Radiation-induced small extracellular vesicles as "carriages" promote tumor antigen release and trigger antitumor immunity," *Theranostics,* vol. 10, no. 11, pp. 4871-4884, 2020, doi: 10.7150/thno.43539.

[126] S. Rastogi, A. Hwang, J. Chan, and J. Y. J. Wang, "Extracellular vesicles transfer nuclear Abl-dependent and radiation-induced miR-34c into unirradiated cells to cause bystander effects," *Mol Biol Cell,* vol. 29, no. 18, pp. 2228-2242, Sep 1 2018, doi: 10.1091/mbc.E18-02-0130.

[127] W. N. Hait, "Anticancer drug development: the grand challenges," *Nat Rev Drug Discov,* vol. 9, no. 4, pp. 253-4, Apr 2010, doi: 10.1038/nrd3144.

[128] L. Hutchinson and R. Kirk, "High drug attrition rates--where are we going wrong?," *Nat Rev Clin Oncol,* vol. 8, no. 4, pp. 189-90, Mar 30 2011, doi: 10.1038/nrclinonc.2011.34.

[129] A. Peirsman *et al.*, "MISpheroID: a knowledgebase and transparency tool for minimum information in spheroid identity," *Nat Methods,* vol. 18, no. 11, pp. 1294-1303, Nov 2021, doi: 10.1038/s41592-021-01291-4.

[130] F. Hirschhaeuser, H. Menne, C. Dittfeld, J. West, W. Mueller-Klieser, and L. A. Kunz-Schughart, "Multicellular tumor spheroids: an underestimated tool is catching up again," *J Biotechnol,* vol. 148, no. 1, pp. 3-15, Jul 1 2010, doi: 10.1016/j.jbiotec.2010.01.012.

[131] R. M. Sutherland, "Cell and environment interactions in tumor microregions: the multicell spheroid model," *Science,* vol. 240, no. 4849, pp. 177-84, Apr 8 1988, doi: 10.1126/science.2451290.

[132] S. Rodriguez-Enriquez *et al.*, "Energy metabolism transition in multi-cellular human tumor spheroids," *J Cell Physiol,* vol. 216, no. 1, pp. 189-97, Jul 2008, doi: 10.1002/jcp.21392.

[133] R. E. Durand and P. L. Olive, "Resistance of tumor cells to chemo- and radiotherapy modulated by the three-dimensional architecture of solid tumors and spheroids," *Methods Cell Biol,* vol. 64, pp. 211-33, 2001, doi: 10.1016/s0091-679x(01)64015-9.

[134] L. Gaedtke, L. Thoenes, C. Culmsee, B. Mayer, and E. Wagner, "Proteomic analysis reveals differences in protein expression in spheroid versus monolayer cultures of low-passage colon carcinoma cells," *J Proteome Res,* vol. 6, no. 11, pp. 4111-8, Nov 2007, doi: 10.1021/pr0700596.

[135] P. C. De Witt Hamer, S. Leenstra, C. J. Van Noorden, and A. H. Zwinderman, "Organotypic glioma spheroids for screening of experimental therapies: how many spheroids and sections are required?," *Cytometry A,* vol. 75, no. 6, pp. 528-34, Jun 2009, doi: 10.1002/cyto.a.20716.

[136] S. E. Yeon *et al.*, "Application of concave microwells to pancreatic tumor spheroids enabling anticancer drug evaluation in a clinically relevant drug resistance model," *PLoS One,* vol. 8, no. 9, p. e73345, 2013, doi: 10.1371/journal.pone.0073345.

[137] B. Djordjevic and C. S. Lange, "Cell-cell interactions in spheroids maintained in suspension," *Acta Oncol,* vol. 45, no. 4, pp. 412-20, 2006, doi: 10.1080/02841860500520743.

[138] K. Storch *et al.*, "Three-dimensional cell growth confers radioresistance by chromatin density modification," *Cancer Res,* vol. 70, no. 10, pp. 3925-34, May 15 2010, doi: 10.1158/0008-5472.CAN-09-3848.

[139] I. Eke and N. Cordes, "Radiobiology goes 3D: how ECM and cell morphology impact on cell survival after irradiation," *Radiother Oncol,* vol. 99, no. 3, pp. 271-8, Jun 2011, doi: 10.1016/j.radonc.2011.06.007.

[140] W. Farhat *et al.*, "Factors predicting recurrence after curative resection for rectal cancer: a 16-year study," *World J Surg Oncol,* vol. 17, no. 1, p. 173, Oct 28 2019, doi: 10.1186/s12957-019-1718-1.

[141] J. Van Deun *et al.*, "The impact of disparate isolation methods for extracellular vesicles on downstream RNA profiling," *J Extracell Vesicles,* vol. 3, 2014, doi: 10.3402/jev.v3.24858.

[142] G. Vergauwen *et al.*, "Robust sequential biophysical fractionation of blood plasma to study variations in the biomolecular landscape of systemically circulating extracellular vesicles across clinical conditions," *J Extracell Vesicles,* vol. 10, no. 10, p. e12122, Aug 2021, doi: 10.1002/jev2.12122.
[143] H. Osorio *et al.*, "Proteomics Analysis of Gastric Cancer Patients with Diabetes Mellitus," *J Clin Med,* vol. 10, no. 3, Jan 21 2021, doi: 10.3390/jcm10030407.
[144] T. Suzuki, K. Fujikura, T. Higashiyama, and K. Takata, "DNA staining for fluorescence and laser confocal microscopy," *J Histochem Cytochem,* vol. 45, no. 1, pp. 49-53, Jan 1997, doi: 10.1177/002215549704500107.
[145] T. R. C. o. Radiologists, *Radiotherapy dose fractionation*, 3rd Edition ed. 2019.
[146] R. Gray *et al.*, "Adjuvant radiotherapy for rectal cancer: a systematic overview of 8507 patients from 22 randomised trials," (in English), *Lancet,* vol. 358, no. 9290, pp. 1291-1304, Oct 20 2001. [Online]. Available: <Go to ISI>://WOS:000171702500008.
[147] F. Letaief *et al.*, "Potential predictive factors for pathologic complete response after the neoadjuvant treatment of rectal adenocarcinoma: a single center experience," *Cancer Biol Med,* vol. 14, no. 3, pp. 327-334, Aug 2017, doi: 10.20892/j.issn.2095-3941.2017.0037.
[148] T. L. Whiteside, "Tumor-Derived Exosomes and Their Role in Cancer Progression," *Adv Clin Chem,* vol. 74, pp. 103-41, 2016, doi: 10.1016/bs.acc.2015.12.005.
[149] E. Endzelins *et al.*, "Extracellular Vesicles Derived from Hypoxic Colorectal Cancer Cells Confer Metastatic Phenotype to Non-metastatic Cancer Cells," *Anticancer Res,* vol. 38, no. 9, pp. 5139-5147, Sep 2018, doi: 10.21873/anticanres.12836.
[150] D. Wang *et al.*, "Exosomal miR-146a-5p and miR-155-5p promote CXCL12/CXCR7-induced metastasis of colorectal cancer by crosstalk with cancer-associated fibroblasts," *Cell Death Dis,* vol. 13, no. 4, p. 380, Apr 20 2022, doi: 10.1038/s41419-022-04825-6.
[151] S. Wang, Z. Zhang, and Q. Gao, "Transfer of microRNA-25 by colorectal cancer cell-derived extracellular vesicles facilitates colorectal cancer development and metastasis," *Mol Ther Nucleic Acids,* vol. 23, pp. 552-564, Mar 5 2021, doi: 10.1016/j.omtn.2020.11.018.
[152] L. Dong *et al.*, "Circulating Long RNAs in Serum Extracellular Vesicles: Their Characterization and Potential Application as Biomarkers for Diagnosis of Colorectal Cancer," *Cancer Epidemiol Biomarkers Prev,* vol. 25, no. 7, pp. 1158-66, Jul 2016, doi: 10.1158/1055-9965.EPI-16-0006.
[153] Y. X. Hao *et al.*, "KRAS and BRAF mutations in serum exosomes from patients with colorectal cancer in a Chinese population," *Oncol Lett,* vol. 13, no. 5, pp. 3608-3616, May 2017, doi: 10.3892/ol.2017.5889.
[154] K. Lin *et al.*, "Comprehensive proteomic profiling of serum extracellular vesicles in patients with colorectal liver metastases identifies a signature for non-invasive risk stratification and early-response evaluation," *Mol Cancer,* vol. 21, no. 1, p. 91, Apr 1 2022, doi: 10.1186/s12943-022-01562-4.
[155] T. Bjornetro *et al.*, "An experimental strategy unveiling exosomal microRNAs 486-5p, 181a-5p and 30d-5p from hypoxic tumour cells as circulating indicators of high-risk rectal cancer," *J Extracell Vesicles,* vol. 8, no. 1, p. 1567219, 2019, doi: 10.1080/20013078.2019.1567219.
[156] U. Strybel *et al.*, "Molecular Composition of Serum Exosomes Could Discriminate Rectal Cancer Patients with Different Responses to Neoadjuvant Radiotherapy," *Cancers (Basel),* vol. 14, no. 4, Feb 16 2022, doi: 10.3390/cancers14040993.
[157] G. Emons *et al.*, "Chemoradiotherapy Resistance in Colorectal Cancer Cells is Mediated by Wnt/beta-catenin Signaling," *Mol Cancer Res,* vol. 15, no. 11, pp. 1481-1490, Nov 2017, doi: 10.1158/1541-7786.MCR-17-0205.
[158] S. Subramaniam, C. Stansberg, and C. Cunningham, "The interleukin 1 receptor family," *Dev Comp Immunol,* vol. 28, no. 5, pp. 415-28, May 3 2004, doi: 10.1016/j.dci.2003.09.016.
[159] E. V. Cutsem *et al.*, "Phase 1/2a trial of nadunolimab, a first-in-class fully humanized monoclonal antibody against IL1RAP, in combination with gemcitabine and nab-paclitaxel (GN) in patients with pancreatic adenocarcinoma (PDAC)," *Journal of Clinical Oncology,* vol.

40, no. 16_suppl, pp. 4141-4141, 2022, doi: 10.1200/JCO.2022.40.16_suppl.4141.
[160] X. X. He *et al.*, "Macrophage migration inhibitory factor promotes colorectal cancer," *Mol Med,* vol. 15, no. 1-2, pp. 1-10, Jan-Feb 2009, doi: 10.2119/molmed.2008.00107.
[161] K. T. Morris, R. A. Nofchissey, I. V. Pinchuk, and E. J. Beswick, "Chronic macrophage migration inhibitory factor exposure induces mesenchymal epithelial transition and promotes gastric and colon cancers," *PLoS One,* vol. 9, no. 6, p. e98656, 2014, doi: 10.1371/journal.pone.0098656.
[162] S. H. Lee *et al.*, "Macrophage migration inhibitory factor (MIF) inhibitor 4-IPP downregulates stemness phenotype and mesenchymal trans-differentiation after irradiation in glioblastoma multiforme," *PLoS One,* vol. 16, no. 9, p. e0257375, 2021, doi: 10.1371/journal.pone.0257375.
[163] P. Pileri *et al.*, "FAT1: a potential target for monoclonal antibody therapy in colon cancer," *Br J Cancer,* vol. 115, no. 1, pp. 40-51, Jun 28 2016, doi: 10.1038/bjc.2016.145.
[164] C. E. de Bock *et al.*, "The Fat1 cadherin is overexpressed and an independent prognostic factor for survival in paired diagnosis-relapse samples of precursor B-cell acute lymphoblastic leukemia," *Leukemia,* vol. 26, no. 5, pp. 918-26, May 2012, doi: 10.1038/leu.2011.319.
[165] K. Chosdol *et al.*, "Frequent loss of heterozygosity and altered expression of the candidate tumor suppressor gene 'FAT' in human astrocytic tumors," *BMC Cancer,* vol. 9, p. 5, Jan 7 2009, doi: 10.1186/1471-2407-9-5.
[166] S. P. Reddy, W. F. Raslan, S. Gooneratne, S. Kathuria, and J. E. Marks, "Prognostic significance of keratinization in nasopharyngeal carcinoma," *Am J Otolaryngol,* vol. 16, no. 2, pp. 103-8, Mar-Apr 1995, doi: 10.1016/0196-0709(95)90040-3.
[167] W. Weichert *et al.*, "Proposal of a prognostically relevant grading scheme for pulmonary squamous cell carcinoma," *Eur Respir J,* vol. 47, no. 3, pp. 938-46, Mar 2016, doi: 10.1183/13993003.00937-2015.
[168] G. Li, D. Li, T. Wang, and S. He, "Pyrimidine Biosynthetic Enzyme CAD: Its Function, Regulation, and Diagnostic Potential," *Int J Mol Sci,* vol. 22, no. 19, Sep 23 2021, doi: 10.3390/ijms221910253.
[169] H. Wang, X. Wang, L. Xu, J. Zhang, and H. Cao, "High expression levels of pyrimidine metabolic rate-limiting enzymes are adverse prognostic factors in lung adenocarcinoma: a study based on The Cancer Genome Atlas and Gene Expression Omnibus datasets," *Purinergic Signal,* vol. 16, no. 3, pp. 347-366, Sep 2020, doi: 10.1007/s11302-020-09711-4.
[170] J. W. Jung, S. Y. Hwang, J. S. Hwang, E. S. Oh, S. Park, and I. O. Han, "Ionising radiation induces changes associated with epithelial-mesenchymal transdifferentiation and increased cell motility of A549 lung epithelial cells," *Eur J Cancer,* vol. 43, no. 7, pp. 1214-24, May 2007, doi: 10.1016/j.ejca.2007.01.034.
[171] R. K. Kim *et al.*, "Radiation driven epithelial-mesenchymal transition is mediated by Notch signaling in breast cancer," *Oncotarget,* vol. 7, no. 33, pp. 53430-53442, Aug 16 2016, doi: 10.18632/oncotarget.10802.
[172] C. Moncharmont *et al.*, "Radiation-enhanced cell migration/invasion process: a review," *Crit Rev Oncol Hematol,* vol. 92, no. 2, pp. 133-42, Nov 2014, doi: 10.1016/j.critrevonc.2014.05.006.

Supplementary Data

Supplementary Table 1 - Tukey's multiple comparison tests for compactness over the several days of culture, for all culture conditions. Row 1- Day 1; Row 2 - Day 2; Row 3 - Day 4; Row 4 - Day 8. Significance level considered was 5%.

Tukey's multiple comparisons test	Summary	Adjusted P Value
DMEM/ F-12_1000		
Row 1 vs. Row 2	ns	0,1830
Row 1 vs. Row 3	ns	0,1186
Row 1 vs. Row 4	ns	0,2397
Row 2 vs. Row 3	ns	0,7683
Row 2 vs. Row 4	ns	0,9520
Row 3 vs. Row 4	ns	0,9930
DMEM/ F-12_2000		
Row 1 vs. Row 2	ns	0,4518
Row 1 vs. Row 3	ns	0,2779
Row 1 vs. Row 4	ns	0,6080
Row 2 vs. Row 3	ns	0,9905
Row 2 vs. Row 4	ns	0,9905
Row 3 vs. Row 4	ns	0,9905
DMEM/ F-12_5000		
Row 1 vs. Row 2	ns	0,8109
Row 1 vs. Row 3	ns	0,2431
Row 1 vs. Row 4	ns	0,7896
Row 2 vs. Row 3	ns	0,5309
Row 2 vs. Row 4	ns	0,9331
Row 3 vs. Row 4	ns	0,8692
DMEM/ F-12_8000		
Row 1 vs. Row 2	ns	0,7578
Row 1 vs. Row 3	ns	0,0860
Row 1 vs. Row 4	ns	0,7683
Row 2 vs. Row 3	ns	0,9995
Row 2 vs. Row 4	ns	0,9803
Row 3 vs. Row 4	ns	0,9997
DMEM/ F-12_10000		
Row 1 vs. Row 2	ns	0,2012
Row 1 vs. Row 3	ns	0,2012
Row 1 vs. Row 4	ns	0,9204
Row 2 vs. Row 3	ns	>0,9999
Row 2 vs. Row 4	ns	0,5851
Row 3 vs. Row 4	ns	0,7969
DMEM/ F-12_15000		
Row 1 vs. Row 2	ns	0,2397
Row 1 vs. Row 3	ns	0,1973
Row 1 vs. Row 4	ns	0,0838
Row 2 vs. Row 3	ns	0,7049

Row 2 vs. Row 4	ns	0,9905
Row 3 vs. Row 4	ns	0,6371
DMEM/ F-12_20000		
Row 1 vs. Row 2	ns	0,4061
Row 1 vs. Row 3	ns	0,5587
Row 1 vs. Row 4	ns	0,9773
Row 2 vs. Row 3	ns	0,4834
Row 2 vs. Row 4	ns	0,9905
Row 3 vs. Row 4	ns	0,0924
RPMI_1000		
Row 1 vs. Row 2	ns	0,2189
Row 1 vs. Row 3	ns	0,3460
Row 1 vs. Row 4	ns	0,3652
Row 2 vs. Row 3	ns	0,9207
Row 2 vs. Row 4	ns	0,9307
Row 3 vs. Row 4	ns	0,9773
RPMI_2000		
Row 1 vs. Row 2	ns	0,2085
Row 1 vs. Row 3	ns	0,6740
Row 1 vs. Row 4	ns	0,5491
Row 2 vs. Row 3	ns	0,7851
Row 2 vs. Row 4	ns	0,9825
Row 3 vs. Row 4	ns	0,2203
RPMI_5000		
Row 1 vs. Row 2	ns	0,3002
Row 1 vs. Row 3	ns	0,4701
Row 1 vs. Row 4	ns	0,4960
Row 2 vs. Row 3	ns	0,5587
Row 2 vs. Row 4	ns	>0,9999
Row 3 vs. Row 4	ns	0,8035
RPMI_8000		
Row 1 vs. Row 2	ns	0,1382
Row 1 vs. Row 3	ns	0,8251
Row 1 vs. Row 4	ns	0,6274
Row 2 vs. Row 3	ns	0,2982
Row 2 vs. Row 4	ns	0,8520
Row 3 vs. Row 4	ns	0,6371
RPMI_10000		
Row 1 vs. Row 2	ns	0,9520
Row 1 vs. Row 3	ns	0,9060
Row 1 vs. Row 4	ns	0,7683
Row 2 vs. Row 3	ns	>0,9999
Row 2 vs. Row 4	ns	0,9872
Row 3 vs. Row 4	ns	0,8692
RPMI_15000		
Row 1 vs. Row 2	ns	0,7049
Row 1 vs. Row 3	ns	0,9973
Row 1 vs. Row 4	ns	0,4777
Row 2 vs. Row 3	ns	0,7683

Row 2 vs. Row 4	ns	0,9934
Row 3 vs. Row 4	ns	0,9251
RPMI_20000		
Row 1 vs. Row 2	ns	0,9942
Row 1 vs. Row 3	ns	0,9307
Row 1 vs. Row 4	ns	0,3862
Row 2 vs. Row 3	ns	0,9995
Row 2 vs. Row 4	ns	0,9060
Row 3 vs. Row 4	ns	0,7956
DMEM_LG_1000		
Row 1 vs. Row 2	ns	0,0604
Row 1 vs. Row 3	ns	0,1638
Row 1 vs. Row 4	ns	0,0706
Row 2 vs. Row 3	ns	0,6413
Row 2 vs. Row 4	ns	0,4834
Row 3 vs. Row 4	ns	0,5252
DMEM_LG_2000		
Row 1 vs. Row 2	ns	0,2922
Row 1 vs. Row 3	ns	0,2097
Row 1 vs. Row 4	ns	0,7296
Row 2 vs. Row 3	ns	0,7683
Row 2 vs. Row 4	ns	0,8996
Row 3 vs. Row 4	ns	0,8704
DMEM_LG_5000		
Row 1 vs. Row 2	ns	0,1597
Row 1 vs. Row 3	ns	0,1749
Row 1 vs. Row 4	ns	0,2841
Row 2 vs. Row 3	ns	0,8569
Row 2 vs. Row 4	ns	0,9520
Row 3 vs. Row 4	ns	0,8300
DMEM_LG_8000		
Row 1 vs. Row 2	ns	0,1495
Row 1 vs. Row 3	ns	0,1295
Row 1 vs. Row 4	ns	0,1135
Row 2 vs. Row 3	ns	0,7919
Row 2 vs. Row 4	ns	0,9307
Row 3 vs. Row 4	ns	0,8364
DMEM_LG_10000		
Row 1 vs. Row 2	ns	0,1512
Row 1 vs. Row 3	ns	0,2184
Row 1 vs. Row 4	ns	0,3165
Row 2 vs. Row 3	ns	0,8035
Row 2 vs. Row 4	ns	0,9571
Row 3 vs. Row 4	ns	0,9060
DMEM_LG_15000		
Row 1 vs. Row 2	ns	0,3819
Row 1 vs. Row 3	ns	0,4517
Row 1 vs. Row 4	ns	0,4962
Row 2 vs. Row 3	ns	0,8251

Row 2 vs. Row 4	ns	0,9373
Row 3 vs. Row 4	ns	0,7683
DMEM_LG_20000		
Row 1 vs. Row 2	ns	0,4619
Row 1 vs. Row 3	ns	0,7295
Row 1 vs. Row 4	ns	0,5635
Row 2 vs. Row 3	ns	0,8833
Row 2 vs. Row 4	ns	0,9060
Row 3 vs. Row 4	ns	0,4217

Supplementary Table 2 - Tukey's multiple comparison tests for diameter over the several days of culture, for all culture conditions. Row 1- Day 1; Row 2 - Day 2; Row 3 - Day 4; Row 4 - Day 8. Significance level considered was 5%

Tukey's multiple comparisons test	Summary	Adjusted P Value
DMEM/ F-12_1000		
Row 1 vs. Row 2	ns	0,0511
Row 1 vs. Row 3	ns	0,0579
Row 1 vs. Row 4	ns	0,0768
Row 2 vs. Row 3	ns	0,2878
Row 2 vs. Row 4	ns	0,2587
Row 3 vs. Row 4	ns	0,5766
DMEM/ F-12_2000		
Row 1 vs. Row 2	*	0,0209
Row 1 vs. Row 3	**	0,0015
Row 1 vs. Row 4	*	0,0150
Row 2 vs. Row 3	ns	0,3039
Row 2 vs. Row 4	ns	0,2614
Row 3 vs. Row 4	ns	0,2745
DMEM/ F-12_5000		
Row 1 vs. Row 2	ns	0,0971
Row 1 vs. Row 3	**	0,0011
Row 1 vs. Row 4	**	0,0090
Row 2 vs. Row 3	ns	0,1856
Row 2 vs. Row 4	ns	0,2159
Row 3 vs. Row 4	ns	0,4004
DMEM/ F-12_8000		
Row 1 vs. Row 2	ns	0,0568
Row 1 vs. Row 3	**	0,0020
Row 1 vs. Row 4	**	0,0033
Row 2 vs. Row 3	ns	0,1029
Row 2 vs. Row 4	ns	0,1024
Row 3 vs. Row 4	ns	0,2308
DMEM/ F-12_10000		
Row 1 vs. Row 2	ns	0,1027
Row 1 vs. Row 3	***	0,0007
Row 1 vs. Row 4	**	0,0053
Row 2 vs. Row 3	ns	0,3746
Row 2 vs. Row 4	ns	0,2787
Row 3 vs. Row 4	ns	0,1733
DMEM/ F-12_15000		
Row 1 vs. Row 2	ns	0,1741
Row 1 vs. Row 3	ns	0,0601
Row 1 vs. Row 4	*	0,0420
Row 2 vs. Row 3	ns	0,0637
Row 2 vs. Row 4	*	0,0443
Row 3 vs. Row 4	ns	0,0542

DMEM/ F-12_20000		
Row 1 vs. Row 2	*	0,0475
Row 1 vs. Row 3	*	0,0207
Row 1 vs. Row 4	**	0,0073
Row 2 vs. Row 3	*	0,0152
Row 2 vs. Row 4	**	0,0065
Row 3 vs. Row 4	*	0,0173
RPMI_1000		
Row 1 vs. Row 2	*	0,0180
Row 1 vs. Row 3	*	0,0464
Row 1 vs. Row 4	ns	0,0869
Row 2 vs. Row 3	ns	0,5449
Row 2 vs. Row 4	ns	0,4885
Row 3 vs. Row 4	ns	0,5900
RPMI_2000		
Row 1 vs. Row 2	**	0,0041
Row 1 vs. Row 3	**	0,0041
Row 1 vs. Row 4	ns	0,0936
Row 2 vs. Row 3	ns	0,1801
Row 2 vs. Row 4	ns	0,2559
Row 3 vs. Row 4	ns	0,3086
RPMI_5000		
Row 1 vs. Row 2	*	0,0147
Row 1 vs. Row 3	**	0,0096
Row 1 vs. Row 4	*	0,0102
Row 2 vs. Row 3	*	0,0127
Row 2 vs. Row 4	ns	0,0613
Row 3 vs. Row 4	ns	0,1682
RPMI_8000		
Row 1 vs. Row 2	***	0,0006
Row 1 vs. Row 3	**	0,0012
Row 1 vs. Row 4	*	0,0191
Row 2 vs. Row 3	ns	0,1046
Row 2 vs. Row 4	ns	0,1558
Row 3 vs. Row 4	ns	0,2002
RPMI_10000		
Row 1 vs. Row 2	*	0,0126
Row 1 vs. Row 3	*	0,0183
Row 1 vs. Row 4	*	0,0251
Row 2 vs. Row 3	ns	0,2615
Row 2 vs. Row 4	ns	0,2105
Row 3 vs. Row 4	ns	0,2191
RPMI_15000		
Row 1 vs. Row 2	**	0,0014
Row 1 vs. Row 3	*	0,0168
Row 1 vs. Row 4	*	0,0299
Row 2 vs. Row 3	ns	0,1107
Row 2 vs. Row 4	ns	0,1124
Row 3 vs. Row 4	ns	0,4578

RPMI_20000		
Row 1 vs. Row 2	*	0,0214
Row 1 vs. Row 3	*	0,0466
Row 1 vs. Row 4	*	0,0342
Row 2 vs. Row 3	ns	0,1571
Row 2 vs. Row 4	ns	0,0556
Row 3 vs. Row 4	*	0,0111
DMEM_LG_1000		
Row 1 vs. Row 2	ns	0,2699
Row 1 vs. Row 3	ns	0,2427
Row 1 vs. Row 4	ns	0,1154
Row 2 vs. Row 3	ns	0,2140
Row 2 vs. Row 4	*	0,0235
Row 3 vs. Row 4	ns	0,9963
DMEM_LG_2000		
Row 1 vs. Row 2	*	0,0219
Row 1 vs. Row 3	*	0,0277
Row 1 vs. Row 4	*	0,0133
Row 2 vs. Row 3	ns	0,2669
Row 2 vs. Row 4	*	0,0176
Row 3 vs. Row 4	ns	0,9870
DMEM_LG_5000		
Row 1 vs. Row 2	ns	0,0921
Row 1 vs. Row 3	ns	0,0674
Row 1 vs. Row 4	ns	0,0630
Row 2 vs. Row 3	ns	0,0948
Row 2 vs. Row 4	ns	0,0577
Row 3 vs. Row 4	ns	0,2620
DMEM_LG_8000		
Row 1 vs. Row 2	ns	0,0620
Row 1 vs. Row 3	**	0,0064
Row 1 vs. Row 4	*	0,0102
Row 2 vs. Row 3	ns	0,0592
Row 2 vs. Row 4	*	0,0188
Row 3 vs. Row 4	ns	0,4494
DMEM_LG_10000		
Row 1 vs. Row 2	*	0,0133
Row 1 vs. Row 3	**	0,0076
Row 1 vs. Row 4	**	0,0014
Row 2 vs. Row 3	ns	0,0611
Row 2 vs. Row 4	*	0,0230
Row 3 vs. Row 4	ns	0,2211
DMEM_LG_15000		
Row 1 vs. Row 2	*	0,0195
Row 1 vs. Row 3	**	0,0093
Row 1 vs. Row 4	*	0,0198
Row 2 vs. Row 3	**	0,0055
Row 2 vs. Row 4	*	0,0437
Row 3 vs. Row 4	ns	0,2484

DMEM_LG_20000		
Row 1 vs. Row 2	*	0,0211
Row 1 vs. Row 3	*	0,0111
Row 1 vs. Row 4	*	0,0231
Row 2 vs. Row 3	*	0,0246
Row 2 vs. Row 4	*	0,0409
Row 3 vs. Row 4	ns	0,1152

Supplementary Table 3 | Tukey's multiple comparison test results regarding the differences in ATP production (luminescence) in spheroids, caused by size and independently of media

Tukey's multiple comparisons test	Summary	Adjusted P Value
1000 vs. 2000	ns	0,0776
1000 vs. 5000	**	0,0041
1000 vs. 8000	****	<0,0001
1000 vs. 10000	****	<0,0001
1000 vs. 15000	****	<0,0001
1000 vs. 20000	****	<0,0001
2000 vs. 5000	ns	0,0935
2000 vs. 8000	**	0,0052
2000 vs. 10000	**	0,0043
2000 vs. 15000	****	<0,0001
2000 vs. 20000	****	<0,0001
5000 vs. 8000	ns	0,1161
5000 vs. 10000	ns	0,0517
5000 vs. 15000	***	0,0005
5000 vs. 20000	***	0,0005
8000 vs. 10000	ns	>0,9999
8000 vs. 15000	**	0,0039
8000 vs. 20000	*	0,0158
10000 vs. 15000	***	0,0009
10000 vs. 20000	***	0,0004
15000 vs. 20000	ns	>0,9999

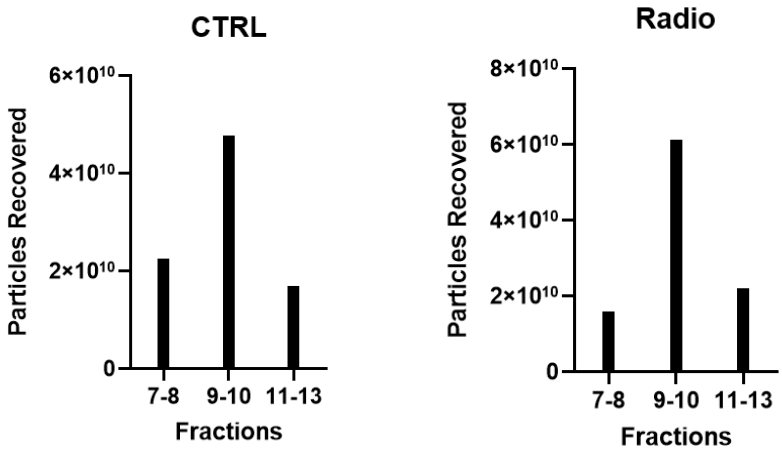

Supplementary Figure 1 - Distribution of particles, measured by NTA, recovered between the 7th and 13th fractions of the OptiPrep Density Gradient. Previous results detected no appreciable number of particles in any other fractions.

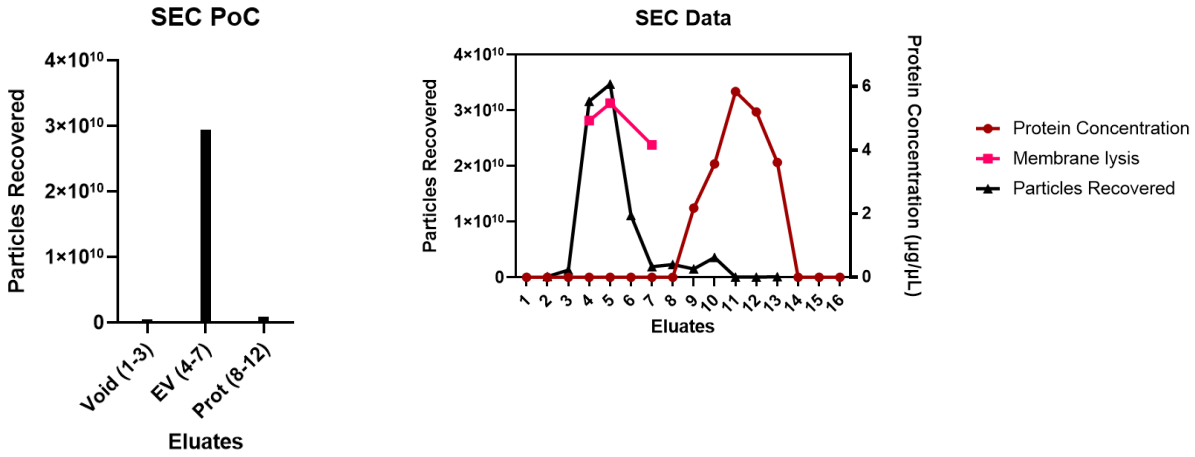

Supplementary Figure 2 - Size Exclusion Chromatography proof of concept (PoC). Particles were only vestigial detected outside eluates 4-7. Protein concentration (without use of Amicon Ultra filters) was barely detectable in the Qubit assay, and only started being detectable on eluate 9, while particles were detected via NTA up to eluate 7. Applying SDS to eluates 4-7 individually allowed for protein detection through EV membrane disruption.

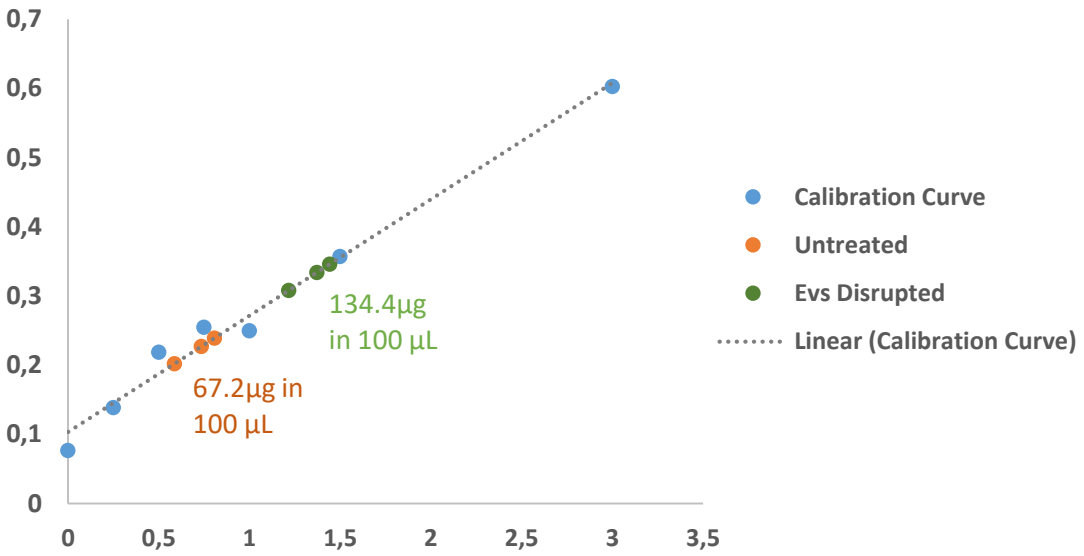

Supplementary Figure 3 - Protein quantification on EV isolates. Untreated EVs in orange and treated EVs with RIPA buffer in green. Calibration curve performed with a series of stock BSA solutions (blue). Membrane disruption through RIPA leads to exposure of intravesicular proteins and an increase in protein concentration.

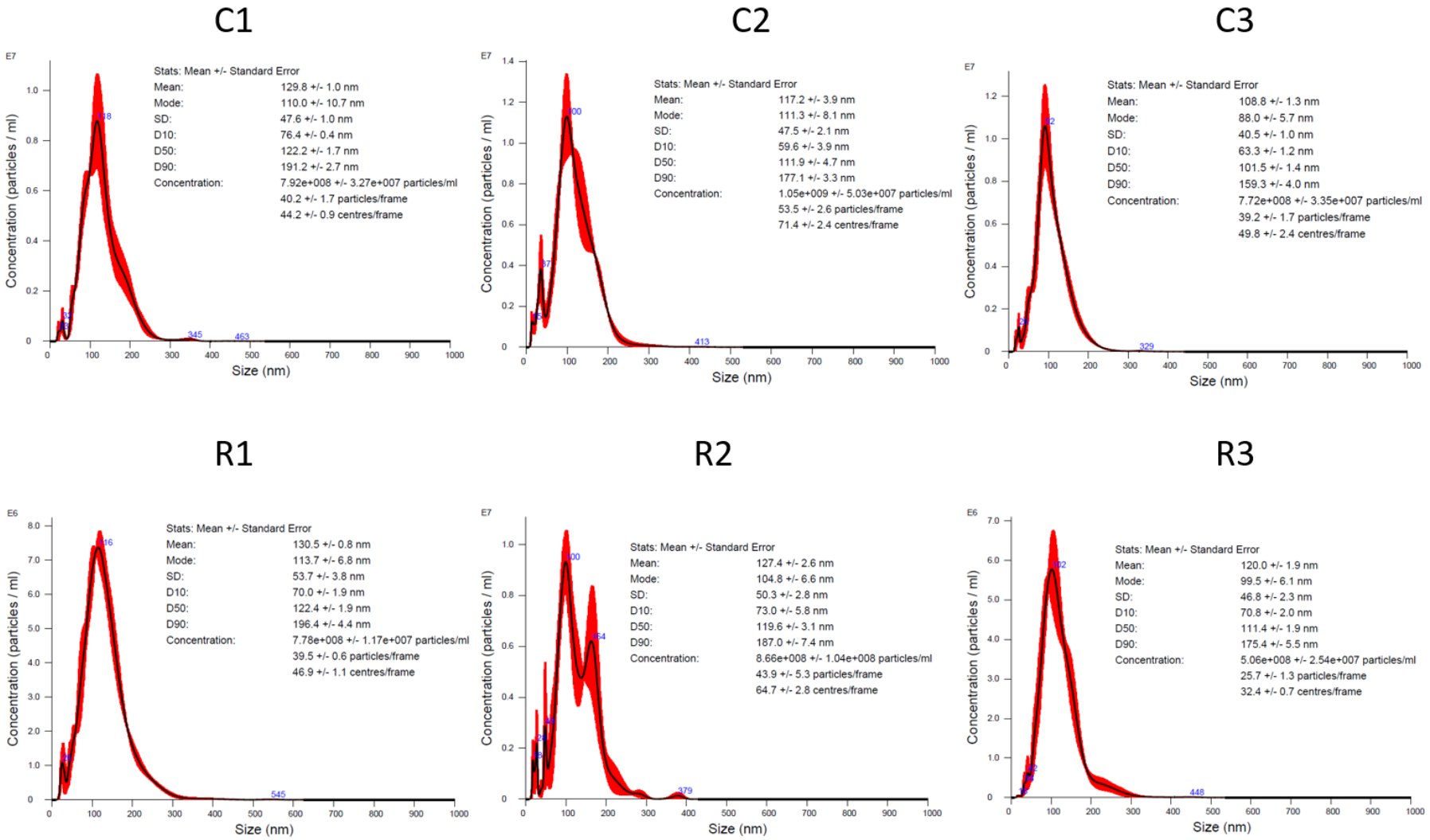

Supplementary Figure 4 | Nanoparticle tracking analysis data for the analysed samples through proteomics.

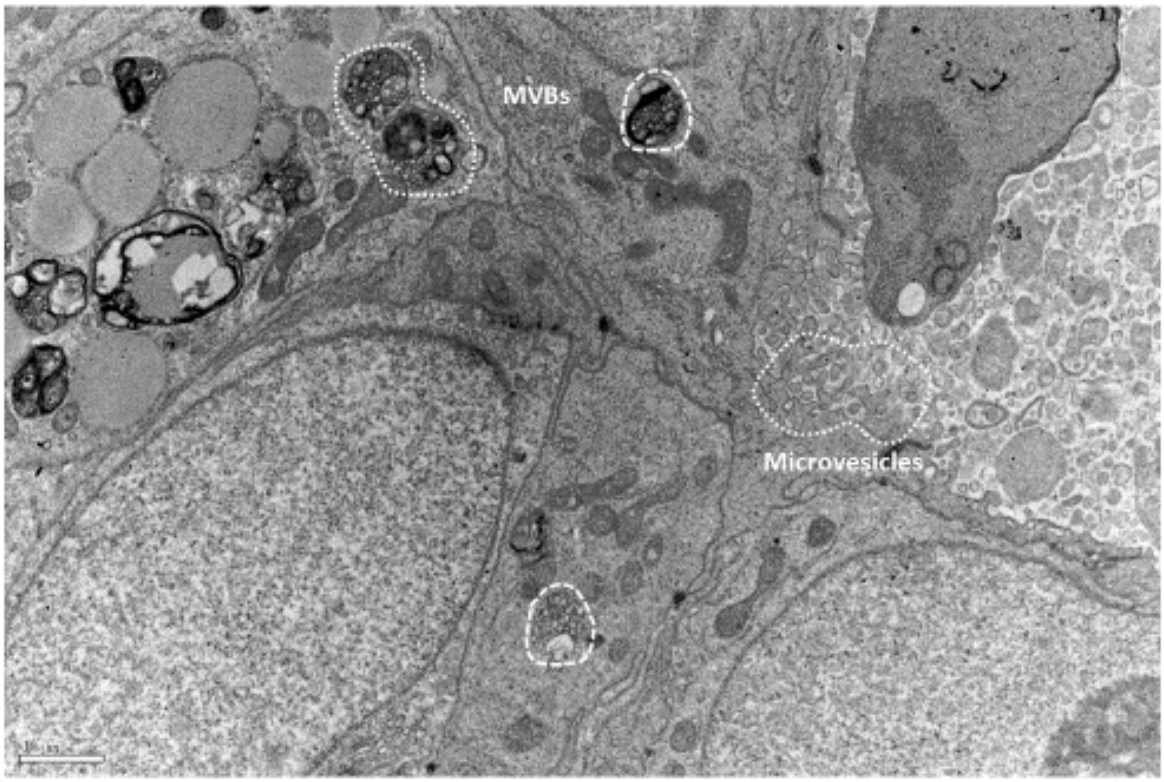

Supplementary Figure 5 - Presence of MVBs and microvesicle shedding in a cell that composes a rectal cancer spheroid. Microvesicles are pinpointed by the dotted circles and MVBs are illustrated by the dashed line circles. A representative image is shown. Scale bar for 1μm.

Supplementary Table 4 - Summary of top hitting proteins in proteomics, among all samples independently of treatment.

	Checked	Protein FDI	Master	Accession	Description
1		High	✓	P98160	Basement membrane-specific heparan sulfate proteoglycan core protein OS
2		High	✓	Q9Y490	Talin-1 OS=Homo sapiens OX=9606 GN=TLN1 PE=1 SV=3
3		High	✓	Q07954	Prolow-density lipoprotein receptor-related protein 1 OS=Homo sapiens OX=
4		High	✓	P21333	Filamin-A OS=Homo sapiens OX=9606 GN=FLNA PE=1 SV=4
5		High	✓	O00468	Agrin OS=Homo sapiens OX=9606 GN=AGRN PE=1 SV=6
6		High	✓	P02768	Albumin OS=Homo sapiens OX=9606 GN=ALB PE=1 SV=2
7		High	✓	O15230	Laminin subunit alpha-5 OS=Homo sapiens OX=9606 GN=LAMA5 PE=1 SV
8		High	✓	P49327	Fatty acid synthase OS=Homo sapiens OX=9606 GN=FASN PE=1 SV=3
9		High	✓	P02751	Fibronectin OS=Homo sapiens OX=9606 GN=FN1 PE=1 SV=5
10		High	✓	P07996	Thrombospondin-1 OS=Homo sapiens OX=9606 GN=THBS1 PE=1 SV=2
11		High	✓	P35579	Myosin-9 OS=Homo sapiens OX=9606 GN=MYH9 PE=1 SV=4
12		High	✓	Q9H6S3	Epidermal growth factor receptor kinase substrate 8-like protein 2 OS=Homo
13		High	✓	P11047	Laminin subunit gamma-1 OS=Homo sapiens OX=9606 GN=LAMC1 PE=1 S
14		High	✓	Q00610	Clathrin heavy chain 1 OS=Homo sapiens OX=9606 GN=CLTC PE=1 SV=5
15		High	✓	P14618	Pyruvate kinase PKM OS=Homo sapiens OX=9606 GN=PKM PE=1 SV=4
16		High	✓	P07942	Laminin subunit beta-1 OS=Homo sapiens OX=9606 GN=LAMB1 PE=1 SV=
17		High	✓	P18206	Vinculin OS=Homo sapiens OX=9606 GN=VCL PE=1 SV=4
18		High	✓	P11142	Heat shock cognate 71 kDa protein OS=Homo sapiens OX=9606 GN=HSPA
19		High	✓	Q15582	Transforming growth factor-beta-induced protein ig-h3 OS=Homo sapiens O
20		High	✓	P04264	Keratin, type II cytoskeletal 1 OS=Homo sapiens OX=9606 GN=KRT1 PE=1
21		High	✓	P04406	Glyceraldehyde-3-phosphate dehydrogenase OS=Homo sapiens OX=9606
22		High	✓	P07355	Annexin A2 OS=Homo sapiens OX=9606 GN=ANXA2 PE=1 SV=2
23		High	✓	P06733	Alpha-enolase OS=Homo sapiens OX=9606 GN=ENO1 PE=1 SV=2
24		High	✓	P35527	Keratin, type I cytoskeletal 9 OS=Homo sapiens OX=9606 GN=KRT9 PE=1
25		High	✓	P08238	Heat shock protein HSP 90-beta OS=Homo sapiens OX=9606 GN=HSP90A

Supplementary Table 5 - Summary of top hitting proteins in proteomics, independent of treatment, excluding the two paired samples isolated at LECR.

	Checked	Protein FDI	Master	Accession	Description
1		High	✓	P98160	Basement membrane-specific heparan sulfate proteoglycan
2		High	✓	P60709	Actin, cytoplasmic 1 OS=Homo sapiens OX=9606 GN=ACT
3		High	✓	P02751	Fibronectin OS=Homo sapiens OX=9606 GN=FN1 PE=1 S\
4		High	✓	O00468	Agrin OS=Homo sapiens OX=9606 GN=AGRN PE=1 SV=6
5		High	✓	P02768	Albumin OS=Homo sapiens OX=9606 GN=ALB PE=1 SV=2
6		High	✓	P07996	Thrombospondin-1 OS=Homo sapiens OX=9606 GN=THBS
7		High	✓	P06396	Gelsolin OS=Homo sapiens OX=9606 GN=GSN PE=1 SV=
8		High	✓	P04406	Glyceraldehyde-3-phosphate dehydrogenase OS=Homo sa
9		High	✓	O00560	Syntenin-1 OS=Homo sapiens OX=9606 GN=SDCBP PE=1
10		High	✓	Q9Y490	Talin-1 OS=Homo sapiens OX=9606 GN=TLN1 PE=1 SV=3
11		High	✓	Q15582	Transforming growth factor-beta-induced protein ig-h3 OS=I
12		High	✓	P14618	Pyruvate kinase PKM OS=Homo sapiens OX=9606 GN=PK
13		High	✓	Q9H6S3	Epidermal growth factor receptor kinase substrate 8-like pro
14		High	✓	P23142	Fibulin-1 OS=Homo sapiens OX=9606 GN=FBLN1 PE=1 S\
15		High	✓	P00734	Prothrombin OS=Homo sapiens OX=9606 GN=F2 PE=1 SV
16		High	✓	P15311	Ezrin OS=Homo sapiens OX=9606 GN=EZR PE=1 SV=4
17		High	✓	P11142	Heat shock cognate 71 kDa protein OS=Homo sapiens OX=
18		High	✓	Q07954	Prolow-density lipoprotein receptor-related protein 1 OS=Ho
19		High	✓	P01024	Complement C3 OS=Homo sapiens OX=9606 GN=C3 PE=
20		High	✓	P21333	Filamin-A OS=Homo sapiens OX=9606 GN=FLNA PE=1 S\
21		High	✓	P04264	Keratin, type II cytoskeletal 1 OS=Homo sapiens OX=9606 (
22		High	✓	P07437	Tubulin beta chain OS=Homo sapiens OX=9606 GN=TUBB
23		High	✓	O15230	Laminin subunit alpha-5 OS=Homo sapiens OX=9606 GN=I
24		High	✓	P35527	Keratin, type I cytoskeletal 9 OS=Homo sapiens OX=9606 C
25		High	✓	P05187	Alkaline phosphatase, placental type OS=Homo sapiens OX

IRON METABOLISM IN COLORECTAL CANCER: A BALANCING ACT

Diogo Estêvão[1,2]*, Miguel da Cruz-Ribeiro[1,2]*, Ana P. Cardoso[1], Ângela M. Costa[1], Maria J. Oliveira[1,3], Tiago L. Duarte[1], Tânia B. da Cruz[1#]

[1]i3S - Institute for Research & Innovation in Health, University of Porto, Portugal;
[2]ICBAS - Institute of Biomedical Sciences Abel Salazar; University of Porto, Portugal;
[3]FMUP - Faculty of Medicine, Pathology department, University of Porto, Portugal.
*Equal contribution

[#]Corresponding author: tcruz@3s.up.pt

ORCID:
Diogo Estêvão: 0000-0001-6457-2356
Miguel da Cruz-Ribeiro: 0000-0001-5630-8635
Ana P. Cardoso: 0000-0003-1987-0316
Ângela M. Costa: 0000-0002-8911-1043
Maria J. Oliveira: 0000-0002-0724-0272
Tiago Duarte: 0000-0002-4901-4580
Tânia B. da Cruz: 0000-0001-7051-040X

Acknowledgements: Not applicable.

ABSTRACT

Background: Colorectal cancer (CRC) is the third most commonly diagnosed cancer and the second deadliest malignancy worldwide. Current dietary habits are associated with increased levels of iron and heme, both of which increase the risk of developing CRC. The harmful effects of iron overload are related to the induction of iron-mediated pro-tumorigenic pathways, including carcinogenesis and hyperproliferation. On the other hand, iron deficiency may also promote CRC development and progression by contributing to genome instability, therapy resistance, and diminished immune responses. In addition to the relevance of systemic iron levels, iron-regulatory mechanisms in the tumor microenvironment are also believed to play a significant role in CRC and to influence disease outcome. Furthermore, CRC cells are more prone to escape iron-dependent cell death (ferroptosis) than non-malignant cells due to the constitutive activation of antioxidant genes expression. There is wide evidence that inhibition of ferroptosis may contribute to the resistance of CRC to established chemotherapeutic regimens. As such, ferroptosis inducers represent promising therapeutic drugs for CRC.

Conclusions and perspectives: This review addresses the complex role of iron in CRC, particularly in what concerns the consequences of iron excess or deprivation in tumor development and progression. We also dissect the regulation of cellular iron metabolism in the CRC microenvironment and emphasize the role of hypoxia and of oxidative stress (*e.g.* ferroptosis) in CRC. Finally, we highlight iron-related players as potential therapeutic targets against CRC malignancy.

KEYWORDS

Colorectal cancer, iron metabolism, hypoxia, oxidative stress, ferroptosis.

1. INTRODUCTION

Colorectal cancer (CRC) is the third most common and the second deadliest malignancy worldwide (*1*). Disease etiology involves genetic and environmental factors, like chronic inflammation, obesity, and nutrition (*2*). Pre-malignant lesions occur through a well-described sequence of genetic and epigenetic modifications (*3*). The genes involved and the sequence in which they are activated result in different pathways of carcinogenesis, leading to tumors with distinct types of genetic instabilities (*4*). These pre-malignant lesions can generally follow two pathways: the adenoma-carcinoma pathway and the serrated neoplasia pathway. The former begins with Adenomatous Polyposis Coli (*APC*) mutation, followed by Rat Sarcoma virus (RAS) protein activation or Tumor-Protein p53 (TP53) loss of function, and accounts for 70-90% of CRC cases. The serrated neoplasia pathway is related to RAS and to proto-oncogene *c-RAF* mutations and CpG island methylation phenotype leading to microsatellite stable (MSS) or unstable (MSI) tumors (*5*). CRC classification currently relies on consensus molecular subtypes (CMS) reflecting both molecular and cellular biological differences: CMS1 (MSI Immune), CMS2 (Canonical), CMS3 (Metabolic) and CMS4 (Mesenchymal) (*6*). CMS1 tumors are hypermutated, generally MSI and have strong immune activation (*7*). Whilst CMS2 and CMS3 are mainly epithelial and account for approximately 50% of colon cancers, CMS3 is characterized by marked metabolic dysregulation (*8*). CMS4 has strong TGF-β activation, stromal invasion, fibrosis, and angiogenesis (*7*). This more recent and sophisticated classification system considers that colon and rectal carcinomas may be infiltrated with numerous immune cells, namely macrophages and T lymphocytes, as well as fibroblasts, adipocytes, and endothelial cells, all of which compose the complex CRC tumor microenvironment (TME). The cell type, density, function, and localization of the cells, as extracellular matrix composition and biomechanical properties, are known to profoundly influence the course of the disease and even the response to therapy (*9*). Specifically, the immune landscape of CRC is highly relevant for predicting patients' prognosis (*10, 11*). Importantly, carcinogenic mechanisms, cell recruitment, and response of CRC to therapy are all affected by the balance in the levels of essential nutrients (*e.g.* iron).

Iron is a crucial nutrient for virtually all living organisms and can be found either directly bound to proteins or as a co-factor, namely in the form of heme or iron-sulfur clusters. These iron-containing proteins are essential for several biological and cellular processes, including oxygen transport, energy production, and cellular proliferation (*12*). In aqueous solution iron can exist in two different forms, ferrous (Fe^{2+}) and ferric (Fe^{3+}) iron, easily engaging in oxidation-reduction reactions due to its ability to donate and accept electrons (*13*). The possibility of interchanging between oxidation states enables this transition element to engage in the Fenton reaction, generating reactive oxygen free radicals (*e.g.* Hydroxyl radical), which promptly react with and damage proteins, fatty and nucleic acids (*14-16*). Therefore, iron levels are finely tuned by a

variety of highly regulated proteins, which act in concert to mediate iron homeostasis and avoid toxicity. Emerging evidences indicate that, in cancer, the balance between iron surplus and iron deficiency is paramount as it impacts tumorigenesis, progression, drug resistance, and immune activation and escape (*17*). In CRC, even though there are some conflicting data, it is clear that a high intake of red and processed meat, iron and heme-rich substances, is associated with an increased risk of disease development and progression (*18-21*). Interestingly, iron deficiency (*e.g.* anemia, iron chelation), the flipside of the coin, also displays controversial roles as it may i) limit cancer cell growth, ii) protect malignant cells from iron-dependent cell death (ferroptosis), and iii) hinder immune surveillance (*16, 22-24*). In addition to the role of systemic iron levels, in CRC the mechanisms behind iron-mediated cellular processes are also known to influence the disease outcome. For example, the up-regulation of the Transferrin Receptor 1 (TfR1) (responsible for cellular iron intake) and ferritin (the cellular iron storage protein) by malignant cells seems to be essential for tumor progression (*25, 26*). Tumor-associated macrophages (TAMs), displaying an anti-inflammatory profile are known to act as "iron donors", that may either feed proliferative cancer cells or contribute to an oxidative graveyard (*27-29*). In advanced CRC tumors, the hypoxic core activates hypoxia-inducible factors (*i.e. HIF*α and β) that bind to Hypoxia Responsive Elements (HREs) altering the expression of several iron metabolism genes (*30*). This review addresses the role of iron in CRC, particularly regarding the consequences of iron over-sufficiency and deprivation in tumor development and progression. The manuscript will also dissect the regulation of cellular iron metabolism in the CRC microenvironment and pinpoint iron-related players as potential therapeutic targets against CRC malignancy.

2. SYSTEMIC IRON: A DOUBLED-EDGE SWORD IN COLORECTAL CANCER

The average of the total amount of iron in the human body is approximately 3 g, with 1 to 4 mg of the metal being taken up daily from the diet through duodenum enterocytes (*14*). Dietary iron is then released into the plasma to compensate for organism losses, mainly by desquamation of epithelia and mucosa surfaces, bleeding, sweating, and urinary excretion (*31*). Dietary habits, particularly the disproportionate consumption of heme iron-rich (red and processed meat) and non-heme iron-containing foods (seeds, nuts, grains, and dark green leafy vegetables) may increase systemic iron levels (*32*). A high intake of iron-rich food, particularly of heme-containing meals, such as red and processed meat, has been reported by the International Agency for Research on Cancer (IARC) to be associated with CRC risk (Figure 1) (*33, 34*). This is supported by several epidemiological studies: Chao *et al.* reported that long-term consumption of red meat was associated with higher rectal cancer risk (*35*); a cohort study in the Netherlands uncovered a direct association between high heme intake and the risk of CRC containing *KRAS* activating and

APC overall mutations (G>A) (*36*); one branch examination of the Iowa Women's Health Study including 34708 postmenopausal women, aged 55–69 years, uncovered that increased dietary heme associates with a higher risk of colon cancer in alcohol-consuming women (*37*); the analysis of 2719 CRC cases from the NIH-AARP Diet and Health Study (USA) concluded that the unrestrained intake of processed meat is associated with a higher risk of rectal cancer than of colon cancer, most likely due to heme iron, nitrate/nitrite, and heterocyclic amines (*38*). Apart from epidemiological studies, numerous meta-analyses aimed at clarifying the impact of dietary heme and iron on CRC risk. Herein we highlight the following: a study that revised 59 epidemiological reports from 1995 to 2012 (*39*), a study that reviewed 20 human reports from 1996-2012 (*40*), and another study that included 14 cohort and 15 case-control studies up to 2017 (*41*). Despite some discrepancies likely due to population specificities or lack of power, all of these reports concluded that excessive iron and heme consumption, mainly from red meat, is positively associated with cancer risk, correlating with a higher incidence of both colon and rectal cancer. The molecular basis of such association has not been fully elucidated, but one possible mechanism is the hypomethylation of oncogenes. Upon iron treatment, *in vitro*, colon cancer Caco-2 cells hyperproliferate and were shown to have over 50 hypomethylated genes from the EGFR, MAPK, and Akt tumorigenic pathways (*42*). Iron excess may also exacerbate colorectal tumorigenesis by promoting Wnt signaling on CRC cells bearing-*APC* mutations (*43*). Additionally, heme iron is a potential pro-oxidant capable of generating reactive oxygen species (ROS), acting as a nitrosating agent, and consequently, increasing lipid peroxidation and carcinogenic N-nitroso compounds (*21, 33, 39*). In line with the evidence presented above, the modulation of elevated iron/heme levels with iron chelators could represent a potential therapeutic approach against CRC. Indeed, the group of François Gaboriau produced a highly selective tumor-targeted iron-chelating molecule, Quilamine HQ1-44, which inhibits DNA synthesis and cell proliferation and was able to reduce HCT116 cell and tumor growth *in vitro* and *in vivo*, respectively (*44*). More recently, desferioxamine (DFO), a clinically approved iron chelator, was shown to decrease the proliferation of HCT116 but not of LoVo cells and to modulate the global histone methylation status of both CRC cell lines (*45*). Interestingly, a number of studies have provided compelling evidence that curcumin, a yellow spice used for centuries in India with iron chelating properties, inhibits HCT-15, HT-29, and LoVo cell proliferation, enhances ROS levels, decreases mitochondrial membrane potential, activates caspase-3 and -9, promotes DNA fragmentation, chromatin condensation, and cell nuclear shrinkage, leading to apoptosis in a dose-dependent manner (*46-48*). Moreover, experimental data obtained from murine models pinpoint curcumin as a radio-sensitization mediator. The efficacy of curcumin in reducing tumor growth when combined with ionizing radiation is likely associated with ROS production, down-regulation of pre-mRNA processing factor 4, and suppression of the NF-kB pathway (*49, 50*). These promising findings led to the development of several clinical trials to test the effect of oral

curcumin supplementation on CRC patients. Although these studies indicate a potential role of curcumin in CRC prevention and treatment, a better knowledge of its properties and mode of action is still required. For example, it remains to be determined whether the above mentioned effects of curcumin are indeed related with iron chelation. Anyhow, the usage of iron chelators alone or in combination with chemotherapeutic agents, together with innovative technologies such as nanotechnology, targeted and cell therapies, and biochemical engineering, remains to be explored as potential therapeutic applications against CRC.

Interestingly, in CRC patients the most common hematological condition is iron deficiency, occurring in about 60% of diagnosed individuals (*16, 51*). Iron deficiency is associated with CRC risk (Figure 1) (*52*) and may benefit disease progression as it hampers immune cell functions, thus compromising tumor surveillance, cytokine production, oxidative defense, response to treatment, and the expression/activation of cancer-associated genes (*i.e. HIF, VEGF, NRF2*) (*16, 24, 53-57*). It was also reported that iron deficiency is associated with lower disease-free survival rates, particularly in individuals with advanced right-side tumors or with T3N0M0 stage colon cancer (*58*). It occurs due to tumor-induced bleeding (particularly in the rectum), chronic inflammation, and reduced iron absorption (*22, 26*), and is often associated with anemia, as more than 70% of CRC patients display decreased hemoglobin and hematocrit levels (*26, 59*). A study performed with a cohort of 339 CRC patients indicated that, at diagnosis, 48.1% of the individuals presented iron deficiency of which 56.4% were anemic. Of note, anemia developed in 50% of the patients with colon cancer, compared to only 20% in rectal cancer cases (*22*). Another study reported that in a cohort of 366 CRC patients, approximately 50% presented iron deficiency and, about 30% of the individuals had anemia (*23*). The development of anemia, either due to low iron levels or inflammation, is associated with a major iron metabolism orchestrator, hepcidin (*60*). This hormone is known to bind the cellular iron exporter Ferroportin 1 (FPN1) promoting its degradation, which results in a decrease in serum iron levels (*61*). In a study performed by Ward *et al.*, hepcidin mRNA expression was detected in 34% of the samples from a small cohort of CRC patients, but not in the adjacent normal colon mucosa (*62*). Another study found that CRC patients have a 2.9-fold decrease in hepcidin mRNA levels in tumor tissues, while serum hepcidin levels were within the range of controls. Despite this, the authors speculated that in CRC patients' serum hepcidin levels may be inappropriately high given their degree of iron restriction, which may reduce duodenal iron absorption, increasing the exposure of the colonic adenocarcinoma to iron. The increased hepcidin may be attributed to the mild inflammation of CRC patients, which was evidenced by significantly increased tumor IL-6 mRNA and serum CRP levels (*63*). In the future it would critical to clarify the role of both systemic and locally produced hepcidin in CRC, by comparing: i) healthy individuals with CRC patients and ii) samples from tumors paired with adjacent normal mucosa, in larger cohorts.

193 Apart from anemia, other parameters used to assess iron stores were also described as possible
194 biomarkers for the relation between iron deficiency and CRC progression. A cohort study by
195 Herrinton *et al.* pinpointed that low levels of transferrin saturation, an indirect measure of tissue
196 iron levels, were associated with a high risk for the development of colon and rectal carcinoma in
197 men (*64*). Three nested case studies that investigated the association between the commonly used
198 iron-related diagnostic markers and CRC revealed that low levels of serum ferritin are associated
199 with an elevated risk of developing colon but not rectal cancer (*65-67*). In these studies, however,
200 contradictory results were obtained for serum iron, transferrin saturation, and total iron binding
201 capacity: two studies showed no association with CRC risk (*65, 66*), while a third study presented
202 an inverse association of these systemic iron indicators with colon cancer risk (*67*). Strikingly, a
203 report on the relationship between preoperative serum ferritin levels, clinicopathological
204 parameters and CRC patient survival showed that individuals with either aberrantly low or high
205 ferritin levels in the serum had a shorter survival rate when compared to those with normal values
206 (*68*). As such, the epidemiologic studies seem to suggest that normal ferritin levels in the blood
207 (women 11-148 ng/mL; men 30-215 ng/mL) are associated with a better outcome in patients with
208 advanced CRC (*68*). Another cohort study with 965 participants demonstrated that the intake of
209 either low (<11.6 mg/day) or excessive (>27.3 mg/day) iron levels increased the risk of
210 developing adenomatous polyps, a lesion that precedes CRC (*69*). These data show that, despite
211 the existence of controversial results in the literature, in CRC, iron unbalance is a potential
212 contributor to both disease development and progression.

213

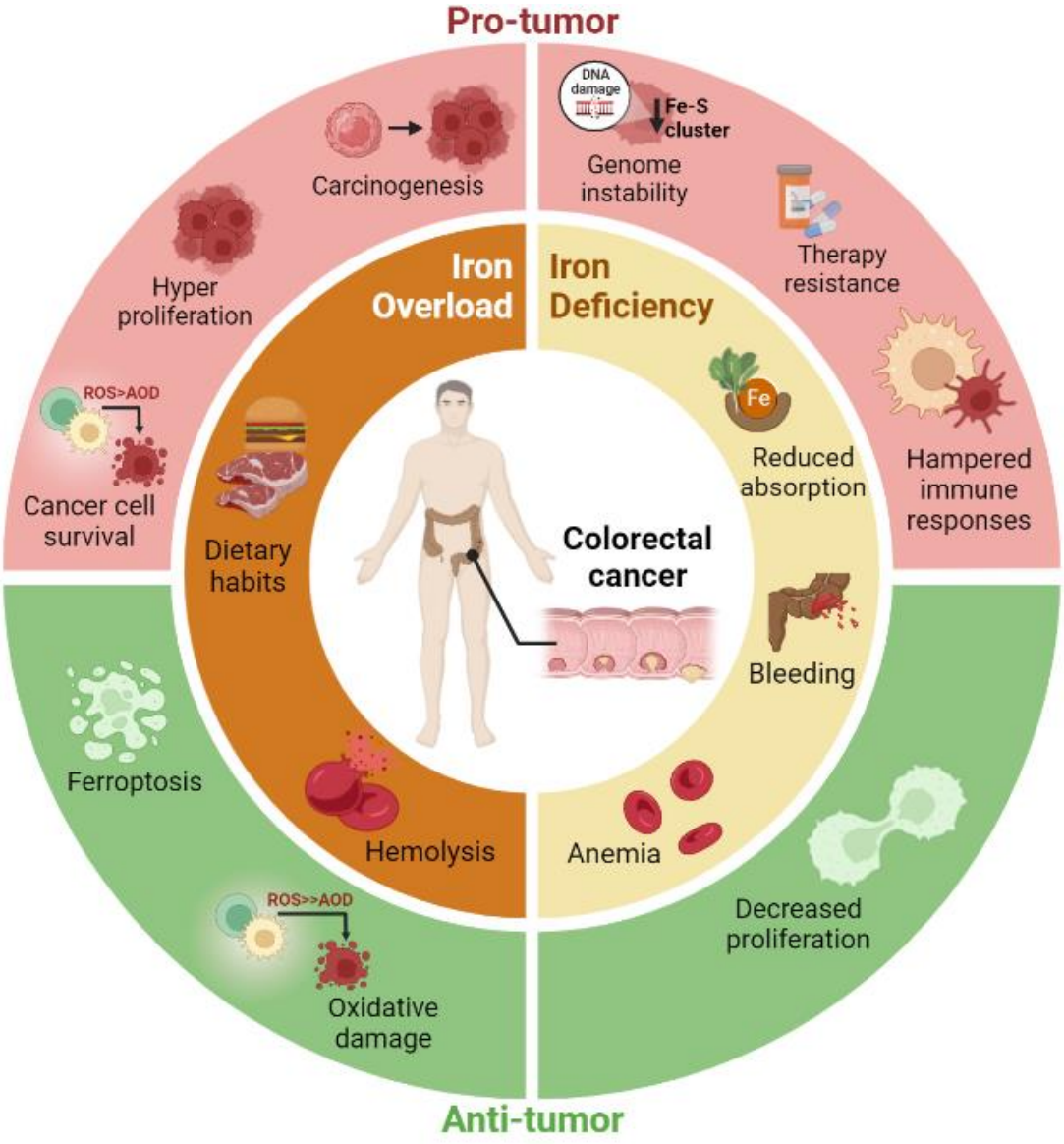

Figure 1 – Balancing systemic iron levels is essential to prevent CRC development. Current dietary habits, particularly in the western world, are associated with increased levels of iron and heme, both of which increase the risk of developing CRC. Hemolysis, often associated with anemia, may also result in systemic iron accumulation and, consequently contribute to a high risk of CRC. The harmful effects of iron overload are related to the induction of iron-mediated pro-tumor pathways namely, WNT-signaling, AKT, MAPK, EGFR, associated with hyperproliferation, cell survival, and consequently carcinogenesis. Interestingly, high levels of iron may also contribute to anti-tumor processes such as oxidative damage of cancer cells and death by ferroptosis. In turn, iron deficiency, associated with reduced absorption, bleeding or anemia, may also assist in CRC containment since iron is an essential nutrient for cancer cell proliferation. On the other hand, iron deficiency, by contributing to genome instability, therapy resistance, and diminished immune responses, may also promote CRC progression. This

complexity highlights the need to carefully study the iron metabolism of CRC patients, at different stages of the disease, when considering iron supplementation or chelation therapeutics.

3. THE YIN YANG OF CELLULAR IRON METABOLISM IN COLORECTAL CANCER

One of the most important hallmarks of cancer is the fact that cancer cells not only proliferate faster but also may divide endlessly (*70*). This higher proliferation rate is linked with an increased biosynthesis of nucleic acids and proteins and consequently a higher demand for energy (*71*). To successfully guarantee the enhancement of their global metabolism, malignant cells require high levels of iron (*72*). To gain access to such a vital nutrient, cancer cells have developed several strategies, namely the modulation of iron acquisition, trafficking, and storage (Table 1) (*73*). Brookes and colleagues were among the first to demonstrate increased expression of iron uptake proteins and increased iron storage in CRC in comparison with normal colorectal mucosa, with CRC samples presenting a higher expression of duodenal cytochrome B ferrireductase (DCYTB), divalent metal transporter-1 (DMT1), and TfR1, along with increased iron content (*74*). Cui *et al.* also reported an increase of TfR1 in primary CRC tissues when compared to paired controls. Further supporting the significance of high TfR1 expression in CRC, the authors down-regulated TfR1 and subsequently demonstrated a decrease in the proliferation of different CRC cells *in vitro* and a suppression of tumor growth in mice (*75*). TfR1 expression was also associated with tumor clinicopathological features: poorly differentiated tumors present lower TfR1 expression (32.1%) when compared to well differentiated tumors (70 %). In addition, CRC patients without lymph node invasion present high TfR1 levels, smaller tumors (< 5cm) and higher TfR1 expression when compared to larger tumors (63% versus 50%, respectively) (*75*). Additionally, TfR1 positive expression is associated with a longer survival time of CRC patients, when compared with TfR1-negative patients (72.06 ± 4.26 months versus 56.05 ± 5.29 months) (*75*). The regulation of TfR1 occurs at several levels, one of which is through Iron Regulatory Proteins (IRP) 1 and 2. These post-transcription regulators bind to mRNA iron-responsive elements (IREs) and stabilize the *TfR1* transcript, increasing its protein expression levels (*76*). In CRC samples, *IRP2* mRNA is overexpressed and correlates positively with TfR1 mRNA when compared to normal adjacent mucosa. Accordingly, *IRP2* knockdown reduced *TfR1* mRNA and protein in RKO cells (*77*). A positive correlation between *IRP2* mRNA expression and *BRAF* mutations (TCGA analysis) was also encountered. The latter was experimentally validated by inhibiting the BRAF downstream molecule MEK with Trametinib, in RKO and HT29 cells (*BRAF* mutated), resulting in the down-regulation of IRP2 and TfR1 when compared to control non-treated cells (*77, 78*). Moreover, the non-coding RNA miR-107, which is down-regulated in several CRC cell lines (LoVo, SW480,

HT29, DLD-1, SW620) and in patient CRC tissue, was proposed to negatively regulate TfR1 expression, affecting the proliferation, invasion, and migration of CRC cells (*79*). While further studies must be performed to clarify the mechanism underlying miR-107-mediated TfR1 regulation, it seems clear that this microRNA is a promising molecular target against CRC.

Recently, an alternative mechanism of iron transfer within the TME has been proposed. It relies on Lipocalin-2 (LCN2), a protein that was first identified as a defense mechanism during innate immune responses, since it binds iron-loaded siderophores, sequestering iron and hampering pathogen survival (*80, 81*). Interestingly, *LCN2* mRNA and protein expression were up-regulated in a cohort of 80 CRC samples, when compared with the adjacent normal tissue (*82*). By modulating LCN2 in CRC cell lines (SW620 and RKO), Feng *et al.* have shown that LCN2 impacts cell proliferation, epithelial-to-mesenchymal transition (EMT), invasion, and metastasis in CRC (*83*). This was also observed *in vivo*, since BALB/c nude mice injected with LCN2-CRC expressing cells exhibited smaller tumors, in both volume and weight, as well as a decreased ki-67 expression, when compared to mice injected with CRC cells with *LCN2* knockdown (*83*). Additionally, the authors verified a decrease in E-cadherin and an increase of vimentin in *LCN2*-knockdown mouse xenograft tissue when compared to control xenografts. These findings indicate that LCN2 regulates crucial markers for the EMT-MET plasticity of CRC (*83*). Nevertheless, more studies are required to determine the exact role of LCN2 in tumor growth and invasion.

In addition to iron uptake, cancer cells may modulate the expression of their key iron storage protein, ferritin (*84*). In a small collection of paraffin-embedded tissue samples, ferritin was significantly less expressed in low- and high-grade dysplastic adenomas and presented no differences in CRC adenocarcinoma samples compared to matched normal mucosa (*74*). Another study comprising only 21 samples, indicated that the mRNA levels of ferritin Heavy chain (*FtH*) were down-regulated in CRC samples when compared to controls (*25*). These contradictory data may be biased by the number of cases studied in the above-mentioned reports, which should be further investigated. Regarding the export of iron, FPN1 levels seemed to be enhanced in CRC samples. However, the iron exporter appears to locate intracellularly, implying that its up-regulation translates into non-functional protein. Nonetheless, poorly differentiated cells at the tumor invasive front presented low levels of FPN1 expression (*74*). Using a sporadic CRC mouse model, Schwartz and colleagues showed that FPN1 while abundant in the adjacent mucosa is not expressed at the tumor tissue (*85*). Moreover, the deletion of *Slc40a1*, encoding FPN1, in the colon epithelium resulted in enhanced tumor burden. The regulation of FPN1 was attributed to an intra-tumoral response to hypoxia which led to an up-regulation of locally produced hepcidin (*85*). Another important player in iron metabolism is heme-oxygenase 1 (HO-1), an enzyme that degrades heme to produce carbon monoxide (CO), biliverdin, and free iron (*86*). In a study with 55 CRC samples, HO-1 expression was detected in 41.8% of the cases and correlated with a better

survival rate (*87*). In another study with 118 CRC patient cases, HO-1 expression was significantly elevated in CRC tumor tissues when compared to paired normal non-tumoral and polyps samples. In addition, well-differentiated colon and rectal cancer tissues expressed the highest levels of HO-1 when compared to moderately/poorly-differentiated cancer samples (*88*). A recent publication, in which 101 CRC cases were studied, reported that HO-1 was expressed in macrophages present at the tumor nest. Moreover, this study correlated the expression of HO-1 with a shorter disease-free survival time and higher number of lymph node metastasis (*89*). However, an Australian retrospective cohort study with 50 cases showed that HO-1 mRNA expression was lower in cancer tissue when compared to adjacent mucosa and that lymphovascular invasion was significantly higher in HO-1 low-expressing patients. The authors also observed a trend for a longer overall survival in patients expressing high HO-1 levels (*90*). This controversy on HO-1 clinicopathological significance is also observed when looking into HO-1 contribution to CRC carcinogenesis. Some reports indicate that, in a functional p53 background, HO-1 has an anti-tumoral role through the induction of cell cycle arrest and apoptosis (*91*), others suggest that HO-1 promotes tumor progression and metastasis by reducing the expression of intercellular adhesion molecule 1 (ICAM-1) and CXCL10 and consequently decreasing T cell-mediated cytotoxicity against CRC cells (*92*). Finally, another study showed that HO-1 is essential for the protection of colonocytes against heme-mediated ROS formation and oxidative DNA damage (*93*). Overall, these conflicting findings highlight, once again, the need for further investigating iron metabolism in the context of CRC.

Another strategy that cancer cells employ to obtain iron is to take advantage of immune cells, such as macrophages and T lymphocytes, present in the tumor milieu (*84*). Tumor-associated macrophages (TAMs) are one of the major immune populations present at the CRC TME (*27*). They mainly differentiate from monocytic precursors from the blood and are chemotactically recruited to the tumor by cancer cell-derived cytokines such as CCL2, VEGF, CCL5 and TGF-β (*94*). In CRC, macrophage infiltration is variable depending on the CMS (*95*) and may affect disease prognosis (*i.e.* overall survival) (*27*). As shown by our group and others, this may be related to the distribution of macrophage sub-populations within the TME: M1-like macrophages, essentially present in the normal adjacent mucosa, display a pro-inflamatory protective role, while M2-like macrophages, mainly located at the invasive front, are a risk factor for CRC patients, harbouring anti-inflamatory and pro-tumor activities (*27, 96, 97*). To meet their high iron demand, malignant cells subvert the profile of TAMs into an anti-inflammatory state characterized by an "iron recycling" phenotype. These "iron donor" phagocytes display lower iron storage and increased iron efflux, primarily due to FPN1 up-regulation, feeding the tumor cells and supporting cancer progression (*28*). Additionally, HO-1 is up-regulated in CRC TAMs, which is associated with a poor prognosis, possibly, due to the iron release from heme (Table 1) (*88, 89*). Malignant

cells can also hijack the macrophage erythrophagocytosis process. Upon *de novo* blood vessel formation at the TME, there is leakage of erythrocytes that will be readily cleared by macrophages and, subsequently, hemoglobin degradation will contribute to the increase of iron availability, boosting cancer cell proliferation (*98, 99*). In addition to the indisputable role of TAMs in the TME, solid tumors contain another important immune cell population, the tumor-infiltrating lymphocytes (TILs) (*100-102*). In CRC, TILs are an heterogeneous population of lymphocytic B and T cells that impacts disease progression (*10, 102*). Infiltration of the tumor with cytotoxic $CD8^+$ T lymphocytes is associated with a better prognosis (*100*). Likewise, high levels of $CD4^+$ Th1 cells in the tumor nest and invasive front are correlated with better overall survival and extended disease-free survival (*102, 103*). On the other hand, T regulatory $FOXP3^{high}$ immunosuppressive population is associated with a worse prognosis, whereas the $FOXP3^{low}$ $CD45RA^-$ pro-inflammatory subset is associated with a better prognosis (*104*). T lymphocyte activation, function, and subsequent response are dependent on iron. In fact, the up-regulation of TfR1 (also known as CD71) is one of the earliest events in T cell activation (*105*). In the TME, the diversion of iron into cancer cell proliferation may result in low iron availability for TILs, inhibiting T cell proliferation, and consequently hampering the action of T cells, while fueling cancer cell activity (*106*). Apart from the TfR1, to our knowledge, nothing is known about the axis between T cell iron metabolism and CRC, thus representing an unexplored niche for the discovery of novel therapeutic targets and possibly biomarkers of therapy response.

Table 1 – The ups and downs of iron metabolism players in colorectal cancer.

BIOLOGICAL PROCESS	PROTEIN	FUNCTION	LOCALIZATION	CELL TYPE	EXPERIMENTAL MODEL	STATUS	REF.
Iron import	**TfR-1**	Binding and endocytosis of Tf-Fe^{3+}	Plasma membrane	Cancer cells	HT-29	Up-regulated (mRNA)	25
				ND	CRC human tissue vs normal adj. mucosa	Up-regulated	74, 75, 77
				TILs		Up-regulated	106
	DMT-1	Fe^{2+} iron importer	Endosomes; Plasma membrane	Cancer cells	HT-29	Up-regulated (mRNA)	25
				ND	CRC human tissue vs normal adj. mucosa	Up-regulated	74
	DCTYB	duodenal cytochrome B ferrireductase	Plasma membrane	ND	CRC human tissue vs normal adj. mucosa	Up-regulated	74
	HO-1	Heme-oxygenase 1	Endoplasmic reticulum	ND	CRC human samples	Up-regulated	88
						Down-regulated (mRNA)	90
				TAMs		Up-regulated	89
Iron storage	**Ferritin-H**	Ferroxidase; Iron reservoir	Cytosol	ND	CRC human tissue vs normal adj. mucosa	Down-regulated (mRNA)	25
						No differences	74
Iron export	**FPN-1**	Iron exporter FPN-1 degradation	Plasma membrane	Cancer cells	HT-29	Up-regulated	25
				ND	CRC human samples	Up-regulated (Intracellular)	74
					CRC mouse tissue vs normal adj. mucosa	Not expressed	85
	Hepcidin	FPN1 regulator	Secreted	ND	CRC human tissues	Up-regulated	62
						Down-regulated (mRNA)	63
Iron chelator	**NGAL/LCN2**	Siderophore chelator	Secreted	ND	CRC human tissue vs normal adj. mucosa	Up-regulated	82
				Cancer cells	CW2, HCT116, SW480, LOVO, LS513, HT29	Up-regulated	83

ND – Not determined

4. THE CROSSTALK OF HYPOXIA AND IRON METABOLISM IN COLORECTAL CANCER

The solid tumor milieu is a harsh hypoxic environment due to aberrant cancer cell growth and abnormal vascularization (*107*). This low oxygen tension induces the stabilization of Hypoxia Inducible Factor (HIF) transcription factors, heterodimer complexes composed by an α subunit, with three different isoforms, 1α, 2α, and 3α, and a β subunit (*108, 109*). The stabilization of HIF is mediated by the inactivation of Prolyl 4-Hydroxylases (PHDs), allowing the rapid translocation of HIFα to the nucleus where it forms a heterodimer with the HIFβ subunit, and induces the activation of genes with Hypoxia responsive elements (HREs) in their promotors (*107-110*). Of note, apart from being oxygen-dependent, PHDs use iron as cofactors. Low iron levels may also lead to their inactivation and consequent HIF stabilization, even in normoxic conditions (*108*).

Intestinal epithelial cells express both HIF1α and HIF2α with non-redundant roles (*111*), and both are overexpressed in several tumors, including CRC (*112, 113*). Previous studies have demonstrated that HIF2α is the isoform associated with the regulation of iron metabolism in a non-cancer context and CRC. In a non-cancer context, it is known that hypoxia links erythropoiesis with iron homeostasis and that the hepcidin/FPN1 axis regulates intestinal HIF2α to modulate iron absorption, through transcriptional activation of *DMT1*, *DCYTB*, and *FPN1* (*114-116*). Moreover, the *HIF2α* promotor has IREs, to which IRPs 1 and 2 bind with high affinity, resulting in the regulation of various iron-related genes (*117*). In a mouse model of colitis-associated colon cancer, HIF2α was shown to regulate *Dmt1* activation, leading to an increment of intracellular iron levels and consequently contributing to increased cell proliferation and tumor growth (*118*). The authors demonstrated that increased iron levels were essential for colon tumor formation after HIF2α activation (*118*), which is particularly relevant since DMT1 is known to be overexpressed in colon cancer compared with normal tissue (*119-121*). Using the same mouse model, HIF2α was demonstrated to also trigger the activation of the iron reductase six-transmembrane epithelial antigen of the prostate 4 (STEAP4), causing mitochondrial iron accumulation, elevated ROS levels, and increased tumor burden (*122*). Interestingly, the link between HIF-2α and iron in CRC may not only result in induced carcinogenesis but also represent a vulnerability that could be explored to develop new therapies against CRC. The fact that HIF-2α activation up-regulates lipid and iron regulatory genes in CRC cell lines and colon tumors leading to a ferroptosis-susceptible cell state, indicates that reprogramming of both iron and lipid metabolism via HIF-2α, could induce malignant cell death contributing to tumor elimination (*123, 124*). Despite the above-mentioned preponderant role of HIF2α in iron metabolism modulation, it is worth mentioning that iron regulates HIF1α protein stabilization by modulating cyclooxygenase-2 (COX-2) signaling in human colon cancer cells (*125*).

5. IRON-ASSOCIATED OXIDATIVE STRESS AND FERROPTOSIS IN COLORECTAL CANCER

In response to alterations in the microbiome and to the breakdown of the colonic barrier integrity, iron may assist inflammatory cells, such as neutrophils and macrophages, to produce ROS via Fenton's/Haber-Weiss reactions. In addition, immune cells also produce reactive nitrogen species (RNS). Together, ROS and RNS directly induce DNA base oxidation (*126, 127*). Premutagenic oxidative DNA base lesions such as 8-hydroxy-2′-deoxyguanosine (8-OHdG) accumulate in the mucosa and may initiate colon carcinogenesis (*128, 129*). ROS can also attack polyunsaturated fatty acids (PUFAs), which are incorporated in the membrane phospholipids of colon tissues, leading to the formation of endogenous lipid-derived electrophiles, including malondialdehyde (MDA) and 4-hydroxynonenal (4-HNE) (*130*). At high levels, MDA and 4-HNE react with several DNA nucleosides to form adducts which, in the absence of repair, may lead to mutations (*131-133*). Of note, 4-HNE-induced COX-2 increases prostaglandin (PG) synthesis, which is also associated with carcinogenesis (*134*). Notably, in CRC, oxidative stress is thought to contribute not just to the initiation but also to disease progression (*135*). CRC cells are more efficient than non-malignant cells in metabolizing lipid-derived electrophiles into non-toxic conjugates due to the higher expression of key biotransformation enzymes, attributable to constitutive Kelch-like ECH-associated protein 1 (KEAP1)/Nuclear factor erythroid 2-related factor 2 (NRF2) activation (*136*). As a result, persistent oxidative stress stimulates the proliferation of CRC cells without inducing cell death, which grants them a selective advantage that favors cancer promotion (*137*). The inactivation of the DNA mismatch repair system by oxidative stress, in turn, may be responsible for the microsatellite instability that is implicated in the initiation and promotion of colitis-associated carcinogenesis (*138*). Interestingly, Ribeiro *et al.* found significantly higher oxidative stress levels in 33 CRC tumor samples when compared to the adjacent normal mucosa. Surprisingly, the authors also verified that tumor samples from the distal colon have a higher risk of oxidative damage than those of the proximal colon (*139*).

As mentioned above, iron can induce and initiate lipid peroxidation through the production of oxygen radicals (mainly hydroxyl radical) via Fenton's/Haber-Weiss reactions. Iron-catalyzed ROS are important initiators and mediators of cell death (*140*), namely of ferroptosis. This non-apoptotic form of programmed cell death caused by the accumulation of iron-dependent lipid peroxides first proposed by Dixon *et al.* in 2012 (*141*) has distinct morphological, biochemical and genetic features from necrosis, apoptosis, and autophagy (*141, 142*). Commonly assessed hallmarks of ferroptosis in cultured cells include: expansion of the intracellular labile iron pool; iron-dependent ROS accumulation; glutathione (GSH) depletion; lipid peroxidation; up-regulation of prostaglandin-endoperoxide synthase (PTGS), acyl-CoA synthetase long-chain family member 4 (ACSL4), HO-1 and transferrin; down-regulation of glutathione peroxidase 4

(GPX4), solute carrier family 7 member 11 (SLC7A11), FtH1, and FPN1; and smaller than normal mitochondria with increased membrane density as well as collapsed mitochondrial cristae (*29*, *142-144*). The contribution of ferroptosis to CRC was first suggested by Sui *et al.* in 2018. The authors reported that the ferroptosis inducer RSL3 caused ROS accumulation, increased labile iron and cell death in three different CRC cell lines (HCT116, LoVo, and HT29), which could be reversed by ferroptosis inhibitors (ferrostatin-1 and liproxstatin-1) and by overexpression of GPX4 (Figure 2) (*29*). In fact, accumulating evidence suggests that triggering ferroptosis by targeting the GPX4/GSH system is an efficient way to inhibit the growth of CRC cells. Also, the suppression of the siderophore-binding protein LCN2, which is elevated in many tumors, results in a cellular iron increase and a decrease in GPX4 and X_C^- expression (Figure 2), which promotes ferroptosis and increases sensitivity to chemotherapy (*e.g.* 5-fluorouracil) in colon cancer cells. Negative regulators of ferroptosis such as LCN2 are thus candidate drug targets in therapy-resistant CRC (*82*). Also, the microRNA-15a-3p (miR-15a-3p) and miR-539, were reported to induce CRC cell death by ferroptosis via the down-regulation of GPX4 (*145*, *146*). When overexpressed, ACADSB, a member of the acyl-CoA dehydrogenase, that negatively regulates glutathione reductase and GPX4, was shown to limit CRC cell migration, invasion, and proliferation by promoting CRC cell ferroptosis (*147*). SLC7A11, a component of the xCT system, which mediates cystine uptake and glutamate release to promote GSH synthesis, an upstream process of ferroptosis, is highly expressed in colon cancer (*148*). The benzopyran derivative 2-imino-6-methoxy-2H-chromene-3-carbothioamide (IMCA), previously shown to inhibit CRC cell viability *in vitro* and tumor growth *in vivo*, was recently demonstrated to be a ferroptosis inducer in CRC cells (*149*, *150*) through the down-regulation of SLC7A11 and decrease of cysteine and GSH levels. Interestingly, Xu *et al.* showed that cisplatin-resistant HT-29 cells displayed higher levels of cysteine, GSH and SLC7A11, lower levels of ROS, and increased stemness-associated features when compared with the parental CRC cells (*151*). Moreover, the knockout of *SLC7A11* reduced the levels of cysteine and GSH, increased ROS levels, and reduced the stem-like properties of cisplatin-resistant CRC cells. These data indicate that SLC7A11 could be a potential candidate for targeted therapies to promote ferroptosis and suppress CRC progression. Notably, erastin, an inhibitor of SLC7A11 and an inducer of ferroptosis, could attenuate stemness features and chemoresistance of CRC cisplatin-resistant cells (*151*). In addition, dichloroacetate (DCA), another ferroptosis-activating agent, was also shown to reduce the stem-like feature of CRC cells (*152*). Thus, promoting ferroptosis is a currently explored strategy that may represent promising therapeutic approaches against CRC (*153*, *154*).

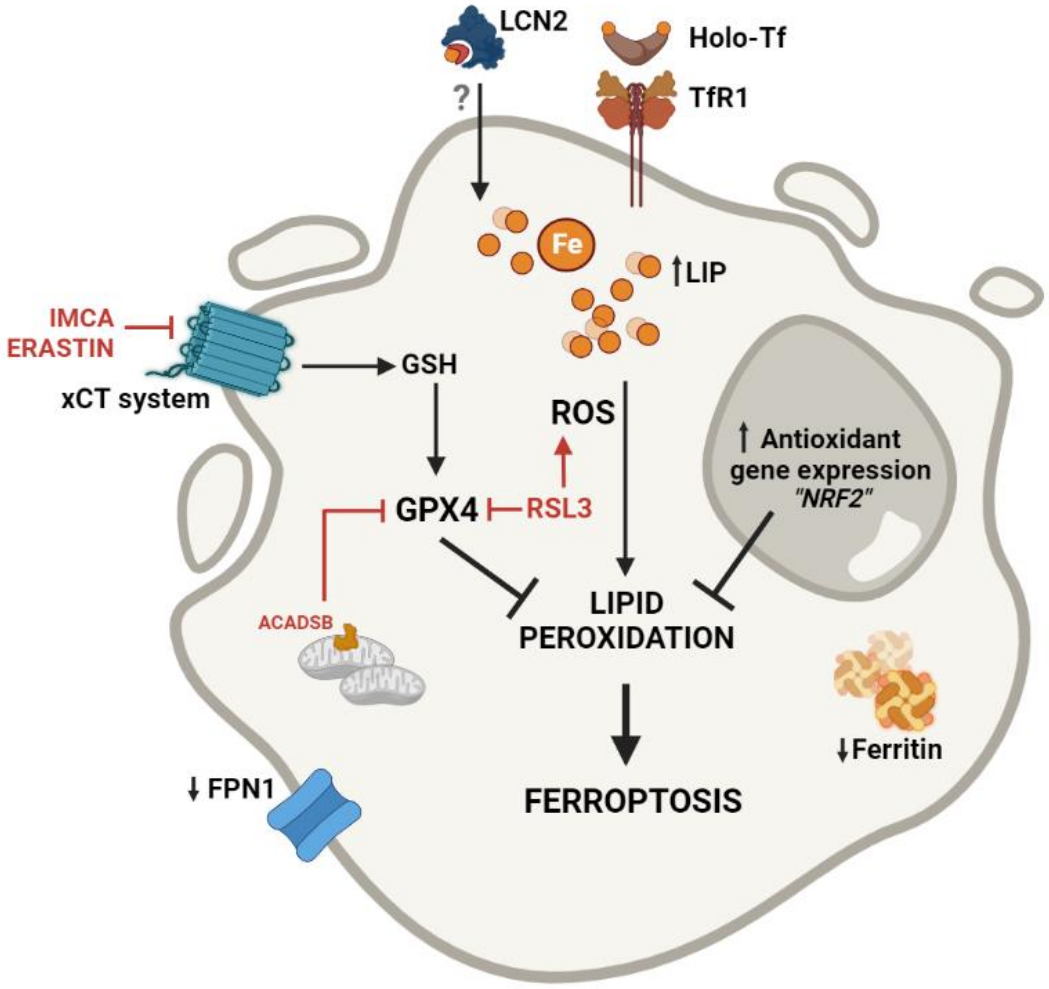

Figure 2 – Ferroptosis modulation as a therapeutic target to promote iron-mediated death of CRC cells. Iron internalization through transferrin receptor 1 (TfR1) and possibly lipocalin 2 (LCN2), as well as decreased iron efflux through ferroportin 1 (FPN1) and diminished ferritin, contribute to an increase in the labile iron pool (LIP). A surplus of intracellular iron results in the production of reactive oxygen species (ROS), which cause lipid peroxidation and ultimately lead to cell death by ferroptosis. Importantly, CRC cells are protected against ROS-induced injury due to the constitutive activation of antioxidant genes (*e.g.* NRF2 pathway). The xCT system fuels the glutathione (GSH) pathway increasing the activity of glutathione peroxidase 4 (GPX4), which inhibits lipid peroxidation and decreases ferroptosis. GPX4 is thus a potential therapeutic target to promote CRC cell death. Both RSL3, a GPX4 inhibitor, and the overexpression of ACADSB, a member of the acyl-CoA dehydrogenase, that also negatively regulates GPX4, were shown to promote ferroptosis in CRC cells. Additionally, erastin and the benzopyran derivative 2-imino-6-methoxy-2H-chromene-3-carbothioamide (IMCA) known to inhibit the xCT system, are able to decrease the levels of GSH and of GPX4, promoting ferroptosis. As such, by exploring the different pathways that activate ferroptosis we may pave the way to the discovery of new therapeutic targets against CRC.

6. CONCLUSIONS

Iron is a double-edged sword as it is essential for life but, when present in excess, may exert deleterious effects. In the context of CRC, both iron deficiency and oversupply negatively associate with disease outcomes. Therefore, systemic iron levels need to be perfectly balanced. At the cellular level, iron metabolism must be finely regulated to avoid toxic by-products and, at the same time, satisfy cell requirements for this essential nutrient. CRC malignant cells display a high demand for iron to sustain their elevated proliferation rate; however, the excess of iron/heme enables death mechanisms by ROS production and ferroptosis. Upon reviewing the current literature, it is clear that several avenues still require further research, namely unanswered issues such as the role of iron in the numerous stromal cells that compose the CRC TME and that modulate cancer cell behaviour, the influence of spatial heterogeneity in cellular iron metabolism, and the mechanisms of iron-combinatory therapies. Finally, further investigation on the use of iron and/or iron chelators for therapeutic purposes is still required to unveil new treatment regimens against CRC.

DECLARATIONS:

Ethics approval: Not applicable.

Competing interests: The authors declare no competing interests.

Author contribution: conceptualization: Tânia B. da Cruz; literature search: Diogo Estêvão, Miguel da Cruz-Ribeiro, Ana P. Cardoso, Ângela M. Costa, Tiago L. Duarte, Tânia B. da Cruz; writing: Diogo Estêvão, Miguel da Cruz-Ribeiro, Ana P. Cardoso, Ângela M. Costa, Tiago L. Duarte, Tânia B. da Cruz; image preparation: Tânia B. da Cruz; reviewing: Diogo Estêvão, Ana P. Cardoso, Ângela M. Costa, Maria J. Oliveira, Tiago L. Duarte. All authors read and approved the final manuscript.

Funding:

Tânia B. da Cruz was financed by Portuguese funds through FCT - Fundação para a Ciência e a Tecnologia/Ministério da Ciência, Tecnologia e Ensino Superior in the framework of the project READOUT (EXPL/BIA-CEL/1225/2021). Miguel C Ribeiro was finnancially supported by the project CANCER-Challenge, financially supported by IPatimup. Diogo Estêvão was financed by UI/BD/151551/2021, Ana P. Cardoso by PTDC/MED-ONC/4165/2021, and Ângela M. Costa by DL57/2016/CP1360/CT0009. This work was partially supported by Programa Operacional Regional do Norte and co-funded by European Regional Development Fund under the project "The Porto Comprehensive Cancer Center" with the reference NORTE-01-0145-FEDER-072678 - Consórcio PORTO.CCC – Porto. Comprehensive Cancer Center Raquel Seruca.

Data availability: Not applicable.

Code availability: Not applicable.

7. BIBLIOGRAPHY

1. H. Sung *et al.*, Global cancer statistics 2020: GLOBOCAN estimates of incidence and mortality worldwide for 36 cancers in 185 countries. *CA Cancer J Clin*, (2021).
2. S. Stintzing, S. Tejpar, P. Gibbs, L. Thiebach, H. J. Lenz, Understanding the role of primary tumour localisation in colorectal cancer treatment and outcomes. *Eur J Cancer* **84**, 69-80 (2017).
3. J. M. Loree *et al.*, Classifying Colorectal Cancer by Tumor Location Rather than Sidedness Highlights a Continuum in Mutation Profiles and Consensus Molecular Subtypes. *Clin Cancer Res* **24**, 1062-1072 (2018).
4. E. R. Fearon, B. Vogelstein, A genetic model for colorectal tumorigenesis. *Cell* **61**, 759-767 (1990).
5. E. R. Kim, D. K. Chang, Colorectal cancer in inflammatory bowel disease: the risk, pathogenesis, prevention and diagnosis. *World J Gastroenterol* **20**, 9872-9881 (2014).
6. J. Guinney *et al.*, The consensus molecular subtypes of colorectal cancer. *Nat Med* **21**, 1350-1356 (2015).
7. K. Thanki *et al.*, Consensus Molecular Subtypes of Colorectal Cancer and their Clinical Implications. *Int Biol Biomed J* **3**, 105-111 (2017).
8. J. Roelands *et al.*, Immunogenomic Classification of Colorectal Cancer and Therapeutic Implications. *Int J Mol Sci* **18**, (2017).
9. Â. Marques-Magalhães *et al.*, Decellularized Colorectal Cancer Matrices as Bioactive Scaffolds for Studying Tumor-Stroma Interactions. *Cancers (Basel)* **14**, (2022).
10. J. Galon *et al.*, Cancer classification using the Immunoscore: a worldwide task force. *J Transl Med* **10**, 205 (2012).
11. D. Bruni, H. K. Angell, J. Galon, The immune contexture and Immunoscore in cancer prognosis and therapeutic efficacy. *Nat Rev Cancer* **20**, 662-680 (2020).
12. R. R. Crichton, J. L. Pierre, Old iron, young copper: from Mars to Venus. *Biometals* **14**, 99-112 (2001).
13. F. Kuang, J. Liu, D. Tang, R. Kang, Oxidative Damage and Antioxidant Defense in Ferroptosis. *Frontiers in Cell and Developmental Biology* **8**, (2020).
14. M. W. Hentze, M. U. Muckenthaler, N. C. Andrews, Balancing acts: molecular control of mammalian iron metabolism. *Cell* **117**, 285-297 (2004).
15. R. R. Crichton, M. Charloteaux-Wauters, Iron transport and storage. *Eur J Biochem* **164**, 485-506 (1987).
16. A. Aksan, K. Farrag, S. Aksan, O. Schroeder, J. Stein, Flipside of the Coin: Iron Deficiency and Colorectal Cancer. *Front Immunol* **12**, 635899 (2021).
17. R. L. Nelson, Dietary iron and colorectal cancer risk. *Free Radic Biol Med* **12**, 161-168 (1992).
18. N. D. Turner, S. K. Lloyd, Association between red meat consumption and colon cancer: A systematic review of experimental results. *Exp Biol Med (Maywood)* **242**, 813-839 (2017).
19. G. C. Kabat, A. B. Miller, M. Jain, T. E. Rohan, A cohort study of dietary iron and heme iron intake and risk of colorectal cancer in women. *Br J Cancer* **97**, 118-122 (2007).
20. V. Bouvard *et al.*, Carcinogenicity of consumption of red and processed meat. *Lancet Oncol* **16**, 1599-1600 (2015).
21. N. M. Bastide *et al.*, A central role for heme iron in colon carcinogenesis associated with red meat intake. *Cancer Res* **75**, 870-879 (2015).
22. M. J. Wilson *et al.*, The role of preoperative iron deficiency in colorectal cancer patients: prevalence and treatment. *Int J Colorectal Dis* **32**, 1617-1624 (2017).

23. H. Ludwig, E. Muldur, G. Endler, W. Hubl, Prevalence of iron deficiency across different tumors and its association with poor performance status, disease status and anemia. *Ann Oncol* **24**, 1886-1892 (2013).
24. M. Costa da Silva *et al.*, Iron Induces Anti-tumor Activity in Tumor-Associated Macrophages. *Front Immunol* **8**, 1479 (2017).
25. W. Sornjai *et al.*, Iron and hepcidin mediate human colorectal cancer cell growth. *Chem Biol Interact* **319**, 109021 (2020).
26. M. Prutki *et al.*, Altered iron metabolism, transferrin receptor 1 and ferritin in patients with colon cancer. *Cancer Lett* **238**, 188-196 (2006).
27. M. L. Pinto *et al.*, The Two Faces of Tumor-Associated Macrophages and Their Clinical Significance in Colorectal Cancer. *Front Immunol* **10**, 1875 (2019).
28. W. Liang, N. Ferrara, Iron Metabolism in the Tumor Microenvironment: Contributions of Innate Immune Cells. *Front Immunol* **11**, 626812 (2020).
29. X. Sui *et al.*, RSL3 Drives Ferroptosis Through GPX4 Inactivation and ROS Production in Colorectal Cancer. *Front Pharmacol* **9**, 1371 (2018).
30. D. Watts *et al.*, Hypoxia Pathway Proteins are Master Regulators of Erythropoiesis. *Int J Mol Sci* **21**, (2020).
31. M. U. Muckenthaler, B. Galy, M. W. Hentze, Systemic iron homeostasis and the iron-responsive element/iron-regulatory protein (IRE/IRP) regulatory network. *Annu Rev Nutr* **28**, 197-213 (2008).
32. O. Phipps, M. J. Brookes, H. O. Al-Hassi, Iron deficiency, immunology, and colorectal cancer. *Nutr Rev* **79**, 88-97 (2021).
33. N. M. Bastide, F. H. Pierre, D. E. Corpet, Heme iron from meat and risk of colorectal cancer: a meta-analysis and a review of the mechanisms involved. *Cancer Prev Res (Phila)* **4**, 177-184 (2011).
34. V. Bouvard *et al.*, Carcinogenicity of consumption of red and processed meat. *Lancet Oncol* **16**, 1599-1600 (2015).
35. A. Chao *et al.*, Meat consumption and risk of colorectal cancer. *JAMA* **293**, 172-182 (2005).
36. A. M. Gilsing *et al.*, Dietary heme iron and the risk of colorectal cancer with specific mutations in KRAS and APC. *Carcinogenesis* **34**, 2757-2766 (2013).
37. D. H. Lee, K. E. Anderson, L. J. Harnack, A. R. Folsom, D. R. Jacobs, Heme iron, zinc, alcohol consumption, and colon cancer: Iowa Women's Health Study. *J Natl Cancer Inst* **96**, 403-407 (2004).
38. A. J. Cross *et al.*, A large prospective study of meat consumption and colorectal cancer risk: an investigation of potential mechanisms underlying this association. *Cancer Res* **70**, 2406-2414 (2010).
39. A. Fonseca-Nunes, P. Jakszyn, A. Agudo, Iron and cancer risk--a systematic review and meta-analysis of the epidemiological evidence. *Cancer Epidemiol Biomarkers Prev* **23**, 12-31 (2014).
40. J. H. Ashmore, C. J. Rogers, S. L. Kelleher, S. M. Lesko, T. J. Hartman, Dietary Iron and Colorectal Cancer Risk: A Review of Human Population Studies. *Crit Rev Food Sci Nutr* **56**, 1012-1020 (2016).
41. Y. Meng, J. Sun, J. Yu, C. Wang, J. Su, Dietary Intakes of Calcium, Iron, Magnesium, and Potassium Elements and the Risk of Colorectal Cancer: a Meta-Analysis. *Biol Trace Elem Res* **189**, 325-335 (2019).
42. H. RD, L. S, B. A, I. TH, S. CT, S. Lai, Ed. (2017).
43. M. J. Brookes *et al.*, A role for iron in Wnt signalling. *Oncogene* **27**, 966-975 (2008).
44. S. Renaud *et al.*, Quilamine HQ1-44, an iron chelator vectorized toward tumor cells by the polyamine transport system, inhibits HCT116 tumor growth without adverse effect. *Biochem Pharmacol* **96**, 179-189 (2015).

45. L. L. Cao *et al.*, Iron chelation inhibits cancer cell growth and modulates global histone methylation status in colorectal cancer. *Biometals* **31**, 797-805 (2018).
46. L. D. Guo *et al.*, Curcumin inhibits proliferation and induces apoptosis of human colorectal cancer cells by activating the mitochondria apoptotic pathway. *Phytother Res* **27**, 422-430 (2013).
47. A. Shehzad, J. Lee, T. L. Huh, Y. S. Lee, Curcumin induces apoptosis in human colorectal carcinoma (HCT-15) cells by regulating expression of Prp4 and p53. *Mol Cells* **35**, 526-532 (2013).
48. A. Agarwal *et al.*, Curcumin induces apoptosis and cell cycle arrest via the activation of reactive oxygen species-independent mitochondrial apoptotic pathway in Smad4 and p53 mutated colon adenocarcinoma HT29 cells. *Nutr Res* **51**, 67-81 (2018).
49. A. Shehzad, J. W. Park, J. Lee, Y. S. Lee, Curcumin induces radiosensitivity of in vitro and in vivo cancer models by modulating pre-mRNA processing factor 4 (Prp4). *Chem Biol Interact* **206**, 394-402 (2013).
50. S. K. Sandur *et al.*, Curcumin modulates the radiosensitivity of colorectal cancer cells by suppressing constitutive and inducible NF-kappaB activity. *Int J Radiat Oncol Biol Phys* **75**, 534-542 (2009).
51. G. N. Ioannou, D. C. Rockey, C. L. Bryson, N. S. Weiss, Iron deficiency and gastrointestinal malignancy: a population-based cohort study. *Am J Med* **113**, 276-280 (2002).
52. N. Hung *et al.*, Risk of cancer in patients with iron deficiency anemia: a nationwide population-based study. *PLoS One* **10**, e0119647 (2015).
53. L. Schito, G. L. Semenza, Hypoxia-Inducible Factors: Master Regulators of Cancer Progression. *Trends Cancer* **2**, 758-770 (2016).
54. S. Menegon, A. Columbano, S. Giordano, The Dual Roles of NRF2 in Cancer. *Trends Mol Med* **22**, 578-593 (2016).
55. J. Eckard *et al.*, Effects of cellular iron deficiency on the formation of vascular endothelial growth factor and angiogenesis. Iron deficiency and angiogenesis. *Cancer Cell Int* **10**, 28 (2010).
56. S. Kuvibidila, R. P. Warrier, Differential effects of iron deficiency and underfeeding on serum levels of interleukin-10, interleukin-12p40, and interferon-gamma in mice. *Cytokine* **26**, 73-81 (2004).
57. A. J. Klecha *et al.*, In vivo iron and zinc deficiency diminished T- and B-selective mitogen stimulation of murine lymphoid cells through protein kinase C-mediated mechanism. *Biol Trace Elem Res* **104**, 173-183 (2005).
58. L. Zhen *et al.*, Iron-deficiency anemia: a predictor of diminished disease-free survival of T3N0M0 stage colon cancer. *J Surg Oncol* **105**, 371-375 (2012).
59. F. Zohora, K. Bidad, Z. Pourpak, M. Moin, Biological and Immunological Aspects of Iron Deficiency Anemia in Cancer Development: A Narrative Review. *Nutr Cancer* **70**, 546-556 (2018).
60. T. Ganz, Molecular pathogenesis of anemia of chronic disease. *Pediatr Blood Cancer* **46**, 554-557 (2006).
61. E. Nemeth *et al.*, Hepcidin regulates cellular iron efflux by binding to ferroportin and inducing its internalization. *Science* **306**, 2090-2093 (2004).
62. D. G. Ward *et al.*, Increased hepcidin expression in colorectal carcinogenesis. *World J Gastroenterol* **14**, 1339-1345 (2008).
63. C. K. Pusatcioglu *et al.*, Systemic and tumor level iron regulation in men with colorectal cancer: a case control study. *Nutrition & Metabolism* **11**, 21 (2014).
64. L. J. Herrinton, G. D. Friedman, D. Baer, J. V. Selby, Transferrin saturation and risk of cancer. *Am J Epidemiol* **142**, 692-698 (1995).
65. I. Kato *et al.*, Iron intake, body iron stores and colorectal cancer risk in women: a nested case-control study. *Int J Cancer* **80**, 693-698 (1999).

66. K. Ekblom *et al.*, Iron biomarkers in plasma, HFE genotypes, and the risk for colorectal cancer in a prospective setting. *Dis Colon Rectum* **55**, 337-344 (2012).
67. A. J. Cross *et al.*, Iron and colorectal cancer risk in the alpha-tocopherol, beta-carotene cancer prevention study. *Int J Cancer* **118**, 3147-3152 (2006).
68. M. Lorenzi, B. Lorenzi, R. Vernillo, Serum ferritin in colorectal cancer patients and its prognostic evaluation. *Int J Biol Markers* **21**, 235-241 (2006).
69. C. L. Bird *et al.*, Plasma ferritin, iron intake, and the risk of colorectal polyps. *Am J Epidemiol* **144**, 34-41 (1996).
70. D. Hanahan, Hallmarks of Cancer: New Dimensions. *Cancer Discov* **12**, 31-46 (2022).
71. M. A. Feitelson *et al.*, Sustained proliferation in cancer: Mechanisms and novel therapeutic targets. *Semin Cancer Biol* **35 Suppl**, S25-S54 (2015).
72. H. W. Hann, M. W. Stahlhut, B. S. Blumberg, Iron nutrition and tumor growth: decreased tumor growth in iron-deficient mice. *Cancer Res* **48**, 4168-4170 (1988).
73. C. Zhang, F. Zhang, Iron homeostasis and tumorigenesis: molecular mechanisms and therapeutic opportunities. *Protein Cell* **6**, 88-100 (2015).
74. M. J. Brookes *et al.*, Modulation of iron transport proteins in human colorectal carcinogenesis. *Gut* **55**, 1449-1460 (2006).
75. C. Cui *et al.*, Downregulation of TfR1 promotes progression of colorectal cancer via the JAK/STAT pathway. *Cancer Manag Res* **11**, 6323-6341 (2019).
76. J. L. Casey *et al.*, Iron-responsive elements: regulatory RNA sequences that control mRNA levels and translation. *Science* **240**, 924-928 (1988).
77. R. D. Horniblow *et al.*, BRAF mutations are associated with increased iron regulatory protein-2 expression in colorectal tumorigenesis. *Cancer Sci* **108**, 1135-1143 (2017).
78. Z. Koveitypour *et al.*, Signaling pathways involved in colorectal cancer progression. *Cell Biosci* **9**, 97 (2019).
79. Y. Fu, L. Lin, L. Xia, MiR-107 function as a tumor suppressor gene in colorectal cancer by targeting transferrin receptor 1. *Cell Mol Biol Lett* **24**, 31 (2019).
80. M. Jung, C. Mertens, R. Bauer, C. Rehwald, B. Brune, Lipocalin-2 and iron trafficking in the tumor microenvironment. *Pharmacol Res* **120**, 146-156 (2017).
81. Z. Liu *et al.*, Regulation of mammalian siderophore 2,5-DHBA in the innate immune response to infection. *J Exp Med* **211**, 1197-1213 (2014).
82. N. Chaudhary *et al.*, Lipocalin 2 expression promotes tumor progression and therapy resistance by inhibiting ferroptosis in colorectal cancer. *Int J Cancer* **149**, 1495-1511 (2021).
83. M. Feng *et al.*, Lipocalin2 suppresses metastasis of colorectal cancer by attenuating NF-κB-dependent activation of snail and epithelial mesenchymal transition. *Mol Cancer* **15**, 77 (2016).
84. C. Pfeifhofer-Obermair, P. Tymoszuk, V. Petzer, G. Weiss, M. Nairz, Iron in the Tumor Microenvironment-Connecting the Dots. *Front Oncol* **8**, 549 (2018).
85. A. J. Schwartz *et al.*, Hepcidin sequesters iron to sustain nucleotide metabolism and mitochondrial function in colorectal cancer epithelial cells. *Nat Metab* **3**, 969-982 (2021).
86. L. Y. Chau, Heme oxygenase-1: emerging target of cancer therapy. *J Biomed Sci* **22**, 22 (2015).
87. J. C. Becker *et al.*, Colonic expression of heme oxygenase-1 is associated with a better long-term survival in patients with colorectal cancer. *Scand J Gastroenterol* **42**, 852-858 (2007).
88. H. Yin, J. Fang, L. Liao, H. Maeda, Q. Su, Upregulation of heme oxygenase-1 in colorectal cancer patients with increased circulation carbon monoxide levels, potentially affects chemotherapeutic sensitivity. *BMC Cancer* **14**, 436 (2014).

89. S. Kimura *et al.*, Increasing Heme Oxygenase-1-Expressing Macrophages Indicates a Tendency of Poor Prognosis in Advanced Colorectal Cancer. *Digestion* **101**, 401-410 (2020).
90. S. M. K. Gamage *et al.*, Heme oxygenase-1 & 2 and their potential contribution in heme induced colorectal carcinogenesis. *Pathol Res Pract* **233**, 153885 (2022).
91. N. C. Andrés *et al.*, Heme oxygenase-1 has antitumoral effects in colorectal cancer: involvement of p53. *Exp Mol Pathol* **97**, 321-331 (2014).
92. G. S. Seo *et al.*, Heme oxygenase-1 promotes tumor progression and metastasis of colorectal carcinoma cells by inhibiting antitumor immunity. *Oncotarget* **6**, 19792-19806 (2015).
93. N. Seiwert *et al.*, Heme oxygenase 1 protects human colonocytes against ROS formation, oxidative DNA damage and cytotoxicity induced by heme iron, but not inorganic iron. *Cell Death Dis* **11**, 787 (2020).
94. P. Allavena, A. Sica, G. Solinas, C. Porta, A. Mantovani, The inflammatory micro-environment in tumor progression: the role of tumor-associated macrophages. *Crit Rev Oncol Hematol* **66**, 1-9 (2008).
95. P. Karpinski, J. Rossowska, M. M. Sasiadek, Immunological landscape of consensus clusters in colorectal cancer. *Oncotarget* **8**, 105299-105311 (2017).
96. J. P. Vayrynen *et al.*, The Prognostic Role of Macrophage Polarization in the Colorectal Cancer Microenvironment. *Cancer Immunol Res* **9**, 8-19 (2021).
97. P. J. Murray *et al.*, Macrophage activation and polarization: nomenclature and experimental guidelines. *Immunity* **41**, 14-20 (2014).
98. D. Hanahan, Hallmarks of Cancer: New Dimensions. *Cancer Discovery* **12**, 31-46 (2022).
99. M. D. Knutson, M. Oukka, L. M. Koss, F. Aydemir, M. Wessling-Resnick, Iron release from macrophages after erythrophagocytosis is up-regulated by ferroportin 1 overexpression and down-regulated by hepcidin. *Proc Natl Acad Sci U S A* **102**, 1324-1328 (2005).
100. Y. Naito *et al.*, CD8+ T cells infiltrated within cancer cell nests as a prognostic factor in human colorectal cancer. *Cancer Res* **58**, 3491-3494 (1998).
101. A. C. Costa, J. M. O. Santos, R. M. Gil da Costa, R. Medeiros, Impact of immune cells on the hallmarks of cancer: A literature review. *Critical Reviews in Oncology/Hematology* **168**, (2021).
102. J. Galon *et al.*, Type, Density, and Location of Immune Cells Within Human Colorectal Tumors Predict Clinical Outcome. *Science* **313**, 1960-1964 (2006).
103. B. Mlecnik, G. Bindea, F. Pagès, J. Galon, Tumor immunosurveillance in human cancers. *Cancer Metastasis Rev* **30**, 5-12 (2011).
104. T. Saito *et al.*, Two FOXP3(+)CD4(+) T cell subpopulations distinctly control the prognosis of colorectal cancers. *Nat Med* **22**, 679-684 (2016).
105. A. Batista, J. Millán, M. Mittelbrunn, F. Sánchez-Madrid, M. A. Alonso, Recruitment of transferrin receptor to immunological synapse in response to TCR engagement. *J Immunol* **172**, 6709-6714 (2004).
106. S. J. F. Cronin, C. J. Woolf, G. Weiss, J. M. Penninger, The Role of Iron Regulation in Immunometabolism and Immune-Related Disease. *Front Mol Biosci* **6**, 116 (2019).
107. K. Graham, E. Unger, Overcoming tumor hypoxia as a barrier to radiotherapy, chemotherapy and immunotherapy in cancer treatment. *Int J Nanomedicine* **13**, 6049-6058 (2018).
108. A. Palazon, A. W. Goldrath, V. Nizet, R. S. Johnson, HIF Transcription Factors, Inflammation, and Immunity. *Immunity* **41**, 518-528 (2014).
109. T. Kietzmann, D. Mennerich, E. Y. Dimova, Hypoxia-Inducible Factors (HIFs) and Phosphorylation: Impact on Stability, Localization, and Transactivity. *Front Cell Dev Biol* **4**, 11 (2016).

110. S. P. Colgan, G. T. Furuta, C. T. Taylor, Hypoxia and Innate Immunity: Keeping Up with the HIFsters. *Annu Rev Immunol* **38**, 341-363 (2020).
111. S. P. Colgan, C. T. Taylor, Hypoxia: an alarm signal during intestinal inflammation. *Nat Rev Gastroenterol Hepatol* **7**, 281-287 (2010).
112. K. L. Talks *et al.*, The expression and distribution of the hypoxia-inducible factors HIF-1alpha and HIF-2alpha in normal human tissues, cancers, and tumor-associated macrophages. *Am J Pathol* **157**, 411-421 (2000).
113. H. Zhong *et al.*, Overexpression of hypoxia-inducible factor 1alpha in common human cancers and their metastases. *Cancer Res* **59**, 5830-5835 (1999).
114. M. Gruber *et al.*, Acute postnatal ablation of Hif-2alpha results in anemia. *Proc Natl Acad Sci U S A* **104**, 2301-2306 (2007).
115. E. B. Rankin *et al.*, Hypoxia-inducible factor-2 (HIF-2) regulates hepatic erythropoietin in vivo. *J Clin Invest* **117**, 1068-1077 (2007).
116. A. J. Schwartz *et al.*, Hepatic hepcidin/intestinal HIF-2α axis maintains iron absorption during iron deficiency and overload. *J Clin Invest* **129**, 336-348 (2019).
117. M. Sanchez, B. Galy, M. U. Muckenthaler, M. W. Hentze, Iron-regulatory proteins limit hypoxia-inducible factor-2alpha expression in iron deficiency. *Nat Struct Mol Biol* **14**, 420-426 (2007).
118. X. Xue *et al.*, Hypoxia-inducible factor-2alpha activation promotes colorectal cancer progression by dysregulating iron homeostasis. *Cancer Res* **72**, 2285-2293 (2012).
119. J. Sabates-Bellver *et al.*, Transcriptome profile of human colorectal adenomas. *Mol Cancer Res* **5**, 1263-1275 (2007).
120. M. Skrzypczak *et al.*, Modeling oncogenic signaling in colon tumors by multidirectional analyses of microarray data directed for maximization of analytical reliability. *PLoS One* **5**, (2010).
121. T. T. Zou *et al.*, Application of cDNA microarrays to generate a molecular taxonomy capable of distinguishing between colon cancer and normal colon. *Oncogene* **21**, 4855-4862 (2002).
122. X. Xue *et al.*, Quantitative proteomics identifies STEAP4 as a critical regulator of mitochondrial dysfunction linking inflammation and colon cancer. *Proc Natl Acad Sci U S A* **114**, E9608-E9617 (2017).
123. R. Singhal *et al.*, HIF-2alpha activation potentiates oxidative cell death in colorectal cancers by increasing cellular iron. *J Clin Invest* **131**, (2021).
124. Y. Zou *et al.*, A GPX4-dependent cancer cell state underlies the clear-cell morphology and confers sensitivity to ferroptosis. *Nat Commun* **10**, 1617 (2019).
125. K. J. Woo, T. J. Lee, J. W. Park, T. K. Kwon, Desferrioxamine, an iron chelator, enhances HIF-1alpha accumulation via cyclooxygenase-2 signaling pathway. *Biochem Biophys Res Commun* **343**, 8-14 (2006).
126. F. Genua, V. Raghunathan, M. Jenab, W. M. Gallagher, D. J. Hughes, The Role of Gut Barrier Dysfunction and Microbiome Dysbiosis in Colorectal Cancer Development. *Front Oncol* **11**, 626349 (2021).
127. Y. Cheng, Z. Ling, L. Li, The Intestinal Microbiota and Colorectal Cancer. *Front Immunol* **11**, 615056 (2020).
128. D. Tardieu *et al.*, The COX-2 inhibitor nimesulide suppresses superoxide and 8-hydroxy-deoxyguanosine formation, and stimulates apoptosis in mucosa during early colonic inflammation in rats. *Carcinogenesis* **21**, 973-976 (2000).
129. L. B. Meira *et al.*, DNA damage induced by chronic inflammation contributes to colon carcinogenesis in mice. *J Clin Invest* **118**, 2516-2525 (2008).
130. A. Ayala, M. F. Muñoz, S. Argüelles, Lipid peroxidation: production, metabolism, and signaling mechanisms of malondialdehyde and 4-hydroxy-2-nonenal. *Oxid Med Cell Longev* **2014**, 360438 (2014).

131. L. J. Niedernhofer, J. S. Daniels, C. A. Rouzer, R. E. Greene, L. J. Marnett, Malondialdehyde, a product of lipid peroxidation, is mutagenic in human cells. *J Biol Chem* **278**, 31426-31433 (2003).
132. L. A. VanderVeen, M. F. Hashim, Y. Shyr, L. J. Marnett, Induction of frameshift and base pair substitution mutations by the major DNA adduct of the endogenous carcinogen malondialdehyde. *Proc Natl Acad Sci U S A* **100**, 14247-14252 (2003).
133. S. Choudhury, M. Dyba, J. Pan, R. Roy, F. L. Chung, Repair kinetics of acrolein- and (E)-4-hydroxy-2-nonenal-derived DNA adducts in human colon cell extracts. *Mutat Res* **751-752**, 15-23 (2013).
134. K. Uchida, HNE as an inducer of COX-2. *Free Radic Biol Med* **111**, 169-172 (2017).
135. S. Pérez, R. Taléns-Visconti, S. Rius-Pérez, I. Finamor, J. Sastre, Redox signaling in the gastrointestinal tract. *Free Radic Biol Med* **104**, 75-103 (2017).
136. M. Baradat *et al.*, 4-Hydroxy-2(E)-nonenal metabolism differs in Apc(+/+) cells and in Apc(Min/+) cells: it may explain colon cancer promotion by heme iron. *Chem Res Toxicol* **24**, 1984-1993 (2011).
137. S. Kondo *et al.*, Persistent oxidative stress in human colorectal carcinoma, but not in adenoma. *Free Radic Biol Med* **27**, 401-410 (1999).
138. C. L. Chang *et al.*, Oxidative stress inactivates the human DNA mismatch repair system. *Am J Physiol Cell Physiol* **283**, C148-154 (2002).
139. M. L. Ribeiro *et al.*, Analysis of oxidative DNA damage in patients with colorectal cancer. *Clin Colorectal Cancer* **7**, 267-272 (2008).
140. S. J. Dixon, B. R. Stockwell, The role of iron and reactive oxygen species in cell death. *Nat Chem Biol* **10**, 9-17 (2014).
141. S. J. Dixon *et al.*, Ferroptosis: an iron-dependent form of nonapoptotic cell death. *Cell* **149**, 1060-1072 (2012).
142. B. R. Stockwell *et al.*, Ferroptosis: A Regulated Cell Death Nexus Linking Metabolism, Redox Biology, and Disease. *Cell* **171**, 273-285 (2017).
143. G. C. Forcina, S. J. Dixon, GPX4 at the Crossroads of Lipid Homeostasis and Ferroptosis. *Proteomics* **19**, e1800311 (2019).
144. B. Hassannia, S. Van Coillie, T. Vanden Berghe, Ferroptosis: Biological Rust of Lipid Membranes. *Antioxid Redox Signal* **35**, 487-509 (2021).
145. L. Liu *et al.*, MiR-15a-3p regulates ferroptosis via targeting glutathione peroxidase GPX4 in colorectal cancer. *Mol Carcinog* **61**, 301-310 (2022).
146. Y. Yang *et al.*, miR-539 activates the SAPK/JNK signaling pathway to promote ferropotosis in colorectal cancer by directly targeting TIPE. *Cell Death Discov* **7**, 272 (2021).
147. D. Lu *et al.*, ACADSB regulates ferroptosis and affects the migration, invasion, and proliferation of colorectal cancer cells. *Cell Biol Int* **44**, 2334-2343 (2020).
148. H. Q. Ju *et al.*, Redox Regulation of Stem-like Cells Though the CD44v-xCT Axis in Colorectal Cancer: Mechanisms and Therapeutic Implications. *Theranostics* **6**, 1160-1175 (2016).
149. L. Zhang *et al.*, Corrigendum to "IMCA Induces Ferroptosis Mediated by SLC7A11 through the AMPK/mTOR Pathway in Colorectal Cancer". *Oxid Med Cell Longev* **2020**, 6901472 (2020).
150. L. Zhang *et al.*, IMCA Induces Ferroptosis Mediated by SLC7A11 through the AMPK/mTOR Pathway in Colorectal Cancer. *Oxid Med Cell Longev* **2020**, 1675613 (2020).
151. X. Xu *et al.*, Targeting SLC7A11 specifically suppresses the progression of colorectal cancer stem cells via inducing ferroptosis. *Eur J Pharm Sci* **152**, 105450 (2020).
152. J. Sun *et al.*, Dichloroacetate attenuates the stemness of colorectal cancer cells via trigerring ferroptosis through sequestering iron in lysosomes. *Environ Toxicol* **36**, 520-529 (2021).

153. J. Yang *et al.*, Cetuximab promotes RSL3-induced ferroptosis by suppressing the Nrf2/HO-1 signalling pathway in KRAS mutant colorectal cancer. *Cell Death Dis* **12**, 1079 (2021).
154. P. Chen *et al.*, Combinative treatment of β-elemene and cetuximab is sensitive to KRAS mutant colorectal cancer cells by inducing ferroptosis and inhibiting epithelial-mesenchymal transformation. *Theranostics* **10**, 5107-5119 (2020).